# Localization and biochemical characterization of the small secreted protein Dld1 from the root endophytic fungus *Piriformospora indica*

# Dissertation

zur

**Erlangung des Doktorgrades**

**der Naturwissenschaften**

**(Dr. rer. nat.)**

Dem Fachbereich Biologie

der Philipps-Universität Marburg

vorgelegt von

**Robin Thomas Nostadt**

aus Offenbach am Main

Marburg/Lahn, 2018

# Localization and biochemical characterization of the small secreted protein Dld1 from the root endophytic fungus *Piriformospora indica*

# Dissertation

**zur**

**Erlangung des Doktorgrades**

**der Naturwissenschaften**

**(Dr. rer. nat.)**

Dem Fachbereich Biologie

der Philipps-Universität Marburg

vorgelegt von

**Robin Thomas Nostadt**

aus Rödermark

Marburg/Lahn, 2018

Die Untersuchungen zur vorliegenden Arbeiten wurden vom Oktober 2012 bis Februar 2016 unter der Betreuung von Prof. Dr. Alga Zuccaro am Max-Planck-Institut für terrestrische Mikrobiologie in der Abteilung Organismische Interaktionen in Marburg durchgeführt.

Vom Fachbereich Biologie

der Philipps-Universität Marburg als Dissertation

angenommen am: 26. Sep. 2018


Erstgutachter: Prof. Dr. Alga Zuccaro

Zweitgutachter: Prof. Dr. Hans-Ulrich Mösch


Tag der mündlichen Prüfung: 19. Dez. 2018

Teile dieser Arbeit wurden in folgenden Artikeln veröffentlicht:

**Nostadt R.,** Hilbert M., Nizam S., Wawra S., Martin J., Küpper H., Mijovilovich A., Ursinus A., Langen G., , Lupas A.N. , Zuccaro , A. Dld1, a novel metal ion-binding protein secreted by the fungus *Serendipita indica* during root colonization confers resistance to metal ion-mediated ROS stress.
*(In Vorbereitung)*

Weitere Veröffentlichungen:

Hilbert M., **Nostadt R.** and Zuccaro, A**.** (2013) Exogenous auxin affects the oxidative burst in barley roots colonized by *Piriformospora indica*.
*Plant Signalling & Behavior.* 8 (4)

Wawra S, Fesel P, Widmer H, Timm M, Seibel J, Leson L, Kesseler L, **Nostadt R,** Hilbert M, Langen G, Zuccaro A. (2016) The fungal-specific β-glucan-binding lectin FGB1 alters cell-wall composition and suppresses glucan triggered immunity in plants.
*Nature Communications*. 7

# Erklärung

Ich versichere, dass meine Dissertation mit dem Titel „Localization and biochemical characterization of the small secreted protein Dld1 from the root endophytic fungus *Piriformospora indica*" selbstständig, ohne unerlaubte Hilfe angefertigt und mich dabei keiner anderen als der von mir ausdrücklich bezeichneten Quellen und Hilfsmittel bedient habe.

Diese Dissertation wurde in der jetzigen oder einer ähnlichen Form noch bei keiner anderen Hochschule eingereicht und hat noch keinen sonstigen Prüfungszwecken gedient.

<br>

(Ort/Datum)  (Robin Nostadt)

*"The good thing about science is that it's true whether or not you believe in it."*

- Neil deGrasse Tyson (*1958)

# Zusammenfassung

*Piriformospora indica* ist ein Symbiont mit einer biphasischen Kolonisierungsstrategie. Er kolonisiert ein breites Spektrum von Wirtspflanzen, inklusive der monokotyledonen Pflanze *Hordeum vulgare* (Gerste), in der er eine Vielzahl von nützlichen Effekten bewirkt. Die Interaktion weißt Charakteristika der pflanzlichen Immunantwort auf, einschließlich der lokalisierten Produktion von reaktiven Sauerstoffspezies (engl. *reactive oxygen species*; ROS) und der Bildung von Zellwandappositionen (engl. *cell wall apposition(s)*; CWA). Ferner wird die Kolonisierung von Gerste durch die Anreicherung von reaktivem $Fe^{3+}$ in CWAs begleitet, die wiederum die Produktion von ROS vermitteln. In der pflanzlichen Immunantwort sind ROS unter anderem für die Festigung und den Ausbau von CWAs durch die Polymerisierung von Ferulasäure und die chemische Quervernetzung von Abwehrproteinen und phenolischen Verbindungen mit Zellwandpolymeren verantwortlich. In den frühen Stadien der *P. indica* / Gerste Interaktion, wenn der Pilz versucht die pflanzliche Zellwand zu durchstoßen, was zu Bildung von CWAs führt, wird die Expression des *P. indica* Gens PIIN_05872 (nachfolgend als *DLD1* bezeichnet) hochreguliert. Das kodierte Protein Dld1 gehört zu einer *P. indica*-spezifischen Proteinfamilie, welche sich durch eine Vielzahl von regelmäßig verteilten Histidinen und Alaninen, sowie einem C-terminal lokalisieren Motiv mit der Konsensussequenz RSIDELD auszeichnet. In dieser Arbeit wurden die Lokalisierung, sowie die biophysikalischen und biochemischen Charakteristika von Dld1 untersucht.

Obwohl die Sekretion von Dld1 durch *P. indica* unklar bleibt, konnte gezeigt werden, dass Dld1 sowohl von *Ustilago maydis* Dld1-Expressionsstämmen *in vitro* und *in planta*, als auch während transienter Expression in Gerstenzellen, sekretiert wird. In Gerste zeigt Dld1 eine Kolokalisation mit $Fe^{3+}$ in CWAs, die als Antwort auf eine Pilzinfektion gebildet werden. Dld1 wurde heterolog in *Escherichia coli* produziert. In Kooperation mit der Arbeitsgruppe von Prof. Lupas aus Tübingen wurde das gereinigte Protein für CD-Spektroskopie und Protein-Röntgen-Kristallstrukturanalyse verwendet. Die Kristallstruktur zeigt, dass Dld1 eine Coiled-coil Struktur aus zwei antiparallelen Alpha-Helices einnimmt. Es konnte gezeigt werden, dass die Struktur pH-sensitiv ist. Während die Histidine auf einer Seite der Helix hervorstehen und wie die Zähne eines Reißverschlusses ineinandergreifen, nehmen die Alanine die meisten Positionen auf der Helix-Innenseite ein, um eine räumlich enge Struktur zu ermöglichen, die in der Vergangenheit als Alacoil benannt wurde. Mit qualitativen und quantitativen Metallbindeassays konnte gezeigt werden, dass Dld1 verschiedene Metallionen binden kann. Die Dissoziationskonstanten für eine Bindung von $Fe^{3+}$ und $Zn^{2+}$ konnten im niedrigen mikromolaren Bereich bestimmt werden. Ursprünglich wurde für Dld1 eine Funktion als Metall-Scavenger vermutet, aber Dld1 kann eine $Fe^{3+}$-katalysierte Oxidation des chemischen Substrats Diaminobenzidin nicht verhindern. Stattdessen, inhibiert Dld1 die Radikal-induzierte Polymerisation von Diaminobenzidin. Diese Beobachtung lässt vermuten, dass Dld1 analoge Reaktionen an der pflanzlichen Zellwand verhindern könnte, z.B. die Polymerisierung von Ferulasäure. Dies könnte schlussendlich dazu beitragen, dass *P. indica* fähig ist die von Gerste gebildeten CWAs zu überwinden, um eine kompatible Interaktion zu etablieren.

# Summary

*P. indica* is a symbiont with a biphasic colonization strategy. It colonizes the roots of a broad range of plant species, including the monocot plant *H. vulgare* (barley) where it has a variety of beneficial effects. The interaction is marked by characteristics of the plant innate immune response, including the localized production of reactive oxygen species (ROS) and formation of cell wall appositions (CWA). In barley, the colonization is furthermore accompanied by a localized accumulation of reactive $Fe^{3+}$ in CWAs, which in turn mediates the production of ROS. In the plant immune response, ROS, among other functions, are responsible for the fortification and maturation of CWAs by polymerization of ferulic acid and crosslinking of defensive proteins and phenolic compounds with cell wall polymers. During the early stages of *P. indica* / barley interaction, when the fungus tries to penetrate the wall of root cells, resulting in the formation of CWAs, the expression of *P. indica* gene *DLD1* is upregulated. The encoded protein Dld1, belongs to a family of small secreted proteins unique to *P. indica*, which exhibit a large number of regularly distributed histidine and alanine residues, as well as a conserved motif with the consensus sequence RSIDELD located at the C-terminus. In this study, the localization of Dld1, as well as its biophysical and biochemical characteristics were investigated.

Although the secretion of Dld1 by *P. indica* remains unclear, it was demonstrated that Dld1 is secreted by *Ustilago maydis* Dld1-expression strains both *in vitro* and *in planta*, and during transient expression in barley. In this host, Dld1 co-localizes with $Fe^{3+}$ in CWAs, formed in response to fungal infection. Dld1 was heterologously produced in *E. coli*. The purified protein was used for circular dichroism spectroscopy and protein x-ray crystallography in cooperation with the group of Prof. Lupas, Tübingen. The crystal structure demonstrates that Dld1 adapts a coiled-coil structure with two antiparallel helices. Its folding was shown to be pH-sensitive. While the histidines protrude from the face of the two helices and interdigitate like teeth of a zipper, alanines occupy most of the helix-inward positions to facilitate a very tight structural assembly, previously termed alacoil. In qualitative and quantitative metal ion binding assays, Dld1 bound several metal ions. The dissociation constants for the binding of $Fe^{3+}$ and $Zn^{2+}$ were determined in the low micromolar range. Originally, a function for Dld1 as metal ion scavenger was postulated, but the protein is unable to prevent the $Fe^{3+}$-catalyzed oxidation of the chemical substrate diaminobenzidine. Instead, Dld1 interferes with the radical-induced polymerization of diaminobenzidine. This observation indicates that Dld1 might interfere with analogous reactions at the plant cell wall, e.g. the polymerization of ferulic acid in maturing CWAs. This might contribute to the ability of *P. indica* to overcome barley CWAs in order to establish a compatible interaction.

# Abbreviations & Technical Terms

| | |
|---|---|
| **Amp** | Ampicillin |
| **$A_X$** | Absorption at x nm |
| **BSA** | Bovine serum albumin |
| **Cam** | Chloramphenicol |
| **Cbx** | Carboxin |
| **CD** | Circular dichroism |
| **CIA** | Chloroform, isoamyl alcohol |
| **CM** | Complete medium |
| **C-terminus/terminal** | Carboxy-terminus/terminal |
| **CWA** | Cell wall apposition |
| **DAB** | 3,3'-Diaminobenzidine |
| **DFO** | Deferoxamine (bacterial siderophore) |
| **dpi** | Days post inoculation |
| **DTT** | Dithiothreitol |
| **EDTA** | Ethylenediaminetetraacetic acid |
| **eGFP** | Ehanced GFP |
| **ER** | Endoplasmatic reticulum |
| **ETI** | Effector-triggered immunity |
| **$Fe^{2+}$** | Ferrous iron ions |
| **$Fe^{3+}$** | Ferric iron ions |
| **FPLC** | Fast protein liquid chromatography |
| **GST** | Glutathione-S-transferase |
| **$H_2O_2$** | hydrogen peroxide |
| **$His_6$** | Hexahistidine |
| **hpi** | Hours post infection |
| **HR** | Hypersensitive response |
| **HRP** | Horseradish peroxidase |
| **Hyg** | Hygromycine |
| **IMAC** | Immobilized metal ion affinity chromatography |
| **IPTG** | Isopropyl β-D-1-thiogalactopyranoside |
| **ITC** | Isothermal titration calorimetry |
| **Kan** | Kanamycin |
| **MAMP** | Microbial-associated molecular pattern |
| **MS** | Mass spectrometry/spectromic |
| **MST** | Microscale thermophoresis |
| **$M_W(X)$** | Molecular weight of protein X |

| | |
|---|---|
| **NB-LRR proteins** | Neucleotide-binding leucine-rich-repeat proteins |
| **NTA** | Nitrilotriacetic acid |
| **N-terminus/terminal** | Amino-terminus/terminal |
| **OD$_x$** | Optical density at x nm |
| **PAMP** | Pathogen-associated molecular pattern |
| **PCR** | Polymerase chain reaction |
| **PP** | PreScission® Protease |
| **PTI** | pattern-triggered immunity |
| **R genes** | Resistance gene |
| **RBOHs** | Respiratory-burst oxidase homologues |
| **Redox reaction** | Reduction-oxidation reaction |
| **ROS** | Reactive oxygen species |
| **rpm** | Rounds per minutes |
| **RxLR** | Arg-x-Leu-Arg (Oomycete translocation motif) |
| **SDS** | Sodium dodecyl sulfate |
| **SDS-PAGE** | Sodium dodecyl sulfate polyacrylamide gelelectrophoresis |
| **SOD** | Superoxide dismutase |
| **SSP** | Small secreted proteins |
| **TCA** | Trichloroacetic acid |
| **UV** | Ultraviolet |

# Table of Contents

# 1. Introduction

## 1.1 The plant immune system and microbial effectors

Plants are sessile organisms that can't evade potential threats by simply changing their location. Instead, they have evolved a two-branched, innate immune system that relies on a number of sophisticated surveillance mechanisms to recognize potential attackers, e.g. bacteria, fungi or herbivores, and rapidly respond via multiple layers of structural, chemical, and protein-based defenses, before the potential attacker has a chance to cause extensive damage (Jones & Dangl, 2006; Boller & Felix, 2009). The first branch of the plant's innate immune system relies on the detection of invading microbes via chemical cues, so called pathogen- or microbe-associated molecular patterns (PAMPs or MAMPs) which are sensed by specific pattern recognition receptors localized on the plant cell surface. Since PAMPs or MAMPs are not exclusively present in pathogenic microbes, the term MAMP is deemed more accurate and will be used hereinafter. MAMPs are essential molecules of the invading microbe that do not necessarily play a role in pathogenicity. A few examples of the best-studied MAMPs are major structural components of bacterial or fungal plasma membrane or cell wall, i.e. bacterial lipopolysaccharides, fungal chitin and ergosterol, or the bacterial flg22-domain of flagellin, a major structural component of the bacterial motility organ (Felix *et al.*, 1999; Nürnberger *et al.*, 2004; Zeidler *et al.*, 2004). Among basal defenses mounted after MAMP recognition, formation of cytoplasmic aggregations, localized cell wall appositions (CWAs or papillae), a burst of reactive oxygen species (ROS), rearrangement of the cytoskeleton and the production of pathogen-related proteins and phytoalexins can be listed (Schulze-Lefert, 2004; Yi & Valent, 2013). Although CWAs and ROS production are key factors in pathogen resistance, they are also found during compatible interactions and in beneficial associations (Hückelhoven *et al.*, 1999; Zuccaro *et al.*, 2011; Lahrmann, U. *et al.*, 2013). If the invading microbe is unable to modulate or suppress the first branch of the plant's innate immune system by prevention of MAMP recognition or interference with downstream responses, the interaction is incompatible and the invader is succesfully repelled. This state has been termed pattern-triggered immunity (PTI) (Jones & Dangl, 2006; Tsuda & Katagiri, 2010). Compatible microbes have evolved so called effectors, proteins produced during the interaction with a potential host plant to overcome, modulate or suppress PTI in order to establish a compatible interaction.

Microbial pathogens have evolved different stategies to deliver their effectors to their respective place of action. Bacterial plant pathogens transport their effectors directly into the target host plant cell cytoplasm or onto the plasma membrane via the type III secretion system, a 3.5 MDa protein complex reminiscent of a syringe (Puhar & Sansonetti, 2014). Oomycete plant pathogens secrete effectors into the apoplastic space, where they either mediate pathogen invasion, e.g. by breaking down the plant's cell wall, or interfere with MAMP

recognition or the plant's defense responses (McLeod *et al.*, 2003; Tian *et al.*, 2007; Damasceno *et al.*, 2008). A subset of secreted oomycete effectors is translocated into the host plant cell via the conserved amino acid motif Arg-x-Leu-Arg (RxLR, where x represents any amino acid), located near the amino-terminus (N-terminus) within the first 40 amino acids after the signal peptide cleavage site (Bos *et al.*, 2006; Wawra *et al.*, 2012).

Similar to oomycete plant pathogens, plant pathogenic as well as mutualistic fungi secrete effectors into the apoplastic space to faciliate colonization in various ways. Some effector proteins inhibit the plant's ability to damage the invading fungus, such as *Cladosporium fulvum* effector Avr4, which protects chitinous fungal cell walls against hydrolysis through host plant chintinases (van den Burg *et al.*, 2006). Other effectors directly inhibit the plant's apoplastic defensive enzymes, such as *C. fulvum* effector Avr2 or *U. maydis* effector Pit2, both of which inhibit extracellular host plant cysteine proteases (Rooney *et al.*, 2005; Mueller *et al.*, 2013). The *U. maydis* effector Pep1 inhibits host plant peroxidases to impair ROS generation, which directly suppresses one of the crucial hallmarks of the plant immune system and any downstream processes (Hemetsberger *et al.*, 2012). One further strategy invading fungi employ, is to mask themselve from recognition. The *C. fulvum* effector Ecp6 sequesters chitin fragments to avoid their detection as MAMPs by the host plant (De Jonge *et al.*, 2010). These are just a few of numerous examples, in which fungal effectors can promote the success of host plant colonization. A small number of fungal effectors target intracellular plant proteins. For example, the *U. maydis* effector Tin2 stabilizes the maize protein kinsase ZmTTK1 and thereby significantly induces anthocyanin biosynthesis, which hypothetically deprives the plant's defense responses of necessary ressources (Tanaka *et al.*, 2014). A further *U. maidis* effector, the secreted chorismate mutase Cmu1, has been shown to to be transloacted into maize cells, where it changes the plant's metabolic status through metabolic primting (Djamei *et al.*, 2011). Consequently, a translocation of particular fungal effectors into the plant cytoplasm has been proposed and investigated (Dodds *et al.*, 2004; Lo Presti *et al.*, 2017). However, a signature sequence similar to the oomycete RxLR motif has yet to be identified.

If the invading microbe has utilized its array of effectors to suppress PTI succesfully, resistant host plants may utilize the second branch of their innate immune system to prevent microbe invasion. The second branch encompasses a set of resistance (R) genes that recognize specific effectors resulting in effector-triggered immunity (ETI) (Collier & Moffett, 2009; Tsuda *et al.*, 2009). ETI is similar to PTI, but both faster and stronger and often culminates in a hypersensitive response (HR) resulting in a localized apoptotic cell death, which potentially hinders or halts the invading microbe (Greenberg & Yao, 2004). The majority of known R genes encode neucleotide-binding leucine-rich-repeat (NB-LRR) proteins, which usually reside within the plant cell. NB-LRR proteins can recognize effectors directly (Tsuda *et al.*, 2009). For example, the *Arabidopsis thaliana* resistance protein RRS1-R directly binds the PopP2 effector

from the plant pathogenic bacterium *Ralstonia solanaecearum* triggering ETI (Deslandes *et al.*, 2003). However, some products of R genes monitor the status of a specific host protein and recognize effectors indirectly, a mode of recognition named as 'guard hpothesis'. For example, the *A. thaliana* RPS2 protein recognizes the *P. syringae* effector AvrRpt2 through the degradation of its 'guarded' *A. thaliana* protein RIN4, which results in ETI (Kim *et al.*, 2005).

The effectiveness of ETI selects for invading microbes that can either evade ETI, by diversification or loss of recognized effectors without compromising virulence, or by ETI suppression by means of acquiring additional effectors, e.g. by gene duplication (Abramovitch *et al.*, 2003; Jones & Dangl, 2006). Supporting this hypothesis, effectors are often subject to diversifying selection, located in the genetic context of transposable elements, telomeres or on dispensable chromosomes (Jones & Dangl, 2006; Raffaele *et al.*, 2010; Rouxel *et al.*, 2011; Balesdent *et al.*, 2013). Similiarly, several R genes show a rapid evolution as well. This might indicate that the respective gene products recognize rapidly evolving effectors directly (Van der Hoorn *et al.*, 2002; Kuang *et al.*, 2004).

In conclusion, plants and microbes are in a constant evolutionary arms raise regarding effectors and R genes, driven by the microbes goal to evade or suppress the plant's immune system and the plant's necessity to defend itself against microbial invaders. Given the significant agricutlural damage caused by microbial pathogens (Rossman, 2009) and the potential benefit of symbiotic microbes, it is essential to elucidate the molecular details of plant-microbe interactions (Hart & Trevors, 2005).

## 1.2 Reactive oxygen species in plant-microbe interactions

Superoxide, hydrogen peroxide ($H_2O_2$) and nitric oxide are the three main forms of ROS produced during plant-microbe interactions, especially in conjunction with MAMP recognition and HR (Torres *et al.*, 2006). A number of different enzymes have been suggested as sources of ROS in plants, including the respiratory-burst oxidase homologues (RBOHs), type III peroxidases, amine oxidases, superoxide dismutases (SODs) and oxalate oxidases (Allan & Fluhr, 1997; Torres *et al.*, 2002; Hückelhoven & Kogel, 2003; Zhang *et al.*, 2004; Torres *et al.*, 2005; Bindschedler *et al.*, 2006; Yoda *et al.*, 2006; Hückelhoven, 2007; Daudi *et al.*, 2012). However, in some plant species individual enzymes are likely responsible for the production of ROS during basal defense and HR, respectively. In *A. thalaiana* for example, the apoplastic oxidative burst after MAMP recognition seems to be exclusively dependent on secreted type III peroxidases (Soylu *et al.*, 2005; Bindschedler *et al.*, 2006). However, ROS-producing enzymes might also interfere with each other, as the $H_2O_2$ produced by peroxidases can induce RBOH activity during HR (Torres *et al.*, 2005). To further complicate the understanding of the role of individual ROS sources and their interplay, $H_2O_2$ production in monocotyledonous plants is associated with the accumulation of free redox-active ferric iron ions at CWAs in response

to fungal penetration attempts (see section 1.3; Liu *et al.*, 2007). As for now, no single source seems to account for ROS production across the continuum of plant-microbe interactions (Torres *et al.*, 2002; Bindschedler, Laurence V. *et al.*, 2006).

The localized generation of ROS by plant cells in response to biotic stimuli has been implicated in a number of defense related processes. Originally, ROS were thought to be generated because of their toxicity for the invading microbe (Peng & Kuc, 1992). However, several plant-associated microbes tolerate relatively high concentrations of ROS in the millimolar range (Molina & Kahmann, 2007; Bolwell & Daudi, 2009), most likely mediated by the production of antioxidant enzymes or compounds (Zhang *et al.*, 2004; Unger *et al.*, 2005).

ROS have also been directly connected to the formation and maturation of CWAs in response to microbial penetration attempts. CWAs mainly consist of crosslinked phenolics, hydroxyproline-rich glycoproteins and callose depositions and $H_2O_2$ accumulation can be observed at sites of CWA formation (Brown *et al.*, 1998; McLusky *et al.*, 1999; Soylu *et al.*, 2005). *In vitro* experiments have shown an oxidative crosslinking of three hydroxyproline-rich proteins purified from French bean cell walls catalyzed by a French bean cell wall peroxidase FBP1, capable of generating $H_2O_2$ at alkaline pH (Wojtaszek *et al.*, 1997). Additionally, FBP1 has been shown to catalyze the oxidative polymerization of ferulic acid, a phenolic compound covalently conjugated with plant cell wall polysaccharides, glycoproteins, lignin and other insoluble biopolymers of the cell wall (Zimmerlin *et al.*, 1994). These results indicate that ROS, such as $H_2O_2$, might be the direct catalyst for the oxidative crosslinking of phenolics and immobilization of cell wall proteins, some of which exert anti-microbial functions, thereby promoting cell wall fortification (Bindschedler *et al.*, 2006).

Finally, ROS serve as signalling molecules in a multitude of different signalling pathways, including growth, development and systemic responses to biotic and abiotic stimuli (Baxter *et al.*, 2014). To partake in such systemic processes, ROS can act as long-distance signals, propagating as a wave in form of ROS accumulation in extracellular spaces in between communicating cells (Miller *et al.*, 2009). This remarkable signalling diversity is most likely achieved by differential co-expression of ROS-generating enzymes in different plant tissues (Suzuki *et al.*, 2011).

Given the important role of ROS during plant-microbe interaction, ROS generators are likely targets for microbial effector proteins. The plant pathogenic oomycete *Phytophthora sojae* for example secretes two effectors that interfere with catalase activity perturbing $H_2O_2$ homeostasis during programmed cell death in order to overcome plant innate immunity (Zhang *et al.*, 2014).

In conclusion, ROS are important signalling molecules and chemical catalysts in plants, with a strong emphasis during plant defense, generated by a number of differentially regulated sources.

## 1.3 The role of iron and iron acquisition in fungal-host-interactions

Iron is a ubiquitous element, which is essential in living cells and is a cofactor in numerous enzymes. However, this element can be toxic at high concentrations, as it is readily engages in one-electron reduction-oxidation (redox) reaction between its reduced ferrous ($Fe^{2+}$) and oxidized ferric ($Fe^{3+}$) form. Redox cycling between both forms can catalyze the formation of highly reactive oxygen radicals through the Fenton reaction (Barb *et al.*, 1951; Koppenol, 2001).

Although iron is one of the most abundant elements on earth, its bioavailability is limited under aerobic and pH neutral conditions. $Fe^{2+}$ rapidly oxidizes under aerobic conditions and $Fe^{3+}$ forms insoluble ferric hydroxide precipitates at a neutral pH. To acquire iron, fungi employ two major high-affinity uptake systems, (i) reductive iron assimilation and (ii) siderophore assisted iron uptake. A number of fungi harbor both systems, e.g. *Schizosaccharomyces pombe* (Askwith & Kaplan, 1997; Schwecke et al., 2006), *Fusarium graminearum* (Greenshields *et al.*, 2007)*, Aspergillus fumigatus* (Schrettl *et al.*, 2004) and *U. maydis* (Mei *et al.*, 1993; Eichhorn *et al.*, 2006), while other fungi seem to have lost the ability to produce siderophores altogether.

The reductive iron assimilation system relies on the extracellular reduction of $Fe^{3+}$ mediated by metalloreductases. Metalloreductase substrate specificity is not limited only to iron salts, but can include low-affinity iron chelates and even siderophores (Johnson, 2008). $Fe^{2+}$ is then transported into the cell through a ferrous iron permease (Askwith *et al.*, 1994). Fungi, which exclusively rely on the reductive iron assimilation system, include *Saccharomyces cerevisiae* (Askwith *et al.*, 1994), *Candida albicans*, *Cryptococcus neoformans* (Howard, 1999) and *Piriformospora indica*.

Siderophores are low-molecular-weight, high-affinity ferric iron specific chelators. Fungi produce a variety of siderophores, but their production almost always relies on a small number of enzymes, including an ornithine oxygenase and several transacylases. The final assembly of siderophores is mediated by non-ribosomal protein synthetases, which activate precursors and incooperate them into small peptides. Subsequently, siderophores can either remain intracellularly to regulate cellular iron pools or are secreted to sequester extracellular $Fe^{3+}$ (Johnson, 2008). Loaded siderophores reenter the cell via specific siderophore transporters, followed by $Fe^{3+}$ reduction to facilitate intracellular release (Ernst & Winkelmann, 1977). Intriguingly, even non-siderophore producing fungi, e.g. *S. cerevisiae* produce siderophore transporters to potentially hijack loaded siderophores produced by other organisms (Lesuisse *et al.*, 1998).

Plant-colonizing fungi are thought to compete with their host for iron. Therefore the ability to acquire iron during colonization is thought to be crucial for the success of the invading fungus. However, which of the two high-affinity uptake systems is required varies from case to case. For example, the virulence of the wheat pathogen *Fusarium graminarum* is dependent on its ability to produce siderophores, but not on the reductive iron assimilation system (Greenshields *et al.*, 2007). In contrast, the virulence of the maize pathogen *U. maydis* is dependent on the reductive iron assimilation system, but not its ability to produce siderophores (Eichhorn *et al.*, 2006). Intriguingly, the abolishment of siderophore production additionally results in a hypersensitivity to $H_2O_2$ in several fungi (Oide *et al.*, 2006).

As stated above, these observations have been mainly attributed to the iron nutritional status of the invading fungus. The plant host is thought employ an iron withholding strategy, consistent with observations made from microbial pathogens in animals (Ong *et al.*, 2006). However, this hypothesis does not apply to all stages of fungal-plant interactions. In 2007, Liu *et al.* demonstrated $Fe^{3+}$ accumulation at CWAs in a number of monocot plant species, namely wheat, corn, barley, oat, sorghum and millet, in response to cell wall penetration attempts by pathogenic fungus *Blumeria graminis* (**Figure 1**). Application of the actin filament disruptor cytochalasin A blocked $Fe^{3+}$ accumulation, indicating that the respective cells were actively redistributing intracellular iron pools to the CWAs, instead of withholding it from the invading pathogen (**Figure 1 C**). Moreover, pretreatment of the plants with bacterial siderophore deferoxamine (DFO) inhibited 3,3'-diaminobenzidine (DAB)-detecatble production of $H_2O_2$ (brown precipitatious staining) in CWAs suggesting that the accumulated $Fe^{3+}$-mediated $H_2O_2$ production (**Figure 1 D**). Iron targeted to the fungal site of attack seems to be a phenomenon specific to cereals since it is not observed in the dicotyledonous model plant *A. thaliana* (Greenshields *et al.*, 2007b; Liu *et al.*, 2007).

Together these observations suggest that, depending on the host plant, the fungus may not only utilize its iron high-affinity uptake system to secure its nutritional status, but is required to sequester iron from CWAs in order to suppress the plant's basal defense response in form of $Fe^{3+}$-mediated $H_2O_2$ production.
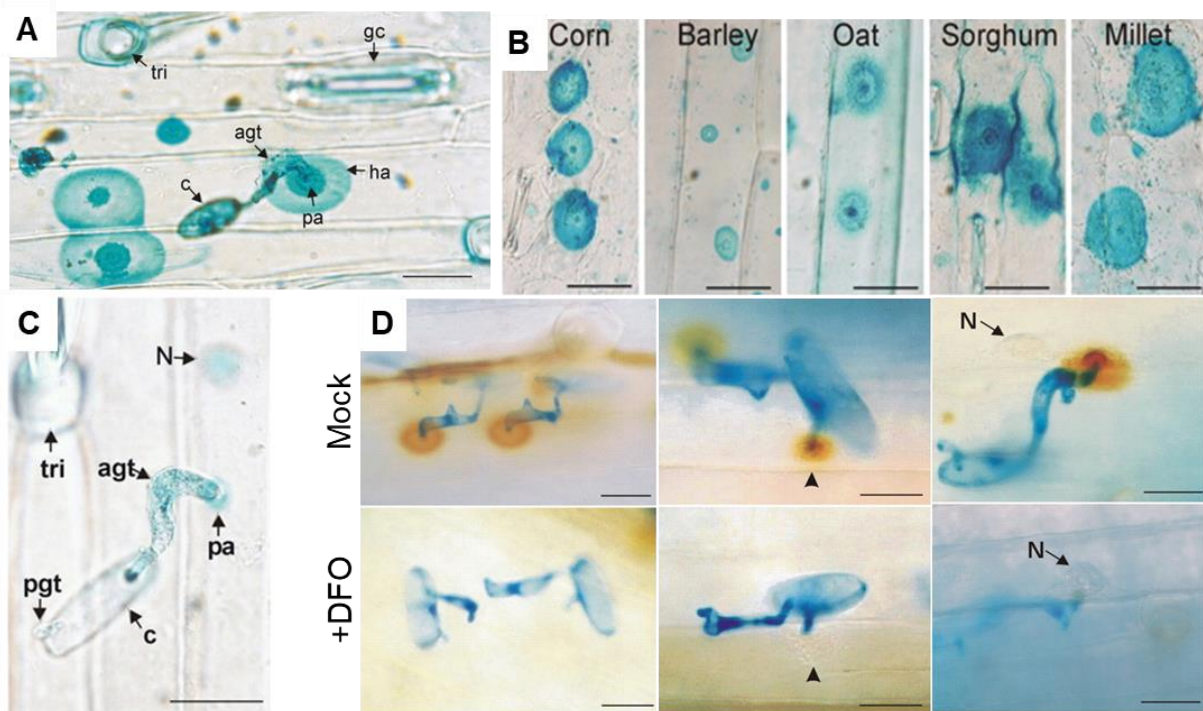
**Figure 1: Targeted iron accumulation mediates $H_2O_2$ production in monocot plant CWAs leaves after _B. graminis_ attack.**
**(A)** _In situ_ $Fe^{3+}$ Prussian Blue staining of wheat epidermis 24 hours post infection (hpi) with _B. graminis_. **(B)** _In situ_ $Fe^{3+}$ Prussian Blue staining of epidermal peels 24 hpi with _B. graminis_ in corn, barley, oat, sorghum and millet. **(C)** The actin filament disruptor cytochalasin A blocks iron accumulation at CWAs. **(D)** DFO blocks $H_2O_2$ generation at appressorial germ tube-associated CWAs. The plants in the bottom panel have been preincubated with the bacterial siderophore DFO. Agt = appressorial germ tube; c = conidium; ha = halo; gc = guard cell; N = epidermal nucleus; n = fungal nucleus; pa = papilla; pgt = primary germ tube; tri = trichome. Scale bar = 20 µm. Adapted fom Liu _et al._, 2007.

## 1.4 The mutualistic root endophyte _Piriformospora indica_

The root endophyte _P. indica_ (Basidiomycota, Sebacinales) is a biotrophic symbiont that colonizes the roots of a broad range of plant species, including _A. thaliana_ and barley. _P. indica_ colonization results in a variety of beneficial effects for the host plant, including growth promotion and heightened resistance against biotic and abiotic stresses (Waller _et al._, 2005; Baltruschat _et al._, 2008; Sherameti _et al._, 2008; Vadassery _et al._, 2009). Depending on its host plant, _P. indica_ exerts different colonization strategies (Lahrmann _et al._, 2013). While in _A. thaliana_, _P. indica_ establishes a long-term biotrophic relationship, the colonization of barley can be divided into an early biotrophic to a late saprophytic phase. The initial interaction with barley is characterized by all hallmarks of plant immune system responses, including CWAs formation, increased vesicle trafficking, accumulation of glycoproteins and production of ROS (Zuccaro _et al._, 2011). Moreover, _P. indica_ colonization in barley leads to an accumulation of iron in cell walls of root epidermal and cortex cells and in particular in CWAs (unpublished data; see **Figure 2**).
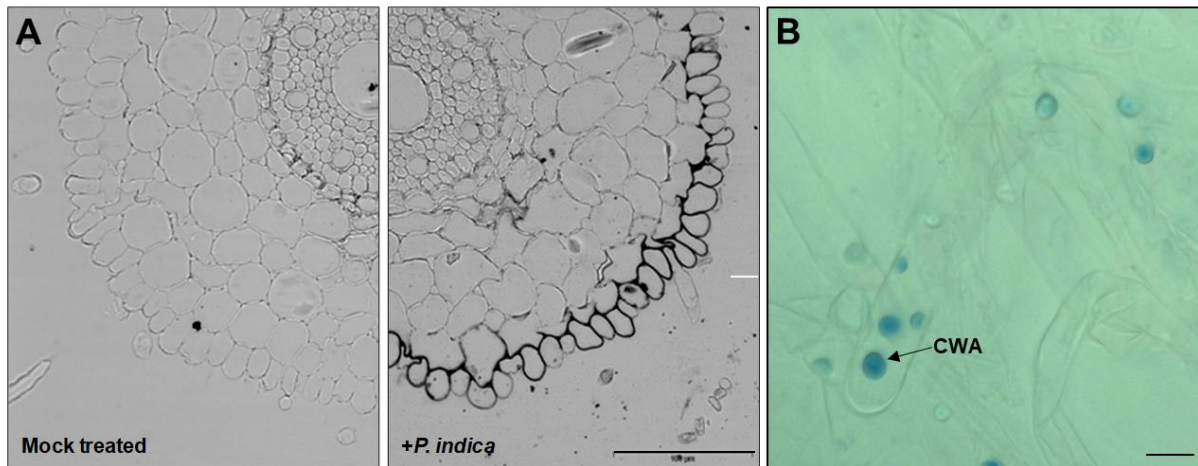
**Figure 2: *P. indica* colonization triggers reallocation of iron to cell walls of root epidermal and cortex cells and CWAs.**
**(A)** Cross sections of barley roots colonized by *P. indica* 6 days post inoculation (dpi) show iron accumulation in epidermal and outermost root cortex cells visualized by sensitive Pearls/DAB staining (visible as black precipitate). Scale bar = 100 µm. **(B)** *P. indica* penetration attempts cause formation of CWAs with strong $Fe^{3+}$ accumulation, visualized by Prussian blue staining. Scale bar = 40 µm. (Dr. Magdalena Hilbert, unpublished data).

*P. indica*-root symbioses is associated with host-specifically induced fungal genes. Most of the induced genes encoding small secreted proteins (<300 amino acids) are either Arabidopsis- or barley-responsive, suggesting that colonization of different hosts may require exploitation of distinct fungal proteins that can interact with elements characteristic to each host (Lahrmann *et al.*, 2015). Genomic and transcriptomic analysis have identified a novel family of small secreted proteins characterized by their high histidine and alanine content, as well as their carboxy-terminal, (C-terminal) seven-amino-acid motif Arg-Ser-Ile-Asp-Glu-Leu-Asp (RSIDELD), therefore named 'DELD' protein family (Zuccaro *et al.*, 2011). Almost all DELD protein family encoding genes are upregulated during plant colonization, the majority during the biotrophic stage of barley colonization when the most CWAs are visible. So far, the localization, biochemical properties and the biological function of the DELD family proteins are unknown. However, the high abundance of histidines as well as the aggregation of charged amino acids at the conserved C-terminus might indicate metal binding properties.

## 1.5 Aims and objectives of this study

The aim of this study is the characterization of the *P. indica* protein Dld1, one member of the DELD protein family, with respect to its localization, structure, biophysical and biochemical properties.

The localization will be analyzed by production of Dld1 fusion proteins in different organisms. As a primary strategy, Dld1:GFP will be constitutively produced in *P. indica* and the secretion will be analyzed. As a secondary strategy, the *in vitro* secretion and *in planta* localization of mCherry:Dld1 will be analyzed with the well-established fungal model organism *U. maydis*. Lastly, the *in planta* localization of Dld1:mCherry will be analyzed by transient expression in barley leaves both untreated and under challenge of the fungal leave pathogen *B. graminis*.

The structural analysis of Dld1 involves the establishment of a sophisticated protocol for the heterologous production of Dld1 in *E. coli* followed by standardized gel filtration chromatography, circular dichroism (CD) spectroscopy and protein x-ray crystallography (in close cooperation with the lab of Prof. Dr. Andrei Lupas, Max-Planck Institute for Developmental Biology, Tübingen). The structure will be compared with available protein structures and differences as well as similarities will be discussed.

Dld1 and mutated derivatives purified from *E. coli*, will be subjected to a number of metal ion binding assays to determine binding properties and to identify amino acids involved in metal ion binding. Furthermore, the impact of Dld1 on the iron catalyzed radical oxidation of the chemical substrate DAB will be analyzed with a respective assay.

From the sum of the results a potential biological function for Dld1 will be inferred and a hypothesis for the role of Dld1 during *P. indica* colonization of barley will be proposed.

# 2. Results

## 2.1 Analysis of Dld1 secretion and localization

### 2.1.1 Secretion of Dld1 by *P. indica*

*In silico* analysis of Dld1 amino acid sequence with SignalP 4.1 predicted an N-terminal signal peptide with a cleavage site between amino acids 19 and 20 (…AST-APL…). In order to verify this prediction, protein secretion was analyzed in three *P. indica* strains (<pGOGFP-DLD1> #1, #5 and #8) producing the fusion protein Dld1:GFP by an immunoblot-based *in vitro* secretion assay. The previously described strain *P. indica* <pGOGFP> (Hilbert *et al.*, 2012) was used as lysis-control, as it produces intracellular eGFP. The mycelium was separated from culture supernatant by filtration. Mycelium proteins were extracted in SDS sample buffer and culture supernatant proteins were precipitated and subsequently solved in equal amounts of buffer. Protein preparations were then analyzed by anti-GFP immunoblot (**Figure 3**).

Three distinct signals between 20 and 25 kDa were detected from lysis-control strain *P. indica* <pGOGFP> mycelium protein preparations. While the highest signal was consistent with the molecular weight of eGFP, the lower two signals most likely originated from eGFP degradation products. No signals were detected in culture supernatant protein preparations of *P. indica* <pGOGFP>. Combined, these results indicate that no leakage of cytoplasmic proteins occurred during sample preparation.

Mycelium protein preparations from all three *P. indica* <pGOGFP:DLD1> strains exhibited two signals at approx. 25 kDa, consistent with the molecular weight of eGFP. One additional signal at approx. 40 kDa was detected from strains #1 and #8, consistent with the molecular weight of Dld1:GFP. Culture supernatant protein preparations of all three strains were devoid of signals. These results indicate that Dld1:GFP was produced, at least in strains #1 and #8, but subsequently cleaved into at least two fragments. The cleavage site or sites reside near the C-terminus of Dld1 and the N-terminus of eGFP. While the C-terminal fragment – mainly consisting of eGFP – was detected at approx. 25 kDa in mycelium protein extractions of all three strains, the N-terminal fragment, which might have undergone secretion, was not detected, due to the missing eGFP epitope. In consequence, no conclusion can be made regarding the secretion of Dld1 by *P. indica* from this experimental setup.

To circumvent the complications of indirect detection of Dld1 via an epitope tag, custom Dld1 antibodies were produced from rabbits in cooperation with Eurogentec (Seraing, Belgium) using Dld1 purified from *E. coli* (see section 2.2.1). Although conclusive results were achieved in immunoblots with protein extractions from *E. coli* and Dld1-expressing *U. maydis* strains, no signals were obtained from *P. indica* protein preparations (**Supplemental Figure 1** and **Supplemental Figure 2**).
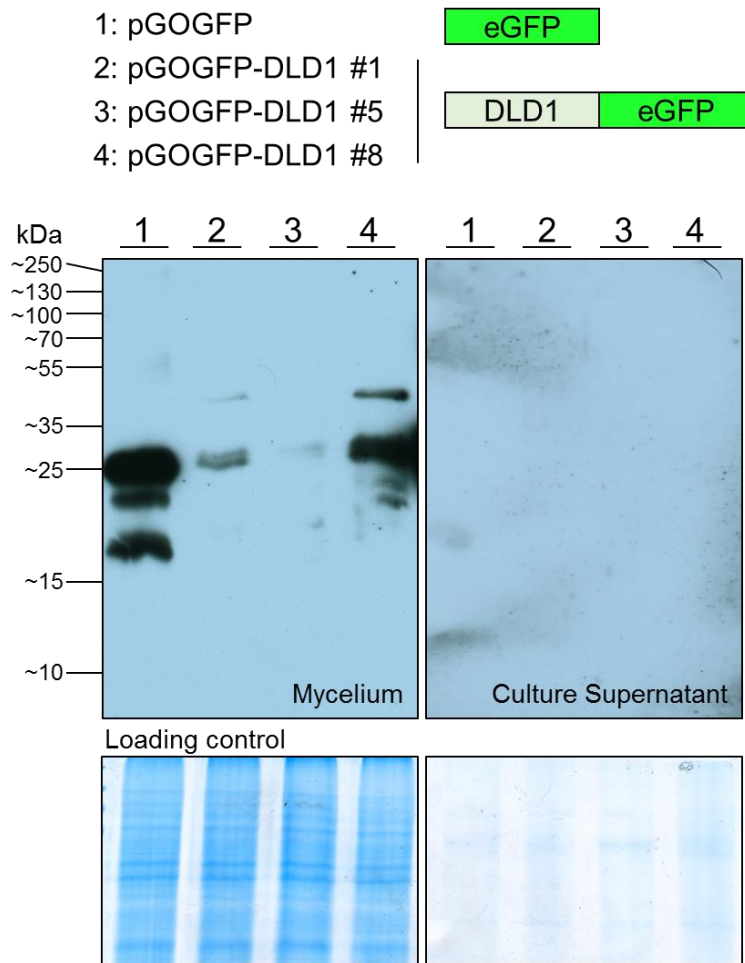
**Figure 3: Anti-GFP immunoblot from *P. indica* secretion assay.**
*P. indica* strains were inoculated in complete medium (CM) and cultivated at 28°C for seven days. The mycelium was separated from culture supernatant by filtration, frozen in liquid nitrogen, ground to fine powder, lysed by mechanical disruption and proteins were extracted with SDS sample buffer. Culture supernatant proteins were precipitated with trichloroacetic acid (TCA), washed and resolved in equal amounts of SDS sample buffer. Protein preparations from mycelium and culture supernatants were analyzed by anti-GFP immunoblot. Gels were stained with Coomassie to ensure that equal amounts of proteins were loaded. $M_W$(eGFP)=26.9 kDa; $M_W$(Dld1:GFP)=41.6 kDa.

As all immunoblot-based approaches to analyze Dld1 secretion by *P. indica* were exhausted, proteins prepared from *P. indica* <pGOGFP:DLD1> culture supernatants were subjected to peptide mass fingerprinting with and without enzymatic deglycosylation. Although a number of secreted *P. indica* proteins were identified (**Supplemental Table 1**) and deglycosylation did increase the number of identified peptides significantly, Dld1 was not detected.

## 2.1.2 Secretion of Dld1 by *U. maydis*

In parallel to the attempts to analyze the secretion of Dld1 by *P. indica*, secretion was also investigated utilizing transgenic, Dld1-expressing *U. maydis* strains. For this experiment, a total of four strains were used. *U. maydis* <p123-mCherry> (Doehlemann *et al.*, 2009) – producing cytoplasmic mCherry – was used as a lysis-control strain. *U. maydis* <p123-PIT2SP:mCherry:DLD1woSP> was used as a positive control for secretion. This strain produces a fusion protein of the signal peptide from *U. maydis* effector Pit2, mCherry and Dld1 without the predicted signal peptide (hereafter named Dld1woSP). The secretion of Pit2 by

*U. maydis* has been verified experimentally by Doehlemann *et al.* in 2011. The strains, *U. maydis* <p123-DLD1SP:mCherry:DLD1woSP> and <p123-DLD1SP:mCherry:DLD1woSP$^{\Delta RSIDELD}$>, produce a fusion protein of the Dld1 signal peptide, mCherry and Dld1woSP, whereas the latter strain produces the fusion protein lacking the C-terminal RSIDELD motif. Both strains were used to investigate if *U. maydis* would be able to utilize the Dld1 signal peptide for secretion and if the RSIDELD motif had any impact on the secretion process. The mCherry epitope was intentionally placed right after the predicted cleavage site of the Pit2 or Dld1 signal peptide to circumvent possible complications with protein cleavage near the C-terminus of Dld1 as observed in the *P. indica* secretion assay. After liquid culture growth, culture supernatant and sporidia were separated by centrifugation and filtration. Proteins from sporidia were extracted and culture supernatant proteins were precipitated. Sporidia and culture supernatant proteins from all aforementioned strains were analyzed in an anti-mCherry immunoblot (**Figure 4**).
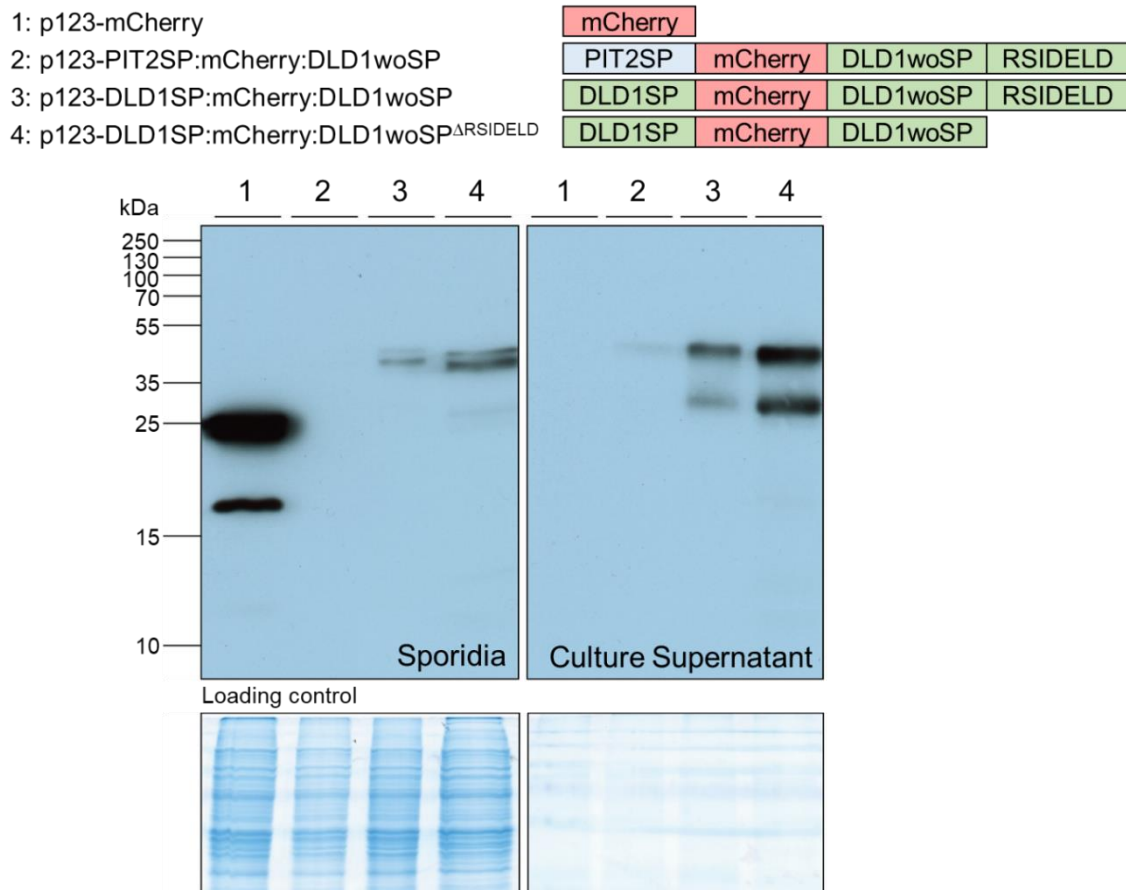


**Figure 4: Anti-mCherry immunoblot-based *U. maydis* secretion assay.**
*U. maydis* strains were grown in CM liquid cultures. Sporidia and culture supernatant were separated by centrifugation and filtration. Sporidia were lysed and proteins extracted with SDS sample buffer. Proteins from culture supernatant were precipitated with TCA and resolved in equal amounts of SDS sample buffer. Sporidia and culture supernatant protein preparations were subjected to an anti-mCherry-immunoblot. Gels were stained with Coomassie to ensure that equal amounts of proteins were loaded in between sporidia and extracellular protein preparations, respectively. $M_W$(mCherry)=28.8 kDa; $M_W$(mCherry:Dld1woSP)=41.5 kDa. Strains used in this assay were provided by Dr. Shadab Nizam.

Sporidia proteins extracted from lysis-control strain *U. maydis* <p123-mCherry> exhibited one strong signal at approx. 25 kDa, consistent with the molecular weight of mCherry, and one signal at approx. 17 kDa, which most likely originated from mCherry degradation. Culture supernatant proteins were devoid of signals. This indicates that no cytoplasmic protein contamination occurred during sample preparation of proteins from the culture supernatant.

Sporidia proteins extracted from *U. maydis* <p123-PIT2SP:mCherry:DLD1woSP> were devoid of signals. Culture supernatant proteins exhibited one faint signal at approx. 40 kDa, consistent with the molecular weight of the fusion protein mCherry:Dld1woSP. Sporidia proteins from *U. maydis* <p123-DLD1SP:mCherry:DLD1woSP> and <p123-DLD1SP:mCherry:DLD1woSP$^{\Delta RSIDELD}$> both exhibited two signals at approx. 40 kDa, consistent with the molecular weight of mCherry:Dld1woSP or mCherry:Dld1woSP$^{\Delta RSIDELD}$, respectively. The two signals likely originated from the respective proteins prior and after signal peptide cleavage. Culture supernatant proteins of both strains exhibited one signal at approx. 40 kDa and one signal at approx. 30 kDa. While the lower signal most likely derived from a protein degradation, the higher signal is consistent with the molecular weight of mCherry:Dld1woSP and mCherry:Dld1woSP$^{\Delta RSIDELD}$, respectively.

Together these results confirm that the basidiomycete fungus *U. maydis* is able to utilize the Dld1 signal peptide for protein secretion and that the RSIDELD motif has no apparent effect on this process. To analyze the localization of Dld1 during plant interaction, maize seedlings were infected with the four aforementioned *U. maydis* strains. These conditions, are deemed more comparable to conditions during *P. indica* plant colonization, as *U. maydis* comes into close contact with plant cells and exerts filamentous growth. Three days after infection, protein localization was analyzed via confocal microscopy (**Figure 5** upper panel).
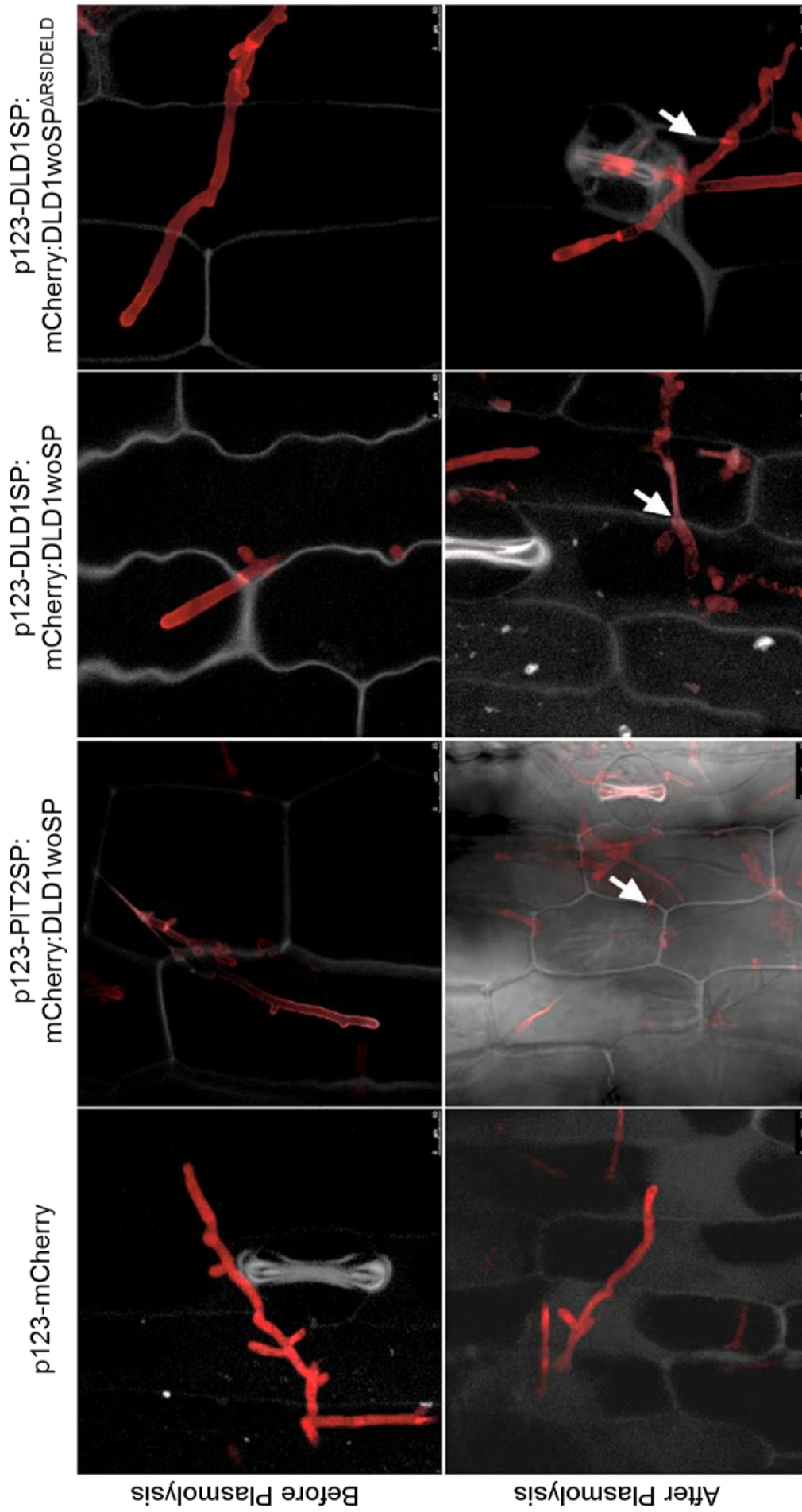
**Figure 5: *In planta* confocal microscopy of *U. maydis* secretion assay strains.**
Maize plants were infected with strains *U. maydis* <p123-mCherry>, <p123-PIT2SP:mCherry:DLD1woSP>, <p123-DLD1SP:mCherry:DLD1woSP>, and <p123-DLD1SP:mCherry:DLD1woSP^ΔRSIDELD>. Three days after infection, the are 1-3 cm below the infection site was excised and analyzed using confocal laser-scanning microscopy (upper panel). To induce plasmolysis, samples were treated with 1 M NaCl (lower panel). mCherry was excited at 561 nm and detected at 580-630 nm. Scale bars represent 35 µm. Strains and pictures provided by Dr. Shadab Nizam.

mCherry fluorescence signals in plants infected with *U. maydis* <p123-mCherry> were detected inside the fungal hyphae, typical for cytoplasmic localization. mCherry signals in plants infected with the *U. maydis* strains <p123-PIT2SP:mCherry:DLD1woSP>, <p123-DLD1SP:mCherry:DLD1woSP> and <p123-DLD1SP:mCherry:DLD1woSP$^{\Delta RSIDELD}$> were detected mainly outside the fungal hyphae. Additionally, in all three strains signals accumulated mostly at the hyphal tip and in plant cell-to-cell passages. These observations strongly suggest that the mCherry fusion proteins were secreted by *U. maydis* during maize infection, regardless of the origin of the signal peptide and presence of the C-terminal RSIDELD motif. These results are consistent with the immunoblot assay.

To further characterize the extracellular localization of mCherry:Dld1woSP and mCherry:Dld1woSP$^{\Delta RSIDELD}$, infected maize samples were treated with 1 M NaCl to induce cell plasmolysis, which resulted in a volumetric extension of the apoplastic space (**Figure 5** lower panel). While plasmolysis did not affect the intra-hyphal signals, signals at the hyphal tip and around the hyphae were dispersed. However, signals in plant to cell-to-cell passages were retained (white arrows). These observations implicate that neither mCherry:Dld1woSP nor mCherry:Dld1woSP$^{\Delta RSIDELD}$ associate with the hyphal surface, i.e. fungal plasma membrane or cell wall, or plant plasma membrane, but associate with the plant cell wall.

## 2.1.3 Dld1 localizes at CWAs in response to *B. graminis* attack

The Dld1-encoding gene is mainly expressed at early stages of *P. indica* / barley interaction and the upregulation correlates with the number of CWAs formed by barley (Zuccaro *et al.*, 2011). The localization of mCherry:Dld1woSP during *U. maydis* / maize infection indicated that Dld1 might associate with the plant cell wall. Combined, these observations lead to the hypothesis that Dld1 might localize at CWAs during the early stages of *P. indica* / barley interaction. Since the production of a detectable Dld1 fusion protein in *P. indica* was not feasible and as no CWAs can be observed in the *U. maydis* / maize pathosystem, the *B. graminis* / barley pathosystem was chosen to analyze the localization of Dld1 in the presence of CWAs. Instead of generating transgenic *B. graminis* lines, barley leaves were transiently transformed by particle bombardment with the two plasmids P35S::eGFP and P35S::DLD1$^{\Delta RSIDELD}$:mCherry:RSIDELD. While P35S::eGFP served as a transformation control, which leads to production of eGFP in transformed cells, P35S::DLD1$^{\Delta RSIDELD}$:mCherry:RSIDELD leads to the production of a fusion protein of full-length Dld1 without the C-terminal RSIDELD motif, mCherry with an added RSIDELD motif (hereafter named Dld1$^{\Delta RSIDELD}$:mCherry:RSIDELD). Bombarded leaves were examined by confocal laser-scanning microscopy (**Figure 6** A)
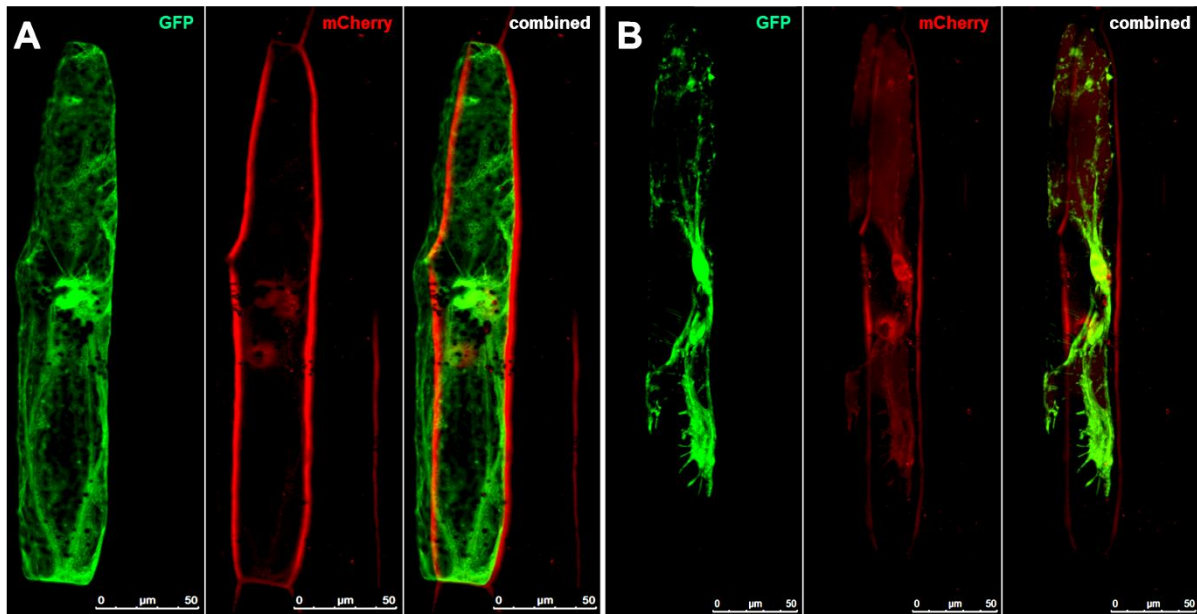
**Figure 6: Confocal laser scanning microscopy of transiently transformed barley leaves.**
The abaxial side of barley leaves from one-week-old seedlings was bombarded with gold microcarriers loaded with plasmids P35S::eGFP and P35S:DLD1$^{\Delta RSIDELD}$:mCherry:RSIDELD. Leaves were examined by confocal laser scanning microscopy three days after particle bombardment **(A)** before and **(B)** after plasmolysis. mCherry was excited at 561 nm and detected at 580-630 nm. eGFP was excited at 488 nm and deteted at 495-530 nm. Scale bars represent 50 μm. Strains and pictures provided by Dr. Magdalena Hilbert.

Transformed cells exhibited strong eGFP-fluorescence signals in cytoplasmic threads and the nucleus. mCherry-fluorescence signals were detected within the plant cytoplasm and nucleus, but with a weaker intensity relative to eGFP signals. Additionally, mCherry signals strongly accumulated at the transformed cells' periphery and spread to the periphery of the neighboring cells. Together these observations are consistent with the secretion of Dld1$^{\Delta RSIDELD}$:mCherry:RSIDELD.

Plasmolysis of the transformed cells was induced by addition of 5 M NaCl (**Figure 6** B). While plasmolysis did not affect the localization of intracellular eGFP and mCherry signals, the mCherry signal intensity in the cell's periphery was slightly reduced, but not dispersed. Together the observations suggest that Dld1$^{\Delta RSIDELD}$:mCherry:RSIDELD localizes in the apoplast, as indicated by the mCherry signal reduction following plasmolysis. However, a subset of the Dld1$^{\Delta RSIDELD}$:mCherry:RSIDELD proteins associate with the plant cell wall and was thereby not affected by the plasmolysis. These results are consistent with the localization of mCherry:Dld1woSP during *U. maydis* / maize infection at the plant cell wall.

To analyze the localization of Dld1$^{\Delta RSIDELD}$:mCherry:RSIDELD during fungal penetration attempts and the formation of CWAs, barley leaves were again transiently transformed by particle bombardment, but additionally spray inoculated with *B. graminis* spores. Leaves bombarded with P35S::eGFP and P35S::mCherry, two plasmids leading to production of cytoplasmic eGFP and mCherry, were used as a control. Fusion protein localization was observed in leaves bombarded with P35S::eGFP and P35S::DLD1$^{\Delta RSIDELD}$:mCherry:RSIDELD.

In control leaves, transformed cells exhibited eGFP- and mCherry-fluorescence signals mainly in cytoplasmic threads. However, *B. graminis* penetration sites (white arrows) were completely devoid of signals (**Figure 7** A). In leaves bombarded with P35S::eGFP and P35S::DLD1$^{\Delta RSIDELD}$:mCherry:RSIDELD, transformed cells exhibited eGFP signals around the nucleus, in cytoplasmic threads and at the cell periphery (**Figure 7** B). mCherry signals were also detected at the cell periphery, but strongly accumulated at sites of *B. graminis* penetration attempts (white arrows).

Together these observations show that transformed barley cells are able to utilize the Dld1 secretion signal in order to secrete Dld1$^{\Delta RSIDELD}$:mCherry:RSIDELD into the apoplast. Moreover, a subset of the protein associates with plant cell wall and accumulates at sites of *B. graminis* penetration attempts, specifically were CWAs are formed. The mechanism behind Dld1's apparent affinity to plant cell walls and preferential localization at CWAs is unclear, but might be explained by its biophysical and biochemical properties.
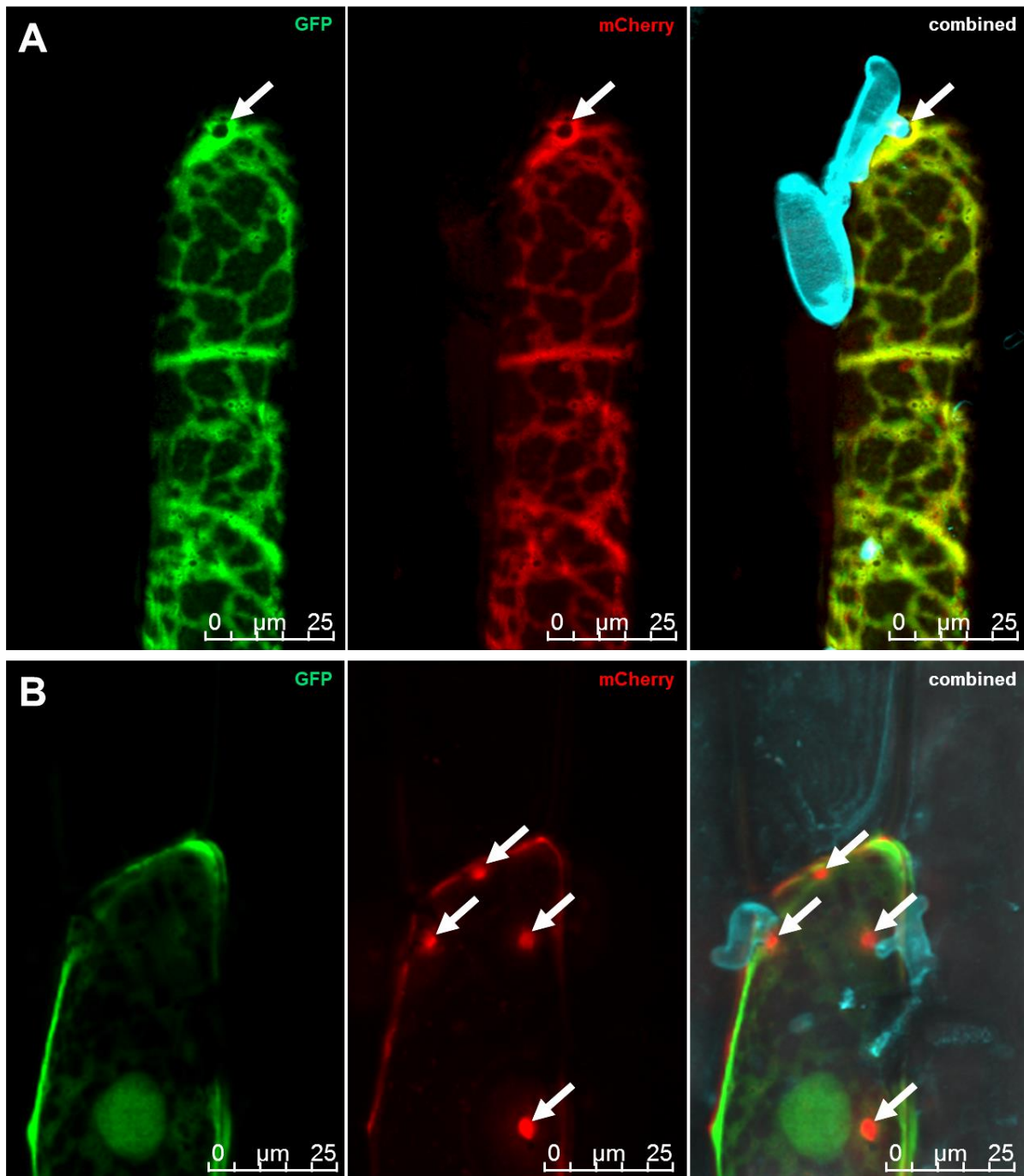
**Figure 7: Confocal micrsocopy of bombarded barley leaves spray inoculated with *B. graminis* spores.**
The abaxial side of barley laves from one-week-old seedlings, where bombarded with gold microcarriers loaded with P35S::eGFP and either P35S::mCherry in **(A)** or P35S::DLD1$^{\Delta RSIDELD}$:mCherry:RSIDELD in **(B)**. Twenty-four (24) hours after bombardment, leaves where spray inoculated with *B. graminis* spores. Leaves were examined by confocal laser-scanning microscopy three days after bombardment. mCherry was excited at 561 nm and detected at 580-630 nm. eGFP was excited at 488 nm and deteted at 495-530 nm. Fungal spores were visualized with Fluorescent brightener 28, which was excited at 405 nm and detected at 420-450 nm. Scale bars represent 25 µm. Strains and pictures provided by Dr. Magdalena Hilbert.

## 2.2 Biophysical and biochemical characterization of Dld1

### 2.2.1 Dld1 can be purified heterologously from *E. coli*

As a prerequisite for biophysical and biochemical characterization, *DLD1* was heterologously expressed in *E. coli* and Dld1 was subsequently purified from cell lysates. As the results from section 2.1 suggest that Dld1 is a secreted protein, the sequence encoding the signal peptide was omitted to avoid secretion by *E. coli*. Hence, all Dld1 variants purified from *E. coli* are lacking the signal peptide. To facilitate the purification procedure, a glutathione-S-transferase (GST)-tag was fused to the N-terminus of Dld1, thereby creating the fusion protein GST:Dld1. A 3C protease cleavage site was introduced in between the GST tag and Dld1 to facilitate removal of GST after purification by treatment with PreScission® Protease (PP).

In a preliminary screen using different *E. coli* expression strains, growth temperatures and concentrations of the chemical inducer isopropyl β-D-1-thiogalactopyranoside (IPTG), the optimal conditions for Dld1 purification were determined. The *E. coli* expression strain BL21(DE3)pLys, grown at 37°C before induction and at 20°C after induction and a final concentration of 1 mM IPTG yielded the highest amount of soluble protein. Visual comparison of total protein extracts before and after induction via sodium dodecyl sulfate polyacrylamide gelelectrophoresis (SDS-PAGE) followed by Coomassie-based staining resulted in a prominent band at approx. 35 kDa after 16 hours growth at 20°C, consistent with the molecular weight of GST:Dld1 (**Figure 8** A).
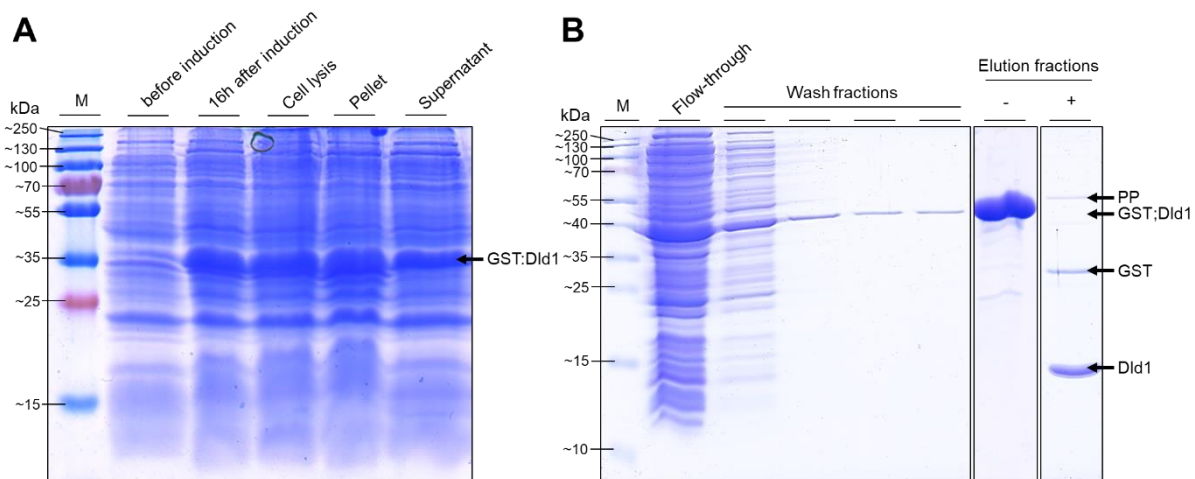


**Figure 8: Dld1 purification from *E. coli*.**
**(A)** SDS-PAGE of total protein extracts from *E. coli* cells at different stages of the induction and lysis procedure. In comparison to total protein extraction before induction, 16 hours after induction a very prominent band was visible at approx. 35 kDa. This band was also visible after cell lysis procedure in the total cell lysate and to equal amounts in insoluble pellet as well as soluble supernatant fraction after centrifugation of the cell lysate. **(B)** SDS-PAGE of Dld1 purification steps via glutathione sepharose columns. Bound proteins were either eluted by competition with reduced glutathione or by addition of a PP, resulting in on-column GST tag cleavage. In elution fractions without addition PP (-), one major band at approx. 40 kDa was visible, consistent to the molecular weight of GST:Dld1. In elution fractions with addition of PP, three bands were visible, one at approx. 55 kDa, consistent with the molecular weight of PP, one at approx. 25 to 35 kDa, consistent with the molecular weight of GST, and one at approx. 15 kDa, consistent with the molecular weight of Dld1. $M_W$(GST:Dld1)=38 kDa; $M_W$(PP)=47 kDa; $M_W$(GST)=26 kDa; $M_W$(Dld1)=12 kDa.

The cell lysis procedure did not change the band pattern significantly and sufficient amounts of GST:Dld1 remained in the soluble supernatant fraction after removal of the insoluble pellet fraction by centrifugation. The supernatant was subsequently applied to glutathione sepharose columns, which were washed with buffer to remove unbound proteins. Immobilized proteins were eluted either by competition with reduced glutathione in the elution buffer or by proteolytic cleavage of the GST tag with PP. Proteins in flow-through, wash- and elution fractions were visualized by SDS-PAGE followed by Coomassie-based staining (**Figure 8** B). Flow-through and wash fraction band patterns contained one prominent band at approx. 35 to 40 kDa, which was decreasing in intensity in final wash fractions. This band is most likely surplus GST:Dld1, exceeding the maximum matrix binding capacity of the column. Elution without addition of PP resulted in one single prominent band at approx. 35 to 40 kDa, consistent with the molecular weight of GST:Dld1 and some fainter bands different in size, most likely originating from degraded GST:Dld1 or other minor protein contaminations. Elution with addition of PP resulted in three bands, one at approx. 40 to 55 kDa, most likely the PP itself, one at approx. 25 to 35 kDa, consistent with the molecular weight of GST and one at approx. 15 kDa, consistent with the molecular weight of Dld1.

Since elution fractions contained significant amounts of other proteins besides GST:Dld1 or Dld1, which might influence experiments conducted with the purified proteins, a secondary purification step was performed using fast protein liquid chromatography (FPLC) with a gel filtration column. To this end, elution fractions from glutathione sepharose purifications were pooled, concentrated and injected onto the FPLC gel filtration system. UV-spectrograms of Dld1 purifications with PP cleavage showed one plateau and two distinct separate peaks (**Figure 9** A).
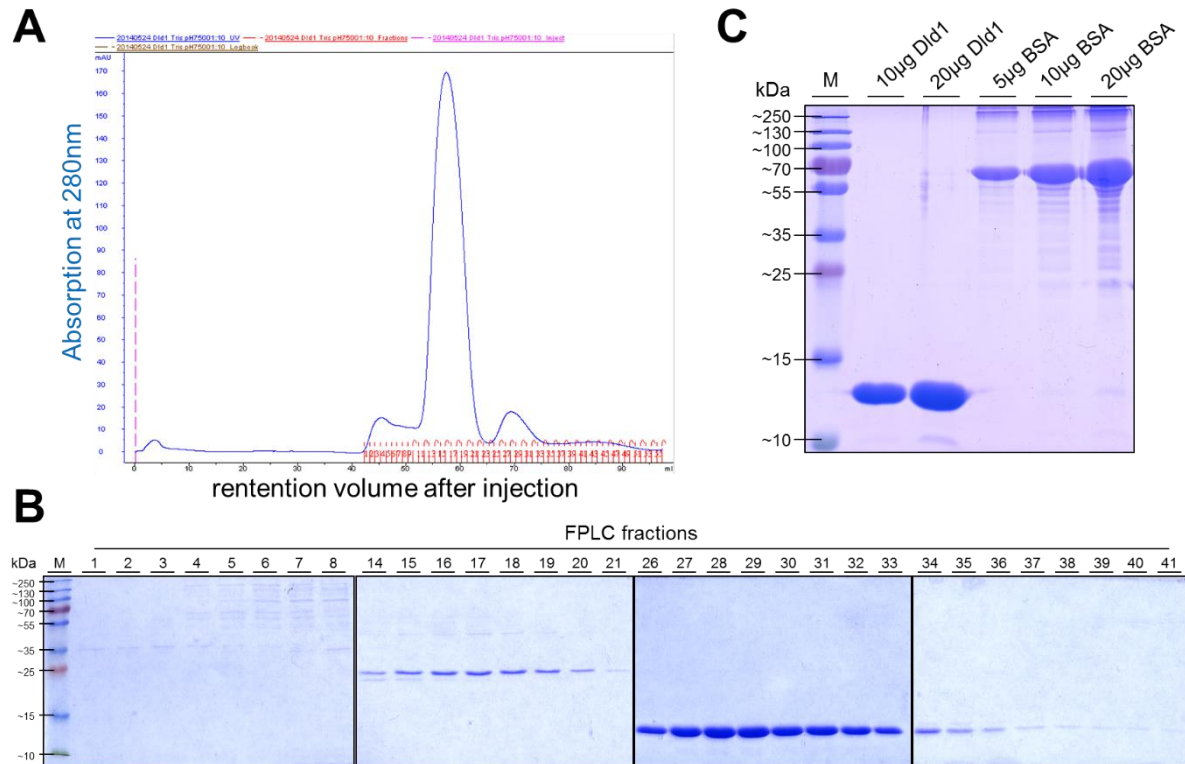
**Figure 9: Purification of Dld1 via FPLC gel filtration.**
**(A)** UV-spectrogram of FPLC gel filtration run with concentrated elution fractions from glutathione-sepharose purification of Dld1 from *E. coli*. The x-axis shows the retention volume after sample injection in mL, the y-axis shows $A_{280}$ in relative absorption units (mAU). The red numbers above the x-axis show the specific fractions in which the device subdivided the elution. **(B)** SDS-PAGE with subsequent Coomassie-based staining of representative FPLC gel filtration fractions. **(C)** Final purification result for Dld1. 10 µg and 20 µg purified Dld1 were analyzed via SDS-PAGE followed by Coomassie-based straining in comparison to three different amounts of commercially available BSA as standard for purity and correct concentration determination.

The plateau ranged from a retention volume of approx. 42 mL to 52 mL (corresponding to fractions 1 to 9) with an absorption at 280 nm ($A_{280}$) of approx. 15 mAU. The first major peak ranged from a retention volume of approx. 52 mL to 65 mL (corresponding to fractions 11 to 22) with $A_{280}$ peak maxima of 170 mAU at approx. 58 mL retention volume. The second minor peak ranged from approx. 65 mL to 75 mL (corresponding to fractions 25 to 33) retention volume with an $A_{280}$ peak maxima of 20 mAU at approx. 70 mL retention volume.

Representative FPLC fractions were analyzed via SDS-PAGE to identify proteins present in absorption peaks (**Figure 9** B). Representative fractions for the plateau (fractions 1 to 8) contained a number of faint bands of higher molecular weight (35 kDa to 250 kDa). The characteristics of the plateau and the high number of bands are typical for protein aggregates with high molecular weight, which elute with a low retention volume. Representative fractions for the first major peak (fractions 14 to 21) also contained very faint bands of high molecular weight and one distinct band at approx. 25 kDa, consistent with the molecular weight of the GST tag. Representative fractions for the second minor peak (fractions 26 to 33) showed a single distinct band at approx. 15 kDa, consistent with the molecular weight of Dld1 without signal peptide.

To avoid contamination a very restrictive number of Dld1 containing FPLC fractions (25 to 33) were pooled and concentrated. $A_{280}$ was measured and the molar and mass concentration of the purified protein was calculated with the *in silico* predicted Dld1 extinction coefficient ($\varepsilon$ = 4470 $M^{-1}cm^{-1}$). Finally, the concentrated protein was analyzed again for purity and accurate concentration determination in comparison to commercially available bovine serum albumin (BSA; **Figure 9** C). Even though high amounts of Dld1 were used, no other bands were visible in the respective lanes, representative of high purity of protein preparation.

In this chapter the primary purification procedure via glutathione sepharose columns for GST:Dld1 and Dld1, as well as the secondary purification procedure via FPLC gel filtration for Dld1 was described. However a number of other proteins were purified for experiments described in this thesis, including the GST alone, GFP and N-terminally GFP-tagged Dld1 and the three mutated versions (GFP:Dld1, GFP:Dld1$^{H107A}$, GFP:Dld1$^{H103A,H107A}$ and GFP:Dld1$^{\Delta RSIDELD}$). For all these purifications the same primary and secondary purifications procedures were applied and concentration and purity of the purified proteins was determined with the same diligence.

## 2.2.2 Dld1 is a monomeric protein with an anti-parallel three-dimensional α-helical structure

To analyze the oligomeric state of Dld1, the FPLC gel filtration column used for purification was calibrated with a protein mixture of conalbumin, carbonic anhydrase, ribonuclease A and aprotinin. Following calibration, the molecular weight of Dld1 was calculated corresponding to its peak retention volume. As a control, two further proteins – GFP and ovalbumin – were analyzed the same way. The molecular weights of all three proteins, as determined by peak retention volume, were compared with the *in silico* molecular weight determination by Expasy ProtParam Tool (Gasteiger *et al.*, 2003) and the deviation was calculated (**Table 1**).

**Table 1: Results of calibrated FPLC gel filtration for ovalbumin, GFP and Dld1.**

| Protein | Peak Retention Volume [mL] | $M_W$ (by Peak Retention Volume) [Da] | $M_W$ (by ProtParam) [Da] | Deviation [%] |
|---|---|---|---|---|
| Ovalbumin | 57.82 | 54028 | 43000 | 25.65 |
| GFP | 63.02 | 39769 | 26430 | 50.47 |
| Dld1 | 69.28 | 27483 | 12700 | 116.40 |

Ovalbumin, with an *in silico* molecular weight of 43 kDa, showed a peak absorbance retention volume of 57.82 mL. Using the determined formula the molecular weight was calculated as 54.03 kDa, which deviates from the *in silico* molecular weight by 25.65%. This indicates that ovalbumin is most likely a monomer in solution. GFP, with an *in silico* molecular weight of 26.43 kDa, showed a peak absorbance retention volume of 63.02 mL. The molecular weight was calculated as 39.77 kDa, which deviates from the *in silico* molecular weight by 50.47%. This result also indicates that GFP most likely is a monomer in solution. Dld1 exhibited a peak

absorbance retention volume of 68.28 mL, which calculated into a molecular weight of 27.48 kDa, which deviates from the *in silico* molecular weight of 12.7 kDa by 116.4%. These results indicate that Dld1 might form dimers in solution and prompted further investigations.

In order to investigate direct protein-protein interactions and potential multimer formation in more detail, purified Dld1 was subjected to formaldehyde crosslinking (**Figure 10** A).
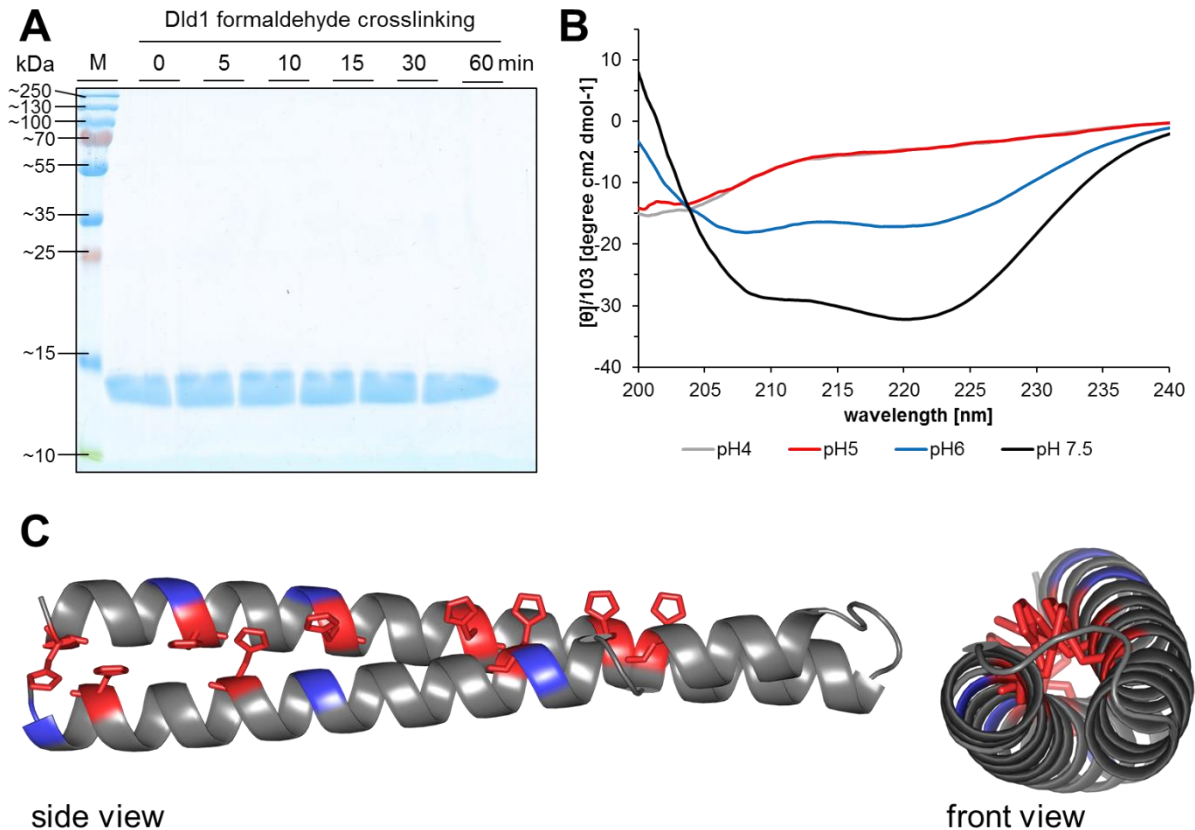


**Figure 10: Analysis of the oligomeric state and structure of Dld1. (A)** 4% formaldehyde was added to a 20 µM Dld1 solution and samples were taken after 0, 5, 10, 15, 30 and 60 min incubation at room temperature. Samples were analyzed via SDS-PAGE followed by Coomassie-based staining without heating the samples to 95°C. **(B)** A 10 µM Dld1 solution was analyzed by CD spectroscopy at pH 7.5, 6, 5 and 4. CD spectra measurements were provided by Dr. Jörg Martin. **(C)** Crystals were formed by sitting-drop vapor diffusion method with a 17 mg/mL Dld1 solution at pH 7.4. For experimental phasing and cryo-protection, single crystals were soaked with zinc acetate and 15% (v/v) PEG 400. The resolved crystal structure of Dld1 contained only the medial part of a single protein molecule. The conserved C-terminus was too flexible to give a definite x-ray image. The structure consisted of two antiparallel helices, separated by a short linker. Conserved histidines (marked in red) protrude from the face of both helices interdigitating like teeth of a zipper. Alanines (marked in blue) occupy most of the helix inward positions. Crystal structure provided from group of Prof. Andrei Lupas.

After crosslinking initiation, samples were taken after 0, 5, 10, 15, 30 and 60 min and analyzed via SDS-PAGE followed by Coomassie-based staining, omitting heating the samples to 95°C to retain potential formaldehyde crosslinks. In all samples only a single band at approx. 15 kDa was visible, consistent with the molecular weight of monomeric Dld1. In contrast to the result obtained from calibrated gel filtration column run, these observations suggest that Dld1 does not form dimers or multimers in solution, but is only present as a monomer.

To further investigate Dld1's structure, in collaboration with the lab of Prof. Andrei Lupas (Max-Planck-Institute for Developmental Biology, Tübingen, Germany) the protein's secondary

structure was analyzed by CD spectroscopy at different pH values (**Figure 10** B). At pH 7.5, the CD spectra of Dld1 showed absorbance peak minima at 208 and 220 nm, characteristic for an alpha helical secondary structure folding. At pH 6, these peak minima were less pronounced, indicating that the structure is pH dependent. At pH 5 and 4, the absorbance peak minima were absent, indicating an unfolded secondary structure.

In collaboration with the group of Prof. Andrei Lupas, the three-dimensional structure of Dld1 was analyzed via protein x-ray crystallography (**Figure 10** C). In crystallization trials with purified recombinant Dld1, a well-diffracting crystals was obtained that yielded a data-set with a resolution of 2 Å. The dimensions of the body-centered tetragonal unit cell indicated a single protein molecule in the asymmetric unit with a solvent content of 50%; the structure could be solved experimentally based on a bound $Zn^{2+}$ ion. The medial part of the protein formed a coiled-coil of two antiparallel alpha helices connected by a short linker with a heptad periodicity (positions *a, b, c, d, e, f, g*). Position *a* was often occupied by alanines, whereas position *d* was occupied by histidines. The histidines of the core were organized in groups of two, with roughly coplanar imidazole rings. The orientation of and the distance between the imidazole pairs indicated that the two histidines were opposite tautomers, with a 3 Å hydrogen bond between a protonated Nδ of one and an unprotonated Nδ of the other histidine. Via their Nε groups, they coordinated solvent molecules or side chains of near-by surface residues. The particular geometry and interactions between the histidine pairs suggested that the assembly would be disrupted at a lower pH, consistent with results obtained from CD spectroscopy measurements. In addition to charge repulsion, further protonation of the imidazole rings would likely disrupt the hydrogen bonds between the histidine pairs.

In conclusion, the structural analyses of Dld1 indicate that the protein is most likely a monomer following the results of crosslinking and x-ray crystallography. Dld1's medial part consists of two antiparallel alpha helices at pH 7.5, which are structurally sensitive to acidic pH. The histidine side-chains all protrude from one side of the two helices and a subset forms a novel and interesting zipper structure.

### 2.2.3 Dld1 binds metal ions resulting in reduced α-helical folding

In the process of x-ray structure analysis, Dld1 crystals were soaked with a zinc acetate solution for experimental phasing and cryo-protection. This procedure increased crystal stability and data analysis with SHELXD (Sheldrick, 2008) identified a single strong $Zn^{2+}$-binding site. These results combined with the abundance of histidines, led to the hypothesis that Dld1 would be capable to bind metal ions. In a qualitative approach, Dld1 purified from *E. coli* was subjected to immobilized metal ion affinity chromatography (IMAC). IMACs were conducted at pH 7.5, pH 6 and pH 5 to observe potential impact of Dld1's secondary structure on metal ion binding. $Fe^{3+}$, $Fe^{2+}$, $Ni^{2+}$, $Cu^{2+}$ and $Zn^{2+}$ ions were immobilized on metal chelating

sepharose according to manufacturer's protocol. An unloaded matrix was used as negative control. After incubation with Dld1, the matrix was washed repeatedly to remove weakly or unbound protein and bound proteins were then eluted with buffer containing a high concentration of imidazole. Proteins from flow-through, wash and elution fractions were precipitated and analyzed by SDS-PAGE followed by Coomassie-based staining (**Figure 11**).
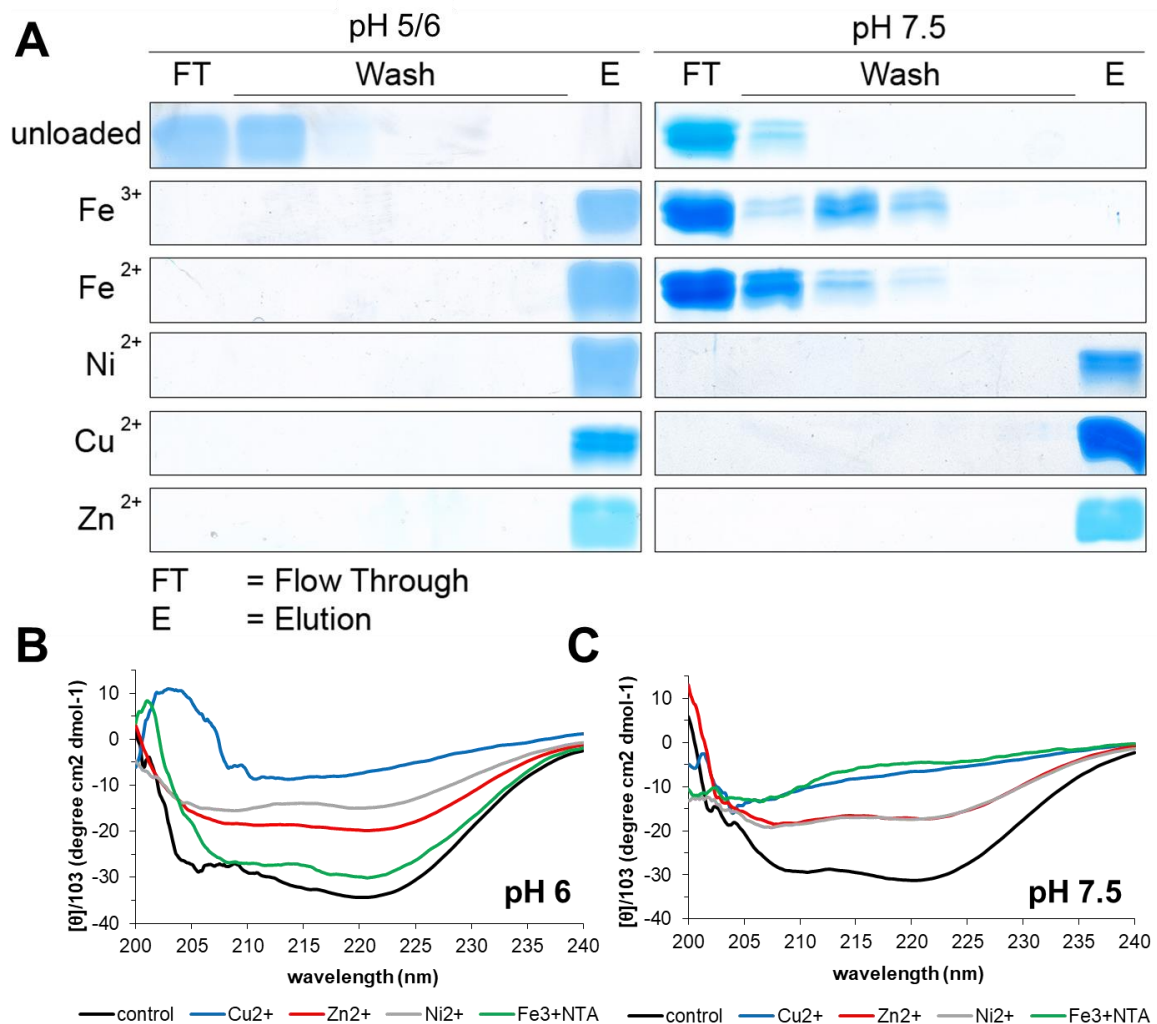


**Figure 11: Dld1 IMAC and CD spectroscopy measurements with metal ions.**
**(A)** SDS-PAGE with fractions from IMAC experiments. Metal chelating sepharose was either used unloaded or loaded with $Fe^{3+}$, $Fe^{2+}$, $Ni^{2+}$, $Cu^{2+}$ or $Zn^{2+}$. Purified Dld1 was incubated with prepared matrix at either pH 5, pH 6 or pH 7.5. Flow-through (FT) was collected and matrix was washed five times with respective assay buffer. Bound proteins were eluted by competition with imidazole in the elution buffer (E). Proteins in all fractions (flow-through, wash and elution) were precipitated, solved in SDS sample buffer and analyzed by SDS-PAGE followed by Coomassie-based staining. Results for IMACs conducted at pH 5 and pH 6 were virtually identical (only one representing picture is shown). **(B)** CD spectroscopy of Dld1 incubated with metal ions at pH 6. All metal ions reduced typical alpha-helical folding peak minima at 208 and 220 nm to different extend: From strong to weak $Cu^{2+}>Ni^{2+}>Zn^{2+}>Fe^{3+}$-NTA. **(C)** CD spectroscopy of Dld1 preincubated with metal ions at pH 7.5. Incubation with metal ions reduced typical alpha-helical folding peak minima at 208 and 220 nm to different extend as well: From strong to weak $Cu^{2+}=Fe^{3+}$-NTA$>Ni^{2+}=Zn^{2+}$. CD spectra provided by Dr. Jörg Martin.

Dld1 was present in flow-through, as well as in first and second wash fractions in IMACs with unloaded metal chelating sepharose, regardless of pH. This result clearly demonstrates that Dld1 has no affinity to unloaded metal chelating sepharose and binding observed in subsequent IMAC experiments could be attributed to the immobilized metal ion.

Results obtained from IMACs at pH 5 and pH 6 were virtually identical and are hence described together. Dld1 was exclusively present in elution fractions in all IMACs at pH 5/6, regardless of the metal immobilized on the sepharose. Similar results were observed at pH 7.5 for IMACs with $Ni^{2+}$, $Cu^{2+}$ and $Zn^{2+}$. In $Fe^{2+}$- and $Fe^{3+}$-IMACs at pH 7.5, Dld1 was present in flow-through up to the third wash fraction. In these IMACs, Dld1 was sometimes visible as a double band, instead of a single band, which might indicate degradation of proteolytic cleavage under these conditions. Together these results indicate that Dld1 was able to bind all of the tested metal ions at pH 5, pH 6, but had a reduced affinity to $Fe^{2+}$ and $Fe^{3+}$ at pH 7.5.

Since results of CD spectroscopy had shown that Dld1's alpha helical folding was sensitive to pH lower than 6 and the IMAC experiments had established an effect of pH on Dld1's metal binding capability, a direct effect of metal ion binding on Dld1's alpha helical structure was investigated via CD spectroscopy, in collaboration with the group of Prof. Lupas. *E. coli*-purified Dld1 was incubated with either $CuCl_2$, $ZnCl_2$, $NiCl_2$ or $Fe^{3+}$-nitrilotriacetic acid (NTA) at pH 6 and 7.5. $Fe^{3+}$-NTA was used rather than $Fe^{3+}$, to avoid precipitation of "free" $Fe^{3+}$ as ferric hydroxide at near neutral pH values. $Fe^{2+}$ was excluded from following experiments because of its high reactivity under aerobic conditions. CD spectra following metal incubation were recorded and analyzed (**Figure 11** B and C). Control samples without metal incubation showed peak absorbance minima at 208 and 220 nm, consistent with previous CD spectroscopy measurements. However, at both pH values, metal incubation reduced alpha helical folding to different extends. At pH 6, the strongest effect on alpha-helical folding was observed when Dld1 was incubated with $Cu^{2+}$, followed by $Ni^{2+}$, $Zn^{2+}$ and $Fe^{3+}$-NTA. At pH 7.5 however, the strongest effect was observed when Dld1 was incubated with $Cu^{2+}$ or $Fe^{3+}$-NTA, followed by $Ni^{2+}$ or $Zn^{2+}$, as both pairs of metals produced almost identical results.

In conclusion, the results of IMAC and CD spectroscopy after metal incubation demonstrate that Dld1 is capable of binding all tested metal ions at pH 6 and pH 7.5. However the affinity to $Fe^{3+}$ and $Fe^{2+}$ seems to be lower at pH 7.5. Moreover, the binding of metal ions affects the alpha helical folding and vice versa, indicating a direct link between protein structure and metal ion binding. Protein structure and pH seem to have the most drastic effect on $Fe^{3+}$ binding. To measure the affinity of Dld1 to the aforementioned metal ions, several quantitative methods were applied.

### 2.2.3.1 Dld1 binds $Fe^{3+}$ and $Zn^{2+}$ with low micro molar affinity

Since metal ions are highly reactive, determining affinity between proteins and metal ions is not trivial. In order to achieve reliable results, several methodical approaches were used for the quantification of Dld1 / metal ion binding, each with their respective advantages and drawbacks.

Isothermal titration calorimetry (ITC) facilitates determination of affinity, stoichiometry, enthalpy and entropy of a binding reaction between two binding partners, given that the experimental setup is optimal. ITC measurements with purified Dld1 titrated with $CuCl_2$, $ZnCl_2$, $FeCl_3$, $Fe^{3+}$-NTA and ferric citrate at pH 7.5 and 6 were performed. However, even after several attempts either only an insignificant difference in temperature was measured or resulting thermograms could not be fitted to any binding model (data not shown). Visual control of the ITC cell after $FeCl_3$ titration revealed that a precipitate had formed, most likely a result of ferric hydroxide formation. Therefore, the pH of ITC measurements with Dld1 titrated with $FeCl_3$ were lowered to 5, where $Fe^{3+}$ ions would remain soluble. The evaluation of resulting thermograms determined the dissociation constant ($K_D$) of Dld1 / $Fe^{3+}$ binding in the lower micromolar range (**Figure 12**).
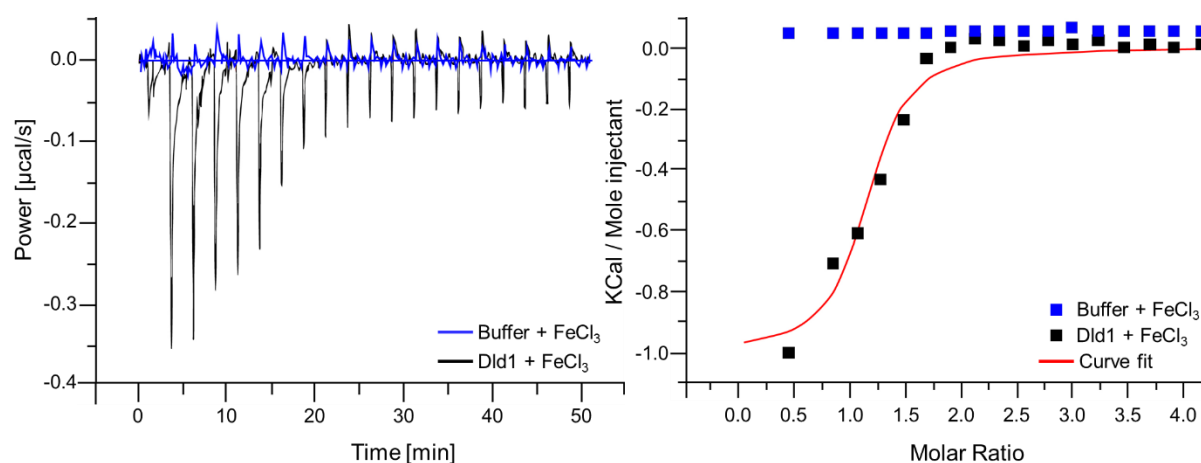


**Figure 12: Isothermal titration calorimetry of Dld1 titrated with $FeCl_3$.**
Purified Dld1 was dialyzed overnight and $FeCl_3$ was solved in buffer dialysate immediately prior to ITC start. ITC run was setup as follows: Total number of injections: 20; cell temperature: 25°C; reference power (µcal/s): 10; initial delay: 60 s; syringe ($FeCl_3$) concentration: 4 mM; cell (Dld1) concentration: 0.2 mM; stirring speed: 1000 rpm; injection volume: 2 µL (0.4 µL for first injection); duration of injection: 4 s (0.8 s for first injection); spacing: 150 s; filter period: 5 s. Power in µcal/s needed to maintain stable cell temperature was plotted against measurement time in min as raw thermograms. Immediately after titration of $FeCl_3$ to Dld1 (black traces), $FeCl_3$ from the same stock was titrated into buffer (blue traces). Both thermograms were evaluated by integration of the area below every spike via Origin-based MicroCal analysis software. Resulting data points (black and blue squares) were plotted as exhausted or consumed energy in KCal/mole of injectant over molar ratio of Dld1 to $FeCl_3$. Several mathematical binding models were applied for both runs. Whereas no mathematical model yielded conclusive results for $FeCl_3$ titration into buffer, the one-binding-site model could be fitted to data points from $FeCl_3$ titrated to Dld1 (red trace), resulting in stoichiometry N = 1.09 ± 0.0419, $K_D$ = 7040 nM ± 2750 nM, enthalpy $\Delta H$ = -998.5 ± 67 cal/mol and entropy of 20 cal/mol/deg ($\Delta S$ =20.2 cal/mol/deg).

Immediately after the measuring $FeCl_3$ titration to Dld1, the exact same $FeCl_3$ stock was titrated into the buffer as control measurement. Both thermograms were analyzed with MicroCal's Origin-based ITC data analysis software, where a binding model with a single set of binding sites resulted in the best fit. According to this model, Dld1 bound $Fe^{3+}$ in a molar ratio of nearly 1:1 (N = 1.09 ±0.0419) and with a $K_D$ of 7040 ± 2750 nM. The binding was an exothermal reaction with an enthalpy $\Delta H$ = -998.5 ± 67 cal/mol and an entropy $\Delta S$ = 20.2 cal/mol/deg.

In an additional approach, microscale thermophoresis (MST) analysis was used for the quantitative analysis of Dld1 / metal ion binding. MST is the defined as the directed movement

of molecules along a temperature gradient. Commercially available MST instruments utilize fluorescence to monitor molecule movement. Binding affinities are determined by analyzing the difference in thermophoresis between molecules with and without their potential binding partner. Since Dld1 exhibits weak intrinsic fluorescence due to its low abundance of tryptophan residues, the protein was purified with eGFP fused to the N-terminus (fusion protein GFP:Dld1), similarly as described in section 2.2.1. Purified eGFP (hereafter just referred to as GFP) was used as a negative control for binding. A fixed concentration of 100 nM of either GFP or GFP:Dld1 was mixed with a range of concentrations of $CuCl_2$, $ZnCl_2$ and ferric citrate from 15 nM up 250,000 nM at pH 7.5. Ferric citrate was used instead of $Fe^{3+}$ to avoid precipitation of $Fe^{3+}$ as ferric hydroxide as observed during ITC measurements. MST measurements at pH 6 were not feasible due to the significantly reduced GFP fluorescence, which resulted in inadequate signal quality (data not shown).

Thermophoresis at pH 7.5 was monitored by GFP fluorescence intensity prior, during and after heating of the capillaries with an infrared laser. To determine the $K_D$ of the binding, normalized fluorescence (in relative fluorescence units = RFU) during thermophoresis for each capillary was plotted against the concentration of metal ion (**Figure 13**). One of the major quality criteria for MST measurements is a significant difference in fluorescence between fluorescent molecule without binding partner and fluorescent molecule with the highest concentration of binding partner. The modulus of normalized fluorescence signal amplitude between both should exceed 10 RFU to achieve reliable results. An amplitude below 10 RFU indicates that MST of the fluorescent molecule was not affected by addition of the potential binding partner, indicating no binding between both molecules.
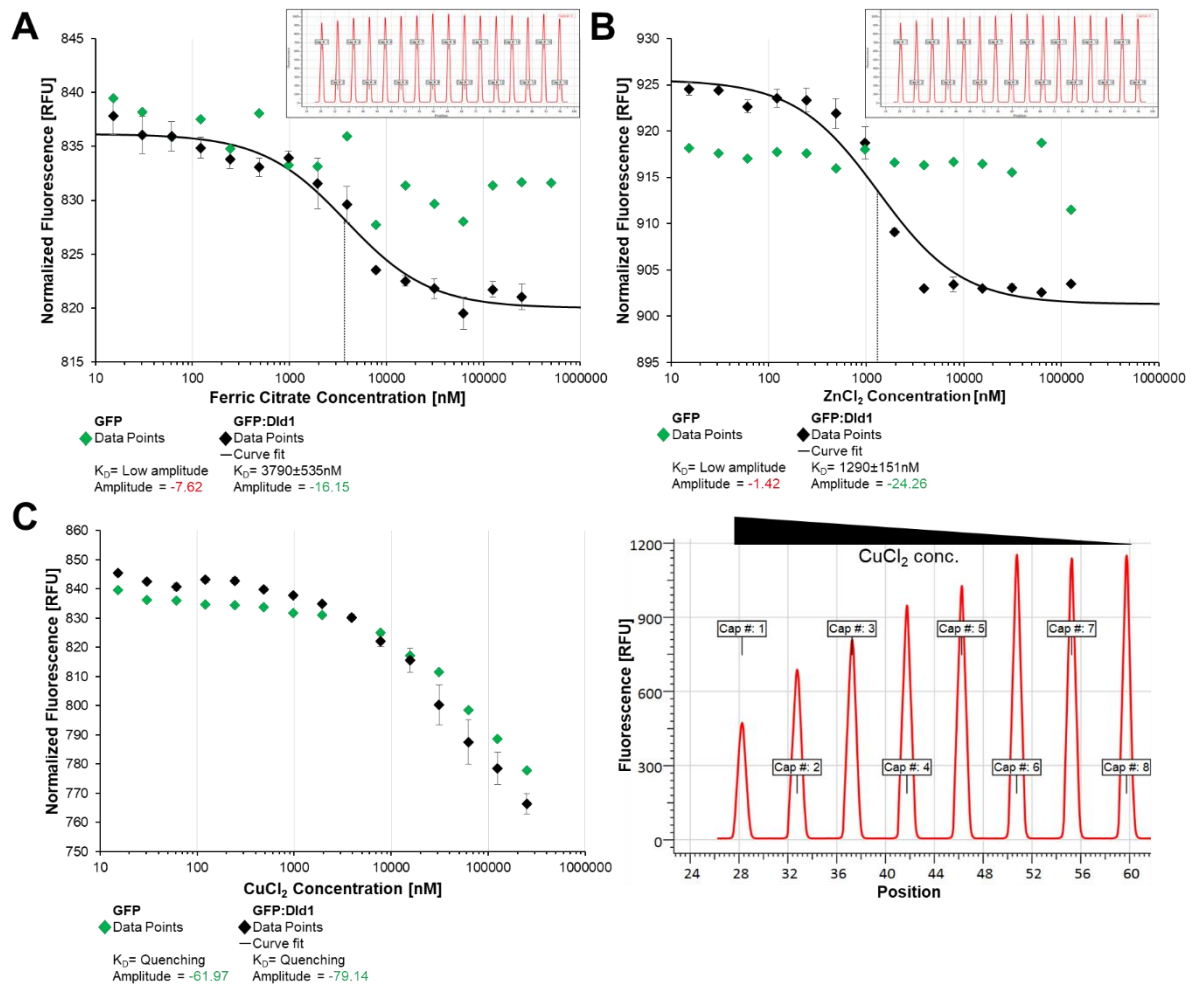
**Figure 13: MST measurements of GFP and GFP:Dld1.**
Either GFP or GFP:Dld1 were incubated with varying concentrations of either ferric citrate, $CuCl_2$ or $ZnCl_2$ from 15 nM up to 250,000 nM at pH 7.5 and room temperature. Protein metal mixture was transferred into small glass capillaries and thermophoresis of GFP or GFP:Dld1 was measured for each capillary by monitoring GFP fluorescence emission prior, during and after heating the capillary. Normalized fluorescence (in relative fluorescence units = RFU) for each of the capillaries was plotted against the respective metal concentration. Binding curves were fitted to the data points, if possible, and $K_D$S were determined by the turning point (vertical black line). **(A)** Results of MST measurements with GFP or GFP:Dld1 and ferric citrate. **(B)** Results of MST measurements with GFP or GFP:Dld1 and $ZnCl_2$. **(C)** Results of MST measurements with GFP or GFP:Dld1 and $CuCl_2$. Data for all GFP:Dld1 measurements was obtained from three independent measurement replicates. Error bars represent the standard error.

No significant difference in normalized fluorescence was observed when GFP was mixed with either ferric citrate or $ZnCl_2$, indicating no binding between GFP and ferric citrate or $ZnCl_2$ (**Figure 13** A+B, green data points).

In contrast, normalized fluorescence changed significantly when GFP:Dld1 was incubated with varying concentrations of ferric citrate. Fitting of a binding curve to the obtained data points determined the dissociation constant of the binding as $K_D$ = 3790 ± 535 nM (**Figure 13** A, black traces). Similarly, incubation of GFP:Dld1 with varying concentrations of $ZnCl_2$ lead to a significant change in normalized fluorescence. Fitting of a binding curve to the resulting data points resulted in a dissociation constant as $K_D$ = 1290 ± 151 nM (**Figure 13** B).

Incubation of GFP and GFP:Dld1 with high concentrations of $CuCl_2$ resulted in a significant decrease of GFP fluorescence (**Figure 13** C). However, this decrease was not only a result of altered thermophoresis, as fluorescence was already decreased before calefaction of the capillaries. This indicated that $CuCl_2$ interfered with GFP fluorescence, which resulted in quenching. As quenching superimposes with a potential change in thermophoresis, determination of the dissociation constant for GFP:Dld1 binding $CuCl_2$ was not possible with this particular MST setup.

Together these results show that Dld1 binds $Fe^{3+}$ and $Zn^{2+}$ ions with low micro molar dissociation constants. However, the dissociation constant for $Fe^{3+}$ binding can only be considered as an estimate, since ITC was conducted at an acidic pH, where Dld1 is mostly unstructured, and MST measurements were only possible at pH 7.5 due to the use of ferric citrate.

### 2.2.3.2 Mutation of conserved histidine residues affect $Fe^{3+}$ binding of Dld1

*In silico* analysis of Dld1's crystal structure with SHELXD identified a strong $Zn^{2+}$ binding site with contribution of histidine residue 107. Moreover the highly conserved histidine 103 was a likely candidate for metal ion binding. The conserved C-terminal RSIDELD motif, with charged amino acids such as arginine, aspartic acid and glutamic acid, can also be considered as a viable source of Dld1's metal binding capability. To verify a contribution of specific amino acids or the RSIDELD motif in metal binding, three mutant derivatives of Dld1 were purified from *E. coli* as described in section 2.2.1.

Primarily, a single amino acid exchange at position 107 from histidine to alanine was introduced by mutation of the corresponding codon resulting in Dld1$^{H107A}$. Subsequently, the histidine at position 103 was exchanged for alanine as well, resulting in a double histidine mutant Dld1$^{H103A,H107A}$. Independently, the C-terminal conserved RSIDELD motif was deleted by substitution of the corresponding codons with a stop codon. The resulting protein is hereafter named Dld1$^{\Delta RSIDELD}$.

All three mutants were tested for qualitative metal ion binding in the same IMAC setups as described in section 2.2.3 (data not shown), but no significant difference was observed, indicating that all proteins were still able to bind metal ions. However, since IMAC experiments are of a purely qualitative nature, MST measurements with all three mutant derivatives were conducted to investigate if any of the mutations had a quanititavie effect on metal ion binding. All proteins were purified as eGFP fusions (hereafter named GFP:Dld1$^{H107A}$, GFP:Dld1$^{H103A,H107A}$ and GFP:Dld1$^{\Delta RSIDELD}$, respectively) as described in section 2.2.1 and incubated with ferric citrate or $ZnCl_2$ concentration from 15 nM up to 250,000 nM at pH 7.5 as described in section 2.2.3.1. $CuCl_2$ was excluded as previous experiments had shown a

quenching effect. The results were compared with $K_D$s previously obtained for GFP and GFP:Dld1. (**Figure 14**).
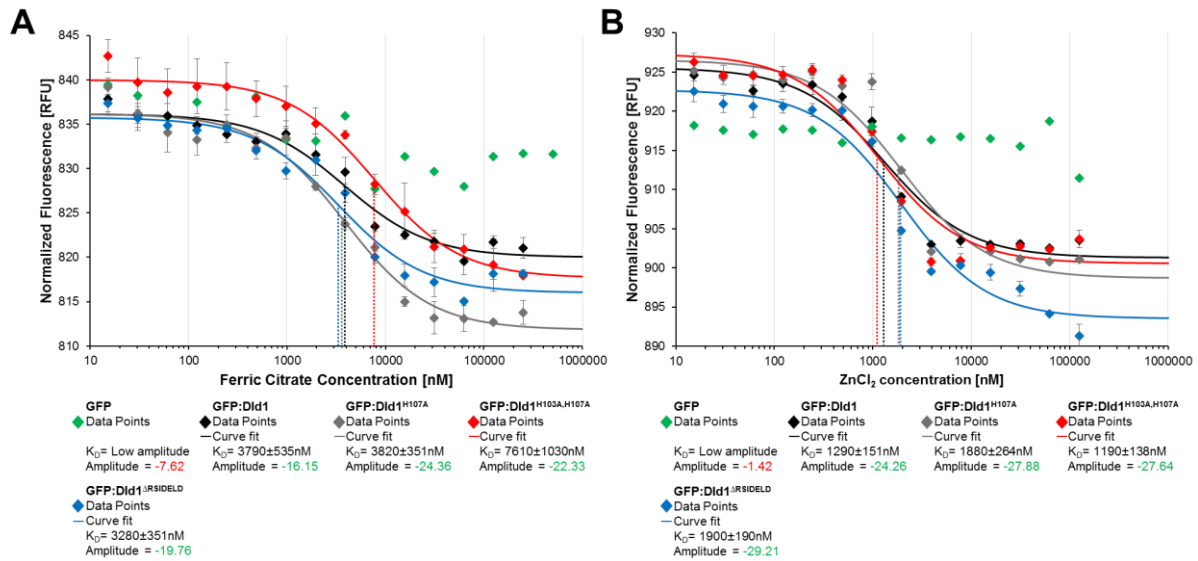


**Figure 14: MST measurements of GFP:Dld1 mutant derivatives.**
Either GFP:Dld1$^{H107A}$, GFP:Dld1$^{H103A,H107A}$ or GFP:Dld1$^{\Delta RSIDELD}$ were mixed with varying concentrations of either ferric citrate or $ZnCl_2$ from 15 nM up to 250,000 nM at pH 7.5. GFP fluorescence intensity was monitored prior, during and after heating the capillary. Normalized fluorescence (in relative fluorescence units = RFU) was plotted against the respective metal concentration. Binding curves were fitted to the individual data points and $K_D$s were determined by turning points (vertical lines). **(A)** Results of MST measurements with GFP or GFP:Dld1 derivatives and ferric citrate. **(B)** Results of MST measurements with GFP or GFP:Dld1 and $ZnCl_2$. Presented data was obtained from three independent measurement replicates. Error bars represent the standard error.

$K_D$s for binding of GFP:Dld1$^{H107A}$ and GFP:Dld1$^{\Delta RSIDELD}$ to ferric citrate were determined as 3820±351 nM and 3280±351 nM, respectively. Both did not deviate significantly from the $K_D$ for binding of GFP:Dld1 to ferric citrate ($K_D$ = 3790±535 nM). However, the $K_D$ for binding of GFP:Dld1$^{H103A,H107A}$ to ferric citrate was recorded as 7610±1030 nM and was significantly higher as compared to GFP:Dld1, indicating a weaker binding.

$K_D$ for binding of GFP:Dld1$^{H103A,H107A}$ to $ZnCl_2$ was determined as 1190±138 nM and did not deviate significantly from the $K_D$ for binding of GFP:Dld1 to $ZnCl_2$ (1290±151 nM). Surprisingly, $K_D$s for binding of GFP:Dld1$^{H107A}$ and GFP:Dld1$^{\Delta RSIDELD}$ to $ZnCl_2$ were determined as 1880±264 nM and 1900±190 nM, respectively. Both values are slightly higher than the $K_D$ for binding of GFP:Dld1 to $ZnCl_2$, indicating a weaker binding.

Together these results suggest that at least histidine 103 partakes in the coordination of $Fe^{3+}$, as its mutation to alanine doubled the respective dissociation constant, while the single mutation of histidine 107 to alanine and the deletion of the RSIDELD motif had no significant effect. Surprisingly, the double mutation of the histidines did not alter the $K_D$ for $ZnCl_2$, while the single mutation of histidine 107 to alanine and deletion of the C-terminal RSIDELD slightly decreased the $K_D$.

### 2.2.3.3 Dld1 inhibits $Fe^{3+}$-dependent Prussian Blue reaction *in vitro*

In 2007, Liu *et al.* provided evidence that "free" reactive $Fe^{3+}$ accumulates at sites of fungal penetration in many monocot plant species under attack by *B. graminis*, including barley. The authors further established a direct link between $Fe^{3+}$ accumulation and the formation of CWAs, the oxidative burst and the expression of pathogenesis-related genes. Transcriptional and microscopic analyses have revealed that barley responds similarly to *P. indica* colonization (Zuccaro *et al.*, 2011). Liu *et al.* used $Fe^{3+}$-specific Prussian Blue (PB) staining to unveil accumulation of reactive $Fe^{3+}$ in CWAs. PB staining of *P. indica*-colonized barley roots demonstrated a similar accumulation of reactive $Fe^{3+}$ in CWAs (**Figure 2**). Moreover, CWAs that successfully repelled *P. indica* seemed larger in diameter and exhibited a stronger PB straining intensity. On the other hand, CWAs that failed to stop *P. indica* were comparably smaller and exhibited a weaker PB staining (Dr. Magdalena Hilbert, unpublished data). Since Dld1 localizes at CWAs in barley and is able to bind $Fe^{3+}$ *in vitro*, the protein seemed a likely candidate for reduced PB staining in failed CWAs.

To investigate if Dld1 might be responsible for reduced PB staining intensity in failed CWAs, an *in vitro* PB assay was performed by incubating purified Dld1 with $FeCl_3$ to mimic a potential sequestering situation. DFO, a bacterial high-affinity $Fe^{3+}$ siderophore was used as positive control and comparison for $Fe^{3+}$ sequestration resulting in PB staining inhibition. PB staining was measured as a percental increase of absorbance at 680 nm ($A_{680nm}$) after addition of PB staining solution. It has to be noted that the PB staining solution itself absorbs at 680 nm and therefore some increase is expected after its addition, even without a staining reaction. The results of the *in vitro* PB staining are shown in **Figure 15**).
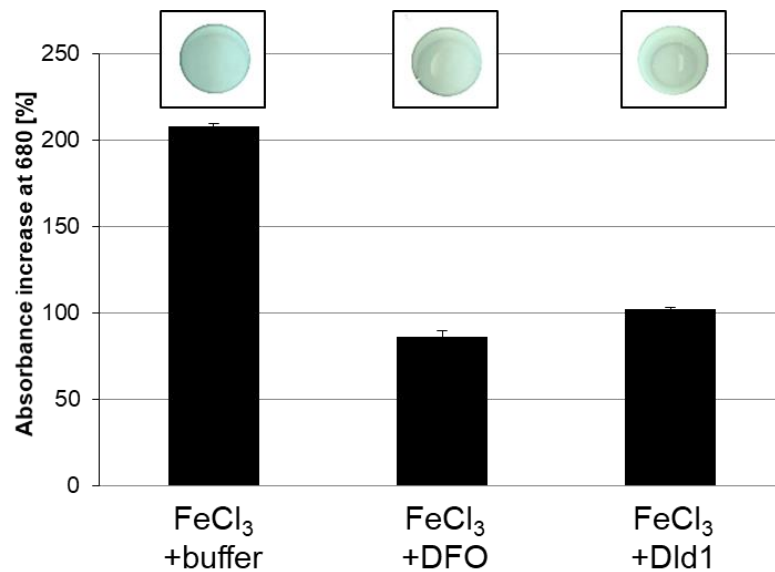
**Figure 15: *In vitro* PB staining assay.**
In a 96-well plate 20 µM $FeCl_3$ were either mixed with buffer (pH 5), 30 µM DFO or 30 µM purified Dld1, respectively, in a total volume of 100 µL. The mixtures were incubated at room temperature for 30 min and the $A_{680nm}$ was measured. 100 µL of PB staining solution was added, the plate was scanned and the increase of $A_{680nm}$ was measured again. The y-axis shows the percental increase of $A_{680nm}$ after addition of PB staining solution. All measurements were performed in technical triplicates. Error bars represent the standard error.

After addition of PB staining solution to $FeCl_3$ with buffer, $A_{680nm}$ increased by more than 200% and respective wells turned a bright blue color indicative of a staining reaction. In contrast, the addition of PB staining solution to $FeCl_3$ incubated with 30 µM DFO increased $A_{680nm}$ by approx. 90% and respective wells turned to a weak blue color, comparable to the PB staining solution itself. Similar effects were observed when $FeCl_3$ was preincubated with 30 µM Dld1, where $A_{680nm}$ increased by approx. 100%. These *in vitro* results indicate that Dld1 is able to bind reactive $Fe^{3+}$ and inhibit PB staining to a similar extend as the bacterial $Fe^{3+}$ high-affinity siderophore DFO. In consequence, Dld1 is a likely candidate for the reduced PB staining intensity in failed CWAs during *P. indica* / barley interaction.

## 2.2.4 Dld1 binds to plant specific cell wall polysaccharides

Localization analysis *in planta* established that Dld1 associates with the plant cell wall and barley CWAs, formed in response to *B. graminis* attack. However, the mechanism through which this localization is mediated remains unclear. To establish whether Dld1 binds to plant cell wall polysaccharides *in vitro*, co-precipitation of *E.* coli-äpurified Dld1 and commercially available plant cell wall polysaccharides xylan and cellulose was tested. As negative control, fungal cell wall polysaccharide chitin was also included. Dld1 was incubated with all three polysaccharides and subsequently pelleted by centrifugation. Unbound proteins from the supernatant were precipitated and solved in SDS sample buffer, whereas the polysaccharide pellet was cooked with SDS sample buffer to denature and release bound proteins. Both supernatant and pellet proteins were analyzed by SDS-PAGE (**Figure 16** A).
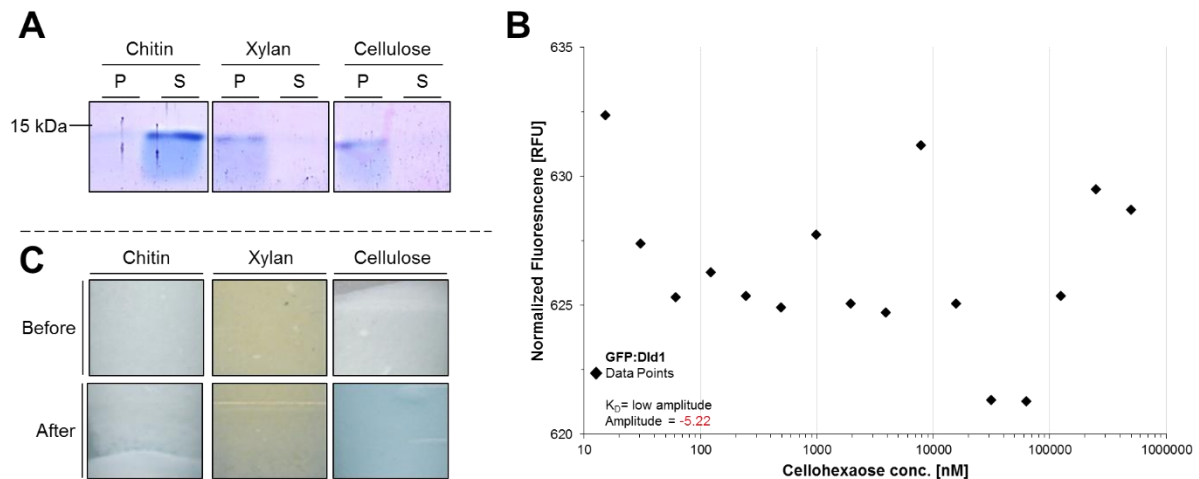
**Figure 16: Dld1 binding to plant cell wall polysaccharides is mediated by their $Fe^{3+}$ content.**
**(A)** Cell wall polysaccharide binding assay. Purified Dld1 was incubated with fungal cell wall polysaccharide chitin or plant cell wall polysaccharides xylan and cellulose. Afterwards, cell wall polysaccharides were pelleted by centrifugation and proteins from the supernatant were precipitated and resolved in SDS sample buffer. Pellet proteins were extracted in SDS sample buffer. Pellet (P) and supernatant (S) proteins were analyzed by SDS-PAGE followed by Coomassie-based staining. **(B)** MST of GFP:Dld1 and cellohexaose. 100 nM GFP:Dld1 was incubated with varying concentrations of cellohexaose from 15 nM up to 250,000 nM at pH 7.5. The mixture was transferred into small glass capillaries and thermophoresis was measured for each capillary by monitoring GFP fluorescence intensity prior, during and after heating. Normalized fluorescence (in relative fluorescence units = RFU) was plotted against the respective cellohexaose concentration. GFP:Dld1 thermophoresis was not significantly altered by cellohexaose incubation (amplitude <10). **(C)** PB staining of commercially available cell wall polysaccharides. Cell wall polysaccharides were prepared the same way as for (A), but were instead mixed with 1 mL of PB staining solution. A picture was taken before and after staining. Whereas chitin and xylan did not change color, cellulose powder, which appeared white before, turned blue, indicating that commercially available cellulose contains reactive $Fe^{3+}$.

For the fungal cell wall polysaccharide chitin, Dld1 was primarily found in the supernatant fraction with only a very faint band visible from the polysaccharide pellet. For the plant cell wall polysaccharides xylan and cellulose, Dld1 was exclusively present in the pellet fractions, whereas only very faint bands were visible for the supernatant. These results suggest, that Dld1 indeed co-precipitates with plant cell wall polysaccharides xylan and cellulose, but not with fungal cell wall polysaccharide chitin.

To quantify cellulose binding, the affinity of GFP:Dld1 to cellohexaose, a synthetic hexamer of six β-1, 4 linked β-D-glucose monomers, was analyzed by MST (**Figure 16** B). Even high concentrations of 250 µM of cellohexaose incubated with 100 nM GFP:Dld1 did not alter thermophoresis, strongly suggesting that GFP:Dld1 did not bind to cellulose diretly, indicating that the binding might be mediated by an unknown third party.

Previous studies have shown that plants utilize cell walls for storage of metal ions (Maier & Cattani, 1965). In consequence, the binding of Dld1 to cellulose and xylan, as observed in the cell wall polysaccharide binding assay, might result from $Fe^{3+}$ or other metals still present in these commercially available polysaccharide preparations. Therefore chitin, xylan and cellulose were prepared as for the cell wall polysaccharide binding assay and stained with PB solution (**Figure 16** C). Pictures before and after staining showed that chitin and xylan did not exhibit any PB staining, indicating that both polysaccharides did not contain reactive $Fe^{3+}$. In

contrast, cellulose exhibited strong PB staining, indicating that this commercially available polysaccharide contains reactive $Fe^{3+}$.

In conclusion, these results suggest that Dld1 does not directly bind cellulose, but the binding is rather mediated by cellulose's $Fe^{3+}$ content instead. How the Dld1's affinity to xylan is mediated remains unclear.

## 2.2.5 Dld1 does not directly interact with horseradish peroxidase

Some effector proteins have been shown to interfere with the plants ability to produce ROS to modulate plant immunity (Hemetsberger *et al.*, 2012; Priller *et al.*, 2016). One way to interfere with ROS generation is to inhibit plant peroxidases, which rely on iron in form of heme as a cofactor (Conesa & Gotz, 2008). Dld1's metal binding capability led to the speculation that the protein might sequester iron from heme to inhibit peroxidases activity. To test this hypothesis, a physical interaction between Dld1 and commercially available horseradish peroxidase (HRP) was investigated. To this end, GST:Dld1 was immobilized on glutathione sepharose and incubated with HRP to allow potential protein-protein-interaction. The assay was conducted at both pH 6 and pH 7.5 to analyze a potential pH effect on the interaction and purified GST was used as negative control. Proteins in flow-through, wash and elution fractions of the binding assay were precipitated and analyzed by SDS-PAGE followed by Coomassie-based staining (**Figure 17**).
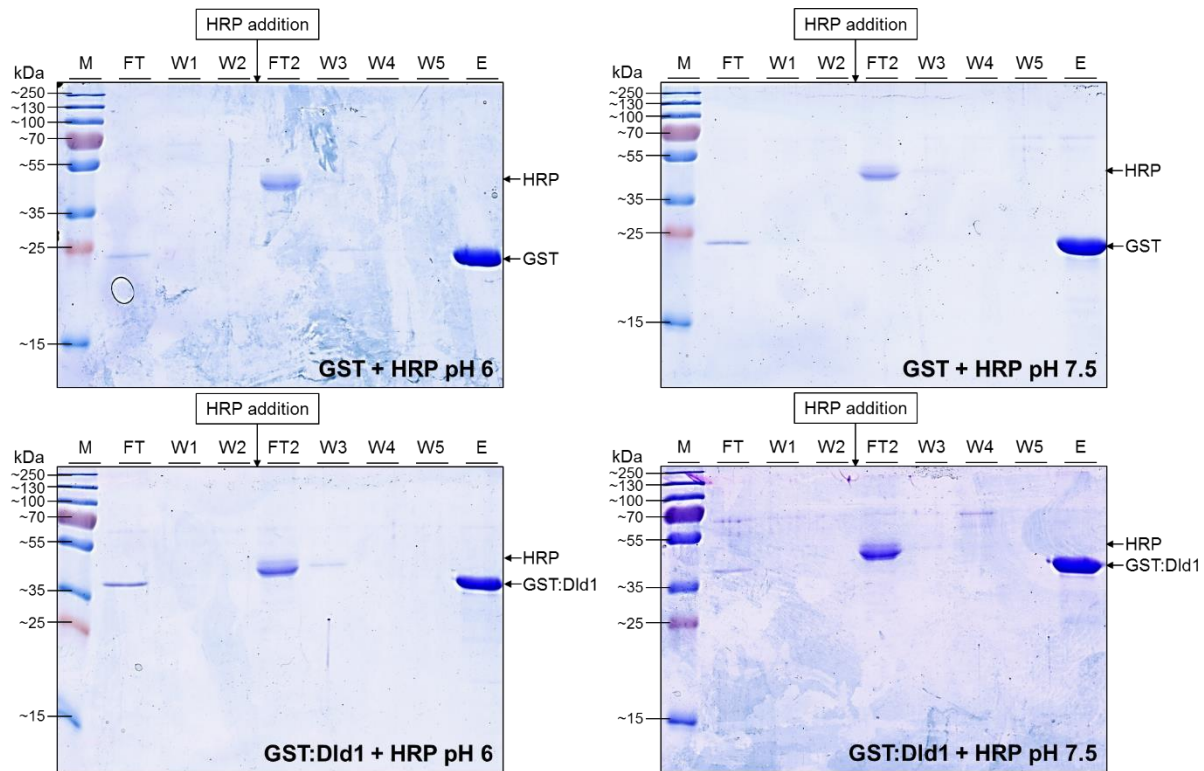
**Figure 17: GST:Dld1/HRP binding assay.**
Purified GST or GST:Dld1 was immobilized on a glutathione sepharose column. Surplus protein was removed by washing the column twice with binding buffer. Initial flow-through (FT) and washing steps (W1 and W2) were collected, precipitated and analyzed by SDS-PAGE followed by Coomassie-based staining. HRP was incubated with loaded sepharose matrix to allow potential protein-protein-interaction. Afterwards the unbound protein was removed by washing the column thrice. Flow-through after HRP addition (FT2) and the three washing steps (W3, W4 and W5) were collected, precipitated and analyzed by SDS-PAGE as well. Proteins bound to the sepharose matrix were eluted by addition of glutathione elution buffer and respective fraction (E) was collected, precipitated and analyzed by SDS-PAGE followed by Coomassie-based staining. $M_W$(GST:Dld1)=38 kDa; $M_W$(GST)=26 kDa; $M_W$(HRP)=44 kDa.

Flow-through fractions after incubation of either GST or GST:Dld1 with glutathione sepharose contained single bands at either approx. 25 or 35 kDA, consistent with the molecular weight of GST or GST:Dld1, respectively, indicating that the column matrix had been loaded over the maximum capacity. After two additional washing steps to remove surplus protein, loaded glutathione sepharose was incubated with HRP. Flow-through after HRP addition contained one single band at approx. 40 kDa, consistent with the molecular weight of HRP, regardless of pH or if GST or GST:Dld1 was immobilized. After three further washing steps, of which the first contained one faint band at approx. 40 kDa, immobilized GST or GST:Dld1 was eluted. Elution fractions only contained bands at either 25 or 35 kDa, consistent with the molecular weight of either GST or GST:Dld1, respectively. No bands corresponding to the molecular weight of HRP were visible in elution fractions. These results suggest that GST:Dld1 does not physically interact with HRP.

Even though no direct physical interaction between Dld1 and HRP was established, a potential influence of Dld1 on HRP activity was investigated. To this end, effects of Dld1 on HRP's catalysis of the oxidation of chemical substrate DAB by $H_2O_2$ was examined. DAB is oxidized in the presence of ROS such as $H_2O_2$ in a two-step process and forms a complex dark brown

precipitate. The reaction is amplified significantly by a catalyst such as HRP, which facilitates electron transfer between $H_2O_2$ and DAB. To examine a potential influence of Dld1 on HRP-catalyzed DAB oxidation, all three components were mixed in different combinations and incubated. Afterwards, $H_2O_2$ was added to all wells. The plate was scanned prior and 10 min after addition of $H_2O_2$ (**Figure 18**).
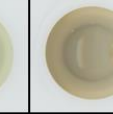
| HRP | - | + | - | + |
|---|---|---|---|---|
| Dld1 | - | - | + | + |
| before add. of $H_2O_2$ | | | | |
| after add. of $H_2O_2$ | | | | |

**Figure 18: HRP catalyzed DAB oxidation assay.**
DAB, HRP and Dld1 were mixed in assay buffer (pH 6) and incubated at room temperature for 10 min. Afterwards, $H_2O_2$ was added and plate was scanned before and 10 min after the addition.

After 10 min, wells without HRP did not show any brown coloring, indicating that no or only an insignificant amount of DAB had oxidized and that Dld1 does not catalyze the oxidation of DAB. Wells with HRP exhibited a strong brown coloring with small, dark brown precipitates, indicating that DAB had oxidized. Addition of Dld1 had no effect on DAB oxidation catalyzed by HRP. However, fewer dark brown precipitates were observed in wells, where Dld1 and HRP were present in comparison to wells with HRP alone. Thus, Dld1 might interfere with DAB radical polymerization.

## 2.2.6 Dld1 interferes with radical polymerization of chemical substrate DAB

The co-localization of Dld1, reactive $Fe^{3+}$ and ROS in CWAs, coupled with Dld1's ability to bind $Fe^{3+}$, led to the speculation that Dld1 might interfere with $Fe^{3+}$-catalyzed oxidation reactions. Similar to HRP, $Fe^{3+}$ is able to act as catalyst in the oxidation of DAB by $H_2O_2$. To test a potential influence of Dld1 on this reaction, all reactants were incubated at room temperature for 10 min. Subsequently, DAB was injected to initiate the reaction. As previous experiments with Dld1 and HRP have shown that Dld1 might interfere with DAB polymerization, the reaction was monitored spectrophotometrically for 5 hours and the plates were scanned afterwards (**Figure 19** A).
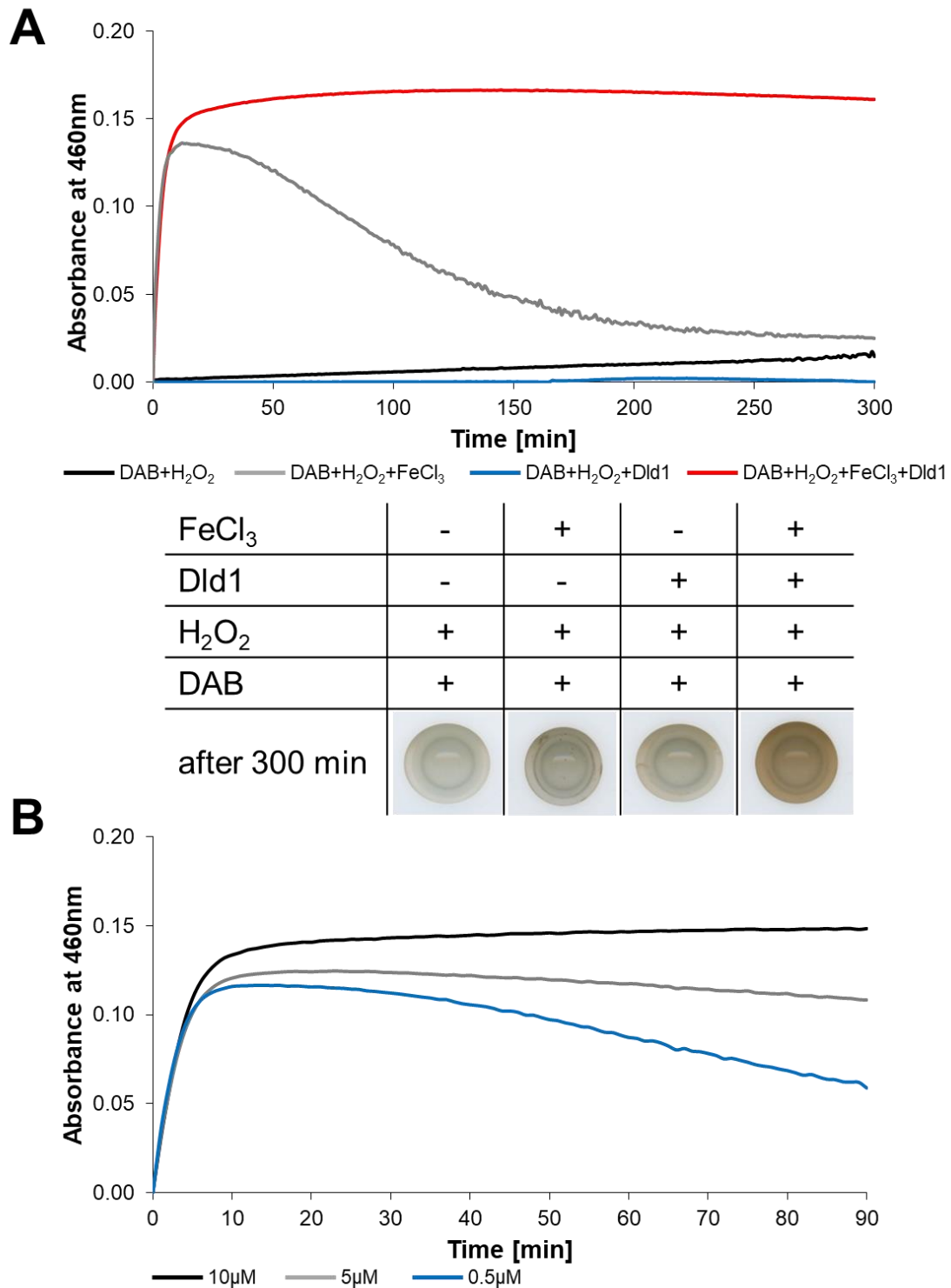
**Figure 19: DAB oxidation assay catalyzed by FeCl₃.**
**(A)** DAB, FeCl$_3$ and Dld1 were mixed in assay buffer (pH 5) and incubated at room temperature for 10 min. After addition of 10 mM $H_2O_2$, $A_{460nm}$ (y-axis) was monitored for 300 min and the wells were scanned. **(B)** The inhibitory effect of Dld1 on DAB polymerization was concentration dependent, as shown by the decrease of $A_{460nm}$ in reactions with lower Dld1 concentration.

Wells only containing DAB or DAB and Dld1, showed only a minor $A_{460nm}$ increase and remained clear and colorless even 5 hours after $H_2O_2$ addition, indicating only minor DAB oxidation. In wells with DAB and FeCl$_3$, $A_{460nm}$ drastically increased within the first 10 min of measurement and gradually decreased until it reached a baseline value at approx. 200 min.

After 300 min respective wells were clear and colorless, but contained dark-brown precipitates. These results indicate, that DAB was completely oxidized within the first 10 min of the experiment, followed by DAB polymerization and precipitation. Where $FeCl_3$ and Dld1 had been added to DAB, a drastic increase of $A_{460nm}$ was observed as well. However, instead of a decline, the absorbance value remained stable at 0.15 until the end of the measurement. Five hours after $H_2O_2$ addition, respective wells exhibited a uniform brown coloring, indicating that that DAB had oxidized but no polymerization and precipitation had taken place.

Together, these results show that Dld1 is unable to prevent the $Fe^{3+}$-catalyzed oxidation of DAB, but interferes with the subsequent DAB polymerization and precipitation, consistent with observations from previous HRP-catalyzed DAB oxidation experiments. To test whether this stabilizing effect on oxidized DAB could be really attributed to Dld1, the experiment was repeated with decreasing concentrations of Dld1, showing a clear concentration dependency (**Figure 19** B).

# 3. Discussion

## 3.1 Dld1 localizes at CWAs during barley colonization

*In silico* analysis of Dld1 proposed the existence of an N-terminal signal peptide. To verify secretion *in vitro*, transgenic *P. indica* strains were generated, which produced a Dld1:eGFP fusion protein. However, due to proteolytic cleavage near the C-terminus of Dld1, eGFP was the main product detected in the protein extracted from the mycelium via an anti-GFP-immunoblot. No signal consistent with Dld1:eGFP was detected in the culture supernatant. Thus, it remains unclear if Dld1 is either not secreted in this setup or the expression is too weak for immunoblot analysis. The generation of a custom antibody against *E.* coli-purified Dld1, as well an attempt to identify Dld1 as part of the *P. indica* secretome via peptide mass fingerprinting, did not confirm the secretion of Dld1 by *P. indica*. Combined, the results lead to two hypotheses: (i) Dld1 is an intracellular protein and was therefore not detectable in the culture supernatant or (ii) Dld1 has a different three-dimensional structure and/or undergoes posttranslational modification and is therefore not accessible to antibodies against Dld1 purified from *E. coli*. Posttranslational modification could prevent detection of Dld1 peptides during mass fingerprinting analysis, as respective masses would not be correctly aligned with *in silico* predictions. To increase peptide mass accuracy, samples were deglycosylated prior to mass spectrometry analysis, which did increase the number of identified proteins. However, Dld1 was not detected in these samples. Consequently, there might be other posttranslational modifications than glycosylation, which altered Dld1 peptide masses enough to prevent identification. Additionally, Dld1 is a relatively small protein, resulting in only a limited number of peptide after tryptic cleavage, which further decreases the chance of peptide mass identification.

In order to overcome the problems encountered by the expression in *P. indica*, Dld1 signal peptide validity was investigated in the maize pathogenic fungus *U. maydis,* which shares the division of Basidiomycota with *P. indica*. Both *in vitro* immunoblot-based analysis and *in planta* microscopy confirmed that *U. maydis* can utilize the Dld1 signal peptide for effective protein secretion. Signal peptide recognition, cleavage and mature protein secretion are highly conserved biological processes and signal peptides can even be functionally exchanged between pro- and eukaryotic organisms (Fraser & Bruce, 1978; Hall *et al.*, 1990; Izard & Kendall, 1994). Since the Dld1 secretion signal facilitated secretion in *U. maydis*, the aforementioned hypothesis (ii) is more likely.

In addition to signal peptide validity, further analysis of mCherry:Dld1woSP localization during *U. maydis* / maize infection indicated that the protein might associate with the plant cell wall. This was confirmed by microscopy of transiently transformed barley leaves producing Dld1$^{\Delta RSIDELD}$:mCherry:RSIDELD, which was not only secreted by transformed barley cells,

further substantiating the validity of the Dld1 signal peptide, but a subset of the secreted protein associated with the plant cell wall even after induction of plasmolysis. Since the expression of *DLD1* coincides with the formation of CWAs during *P. indica* / barley interaction (Zuccaro *et al.*, 2011), transiently transformed barley cells were challenged with *B. graminis* to induce the formation of CWAs. Consequently, Dld1$^{\Delta RSIDELD}$:mCherry:RSIDELD co-localized with CWAs, indicating that the protein was recruited to the penetration sites where it could not diffuse away.

*In vitro* experiments with purified Dld1 from *E. coli* showed that the protein bound several transition metals, including $Fe^{3+}$. Furthermore, Dld1 co-precipitated with plant cell wall polysaccharides cellulose and xylan *in vitro*, but showed no affinity to soluble cellohexaose. PB staining of cellulose used in co-precipitation experiments showed the presence of $Fe^{3+}$, while no $Fe^{3+}$ can be expected in the chemically synthesized cellohexaose. These observations argue that Dld1 co-precipitated with cellulose as a result of its $Fe^{3+}$ content rather than by direct affinity to cellulose.

For decades the plant apoplast, roots and cell walls have been recognized to accumulate significant amounts of iron (Maier & Cattani, 1965; Longnecker & Welch, 1990). Previous studies have also shown that in monocot plant species a pathogen attack triggers an actin-dependent, vesicle-based intracellular iron efflux towards CWAs, where $Fe^{3+}$ is deposited in a redox active form and mediates ROS production (Greenshields *et al.*, 2007; Liu *et al.*, 2007). An accumulation of iron in barley root epidermal and cortex cell walls, as well as in CWAs formed in response to *P. indica* colonization has been observed as well (Dr. Magdalena Hilbert, unpublished data, **Figure 2**). In contrast to barley, no iron accumulation has been observed in CWAs of Arabidopsis, where the production of $H_2O_2$ has been primarily associated with two respiratory burst oxidase homologues (Torres *et al.*, 2002; Greenshields *et al.*, 2007). Interestingly, microarray data show that the expression of *DLD1* is not upregulated during *P. indica* colonization of Arabidopsis, indicating that Dld1 is not needed during *P. indica* / Arabidopsis interaction (Zuccaro *et al.*, 2011). These studies in combination with Dld1 *in planta* localization, *in vitro* metal-binding and co-precipitation experiments, lead to the hypothesis that secreted Dld1 localizes at barley cell walls as a result of their iron content. Moreover, Dld1 shows a focal accumulation at CWAs in response to the deposition of redox-active $Fe^{3+}$. Since this $Fe^{3+}$ mediates ROS production, one can speculate that Dld1 might interfere with downstream processes or ROS production itself.

## 3.2 Dld1 is a structural relative to SmbP from *Nitrosomonas europaea*

Crystallization of Dld1 purified from *E. coli* revealed that the medial part of the protein forms a coiled-coil of two antiparallel alpha helices connected by a short linker. The core of the structure shows a sequence of 11 heptad repeats with *a, b, c, d, e, f* and *g* positions. The majority (8 out of 11) of *a* positions are occupied by alanines. Such positioning of the alanines allow a very tight coiled coil assembly and has been previously described as alacoils (Gernert *et al.*, 1995). Alacoils occur between helices in multi-helical bundles in large proteins as ferritin, but the structure of Dld1 shows that alacoils can also form in small monomeric proteins.

The majority (9 out of 11) of *d* positions are occupied by histidines. Respective side-chains protrude from the face of the two helices and interdigitate like teeth of a zipper. The configuration closely resembles the original model proposed for the leucine zipper, although analysis of the respective crystal structures revealed that the leucine side-chains were arranged side-by-side, like rungs of a ladder (Landschulz *et al.*, 1988). The structure of Dld1 shows that the original zipper structure is possible, albeit with histidines instead of leucines.

A search for structural homologues to Dld1 in the RCSB Protein Data Bank identified Small metal binding Protein (SmbP) from the ammonia-oxidizing bacteria *N. europaea*, entered into the database by Allen & Francisco in 2011 (no publication available). Both proteins are similar in length (Dld1: 133 amino acids; SmbP: 117 amino acids), molecular weight ($M_W$ [Dld1] = 14.7 kDa; $M_W$ [SmbP] = 12.4 kDa) and exhibit a high percentage of alanines (Dld1: 18.8%; SmbP: 16.2%) and histidines (Dld1: 10.5%; SmbP: 13.7%). Furthermore, SmbP exhibits similar heptad periodicity as Dld1, with a total of 10 repeats in which all *d* positions are occupied by histidines (**Figure 20 A**).
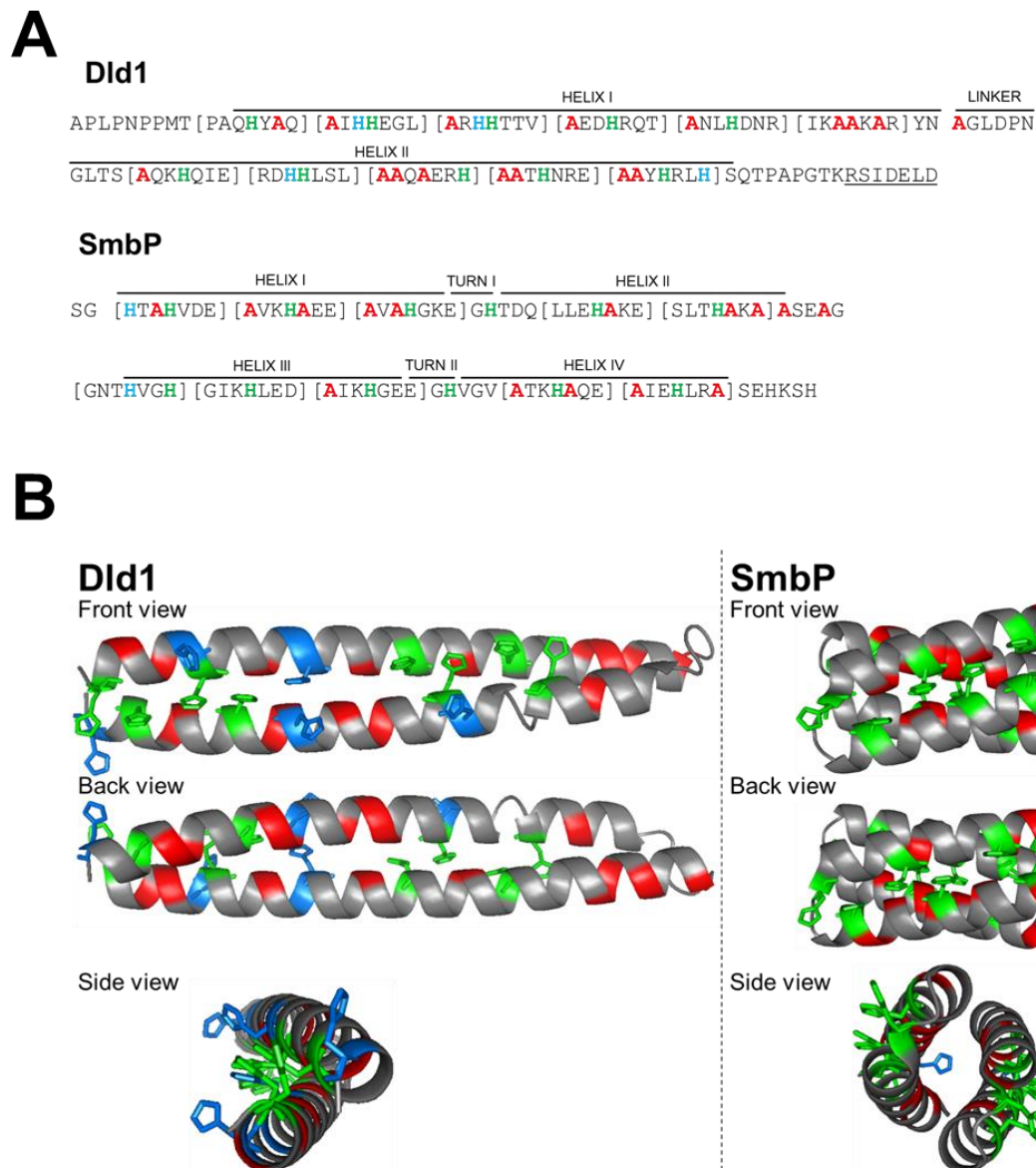
**Figure 20: Comparison of Dld1 and SmbP.**
**(A)** Sequential comparison of Dld1 and SmbP. Analysis of the amino acid sequence of Dld1 and SmbP reveals the existence of 11 heptad repeats in Dld1 and 10 heptad repeats in SmbP (indicated by square brackets). In both proteins a number of the *a* positions of the heptad repeats are occupied by alanines (8 out of 11 in Dld1; 5 out of 10 in SmbP) allowing a tight coiled coil assembly of the two or rather four alpha helices. Moreover a number of *d* positions are occupied by histidines (9 out of 11 in Dld1 and 10 out of 10 in SmbP), facilitating the protrusion of said histidine side chains and the formation of the histidine zipper. **(B)** Structural comparison. Both proteins exhibit a coiled-coil structure of 2 (Dld1) or 2x2 (SmbP) alpha helices. The vast majority of histidine side chains protrude from the side of alternating helices and interdigitate forming a zipper. Alanines are highlighted in red. Histidines are highlighted in blue if they are not part of the zipper. Histidines contributing to the zipper are highlighted in green.

Half of the repeats *a* positions are occupied by alanine residues, indicating that SmbP is potentially able to form a tight alacoil as well. A direct structural comparison of Dld1 and SmbP reveals that SmbP also forms a histidine zipper (**Figure 20 B**). SmbP has been functionally characterized as a periplasmic protein that binds different metal ions, including $Ni^{2+}$, $Zn^{2+}$, $Fe^{3+}$ and $Cu^{2+}$ (Barney *et al.*, 2004). Binding stoichiometry was determined as 6 metal ions per 1 molecule SmbP. Its metal binding capacity coupled with the fact that periplasmic SmbP abundance increased with higher copper concentration in *N. europea* liquid media, led the authors to speculate that the protein scavenges extracellular metal ions, especially $Cu^{2+}$, to

help the cell cope with cytotoxic effects of high concentrations of "free" redox-active metals. Due to the striking similarities between Dld1 and SmbP in terms of amino acid composition, sequential heptad repeat arrangement and overall protein structure, it is tempting to speculate that Dld1 might play a similar role during *P. indica* plant colonization, with an optimization for iron and zinc. The large number of DELD members in *P. indica* genome argue that these proteins may resemble metal ion binding proteins with different specializations.

## 3.3 Dld1 belongs to a paralogous group of small, histidine-rich metal binding proteins

Besides the striking structural similarities to SmbP, other histidine-rich proteins with similar features to Dld1 have been previously described.

Histidine-rich protein 2 (PfHRP2) is a histidine and alanine rich protein from malaria parasite *Plasmodium falciparum*. With 34% and 37% respectively, PfHRP2 exceeds Dld1 in both histidine and alanine abundance and has been shown to bind $Zn^{2+}$ and heme (Wellems & Howard, 1986; Panton *et al.*, 1989). Similar to Dld1, PfHRP2 undergoes a significant structural reorganization either by ligand binding or change of pH. While the protein normally assumes a random coil, the secondary structure switches to a 3/10 helix by binding of heme (Schneider & Marletta, 2005). Depending on the pH, PfHRP2 exerts two contrary functions: At pH 5.2 PfHRP2 binds and promotes detoxification of the iron containing heme and prevents generation of ROS. At pH 7.4, PfHRP2 stabilizes heme and prevents its glutathione mediated degradation (Papalexis *et al.*, 2001). The protein contains two types of consensus sequences. The nonapeptide D-A-H H-A-H H-A-A occurs 15 times, while the hexapeptide D-A-H H-A-A is found 17 times. With a three amino acid spacing in a 3/10 helix structure histidines and alanines assume a similar relative position in every helix turn (Panton *et al.*, 1989), which is reminiscent of the placement of both amino acids within Dld1.

Small histidine-rich human salivary peptides called histatins exhibit a large variety of potential functions, including potent antibacterial and antifungal activity (Melino *et al.*, 2014). Composed of 24 to 38 amino acids, histatins are products of the two genes *his1* and *his2* (Sabatini & Azen, 1989). Structural and functional characterization of HST5, one member of the histatin family, revealed the presence of two metal binding motifs, a Cu(II)/Ni(II)-binding ACTUN motif (consensus sequence D-X-H) and a $Zn^{2+}$-binding motif (consensus sequence H-E-X-X-H) (Harford & Sarkar, 1997; Melino *et al.*, 1999). Like Dld1, HST5 can bind metal ions with low micro molar affinity. The antimicrobial function of most likely originates from inhibition of Zn(II)-dependent metalloproteases (Melino *et al.*, 1999; Porciatti *et al.*, 2010) and increase of intracellular ROS in target bacterial of fungal cells (Helmerhorst *et al.*, 2001). Although the exact mechanisms are still unclear, both the protease inhibition as well as ROS generation are dependent on $Zn^{2+}$ and $Cu^{2+}$ binding, respectively (Cabras *et al.*, 2007).

The human gastric pathogen *Helicobacter pylori* colonizes the stomach of about half of the human population and its virulence strongly depends on the ability to maintain the cytoplasmic pH at a near neutral level in the highly acidic milieu of the stomach (Scott *et al.*, 1998; Yamaoka, 2010). The pathogen accomplishes this by catalyzing the hydrolysis of urea via an intracellular urease into ammonia and bicarbonate, two potent buffering components. $Ni^{2+}$ is part of the active center of the urease enzyme and can be considered an essential virulence determinant of *H. pylori* (Eaton *et al.*, 2002). *H. pylori* produces the two small histidine-rich proteins, Hpn and Hpn-2, both of which are essential for colonization of the mouse model (Vinella *et al.*, 2015). Hpn is composed of 60 amino acids, of which histidine is the most abundant with 28 residues, while glycine takes second place with 8 residues. Hpn-2 is composed of 66 amino acids and its N-terminal part is very similar to Hpn. However, Hpn-2 is enriched for glutamine (27 residues), histidine (17 residues) and alanine (8 residues) (Tomb *et al.*, 1997). As Dld1, heterologously expressed and purified Hpn and Hpn-2 from *E. coli* bind several transition metals *in vitro*, including $Ni^{2+}$, $Zn^{2+}$ and $Cu^{2+}$. Mutation of Hpn histidine 29 and 30 severely impaired the proteins ability to bind $Ni^{2+}$ ions and rendered and *E. coli* Hpn expressing strain less tolerant to high concentrations of extracellular $Ni^{2+}$ (Zeng *et al.*, 2011). According to recent studies, Hpn serves as a $Ni^{2+}$ sequestration and storage protein and together with Hpn-2, both proteins tightly regulate intracellular $Ni^{2+}$ storage, prevent toxic metal concentrations and control urease activity (Vinella *et al.*, 2015).

Together with SmbP, these are four examples of a pool of small histidine-rich proteins which share structural or compositional features with Dld1. In these proteins, histidine residues are often paired with an abundance of amino acids with small side-chains, like glycine (*H. pylori* Hpn1) or alanine (*H. pylori* Hpn-2, *N. europaea* SmbP, *P. falciparum* PfHRP2). All proteins are able to coordinate a variety of transition metal ions *in vitro*, but have been preferentially associated with the binding of one transition metal ion in order to fulfill their proposed biological function. A subset of these proteins seem to be involved in either inhibition or induction of metal-catalyzed ROS generation.

## 3.4 The role of histidines in Dld1's structure and metal binding capability

The abundance of histidines in Dld1 and their organized positioning suggest that these amino acid fulfill a crucial role for the protein's structure and likely participate or are solely responsible for Dld1's affinity to metal ions. Investigation of Dld1's secondary structure via CD spectroscopy have shown that the protein exhibits an alpha helical folding at pH 7.5. X-ray crystallography revealed that structure of Dld1's medial part consists of two antiparallel helices in a tight coil-coil assembly, in which the imidazole rings of histidines interdigitate like teeth of a zipper.

Histidine side chains are composed of imidazole, a planar five-membered ring containing two non-adjacent nitrogen atoms. One of the two nitrogen atoms is covalently bond with one hydrogen atom and two of the ring-adjacent carbon atoms, while the other nitrogen atom has a single bond with one ring-adjacent carbon atom and a double bond with the other ring-adjacent carbon atom. Imidazole exists in two equivalent tautomeric forms, as the hydrogen atom and the double blond can alternate between both nitrogen atoms. The $pK_a$ value of a nitrogen atom without hydrogen in histidines imidazole ring is 6. Following these principles, lowering the pH equal to or below 6 would likely result in protonation of this nitrogen atom in the imidazole rings of a majority of Dld1's histidines. Given the close proximity of the histidines in the zipper-formation, the positive charges would likely repel each other and consequently result in unfolding of the coiled-coil assembly and denaturation of Dld1's structure. This hypothesis is consistent with the results of CD spectroscopy where a decrease in alpha helicity was observed at pH 6 and the protein was devoid of characteristic secondary structures at pH 5.

If Dld1's metal ion binding is mediated by its histidines, each binding would reduce alpha helicity similarly to lowering of the pH. Large metal ions bound by histidine side chains would drive the zipper-formation apart, resulting in unfolding of the coiled-coil assembly and denaturation of Dld1's structure. This hypothesis is consistent with the results of Dld1 CD spectroscopy at pH 7.5 and 6 incubated with $Zn^{2+}$, $Ni^{2+}$, $Cu^{2+}$ and $Fe^{3+}$ in which a varying decrease of alpha helicity in comparison to Dld1 without metal ion incubation was observed. The decrease in alpha helicity was comparable for $Ni^{2+}$, $Cu^{2+}$ and $Zn^{2+}$ at both pH values. Intriguingly, incubation of Dld1 with $Fe^{3+}$-NTA lead to a strong decrease in alpha helicity at pH 7.5, while only a minimal decrease was observed at pH 6. This observation argues that $Fe^{3+}$ binding of Dld1 is weaker at a pH below 7.5.

This assumption is inconsistent with results from IMAC experiments, in which Dld1 showed a markedly reduced affinity to $Fe^{3+}$ at pH 7.5 relative to pH 6 and 5. However, as $Fe^{3+}$ reacts to ferric hydroxide at neutral pH values, immobilized $Fe^{3+}$ ions possibly reacted to ferric hydroxide, which were not able to retain Dld1 on the column, resulting in the presence of Dld1 in flow-through and wash fractions of the $Fe^{3+}$-IMAC at pH 7.5, falsely interpreted as reduced $Fe^{3+}$ affinity. Moreover, the assumption that $Fe^{3+}$ binding of Dld1 is weaker at a pH below 7.5 is consistent with quantitative affinity measurements, i.e. ITC measurements at pH 5 and MST measurements at pH 7.5, where the dissociation constant had doubled between pH 7.5 to 5. The most likely explanation for the decreased affinity for $Fe^{3+}$ at lower pH values would be the protonation of a subset of histidines involved in $Fe^{3+}$ binding most likely accompanied by a denaturation of the binding site.

On the contrary, lowering the pH from 7.5 to 6 did not influence the observed decrease in alpha helicity following Dld1 incubation with $Zn^{2+}$, $Ni^{2+}$ and $Cu^{2+}$, hence there was no significant impact on the binding. If both hypotheses for $Fe^{3+}$ and $Zn^{2+}/Ni^{2+}/Cu^{2+}$ binding are valid, this would indicate that a different set of histidines would mediate the binding of either $Fe^{3+}$ and $Zn^{2+}/Ni^{2+}/Cu^{2+}$.

## 3.5 Characterization of potential metal binding-sites in Dld1

Based on the results of the x-ray crystallography analyzed by SHELXD (Sheldrick, 2008), a single strong $Zn^{2+}$ binding site was predicted, consisting of histidines at position 46 and 107. Both histidines have roughly coplanar imidazole rings which are offset by one helix turn in which an alanine occupies the helix-inward position. Dld1's capability to bind $Zn^{2+}$ was confirmed by $Zn^{2+}$-IMAC, CD spectroscopy and MST. However, a comparison of the predicted $Zn^{2+}$-binding site with available information published in scientific literature indicated that it is far more likely that $Zn^{2+}$ is coordinated by more than just the two predicted histidine ligands. An analysis of available crystal structures in the Cambridge Structural Database in 1998 showed that $Zn^{2+}$ is usually coordinated by at least four ligands with either tetrahedral, square-based pyramidal, trigonal-bipyramidal or octahedral coordination geometries, whereas a tetrahedral coordination is prevailing (Alberts *et al.*, 1998). A broader search of $Zn^{2+}$ binding sites published in scientific literature did not reveal any other proteins with $Zn^{2+}$ coordination by only two amino acid ligands, even with participation of non amino acid ligands. Moreover, quantitative analysis of $Zn^{2+}$ binding by MST with GFP:Dld1, GFP:Dld1[H107A] and GFP:Dld1[H103A,H107A] did not lead to a strong difference in determined dissociation constants between the three proteins. Although a $K_D$ increase from approx. 1.3 µM to 1.9 µM was observed for GFP:Dld1[H107A], paradoxically, the $K_D$ determined for $Zn^{2+}$ binding of GFP:Dld1[H103A,H107A] was almost identical to GFP:Dld1. A possible explanation for these observations would be, that other amino acids would be able to 'step in' for the exchanged histidine at position 107. Indeed, if compared to the SHELDX predicted binding site, histidine pairs 60 and 93 as well as 39 and 114 adopt a similar relative positioning as the histidine pair 46 and 107 (**Figure 21**). These pairs also have roughly coplanar imidazole rings alanine positioned at the helix-inward position in between.
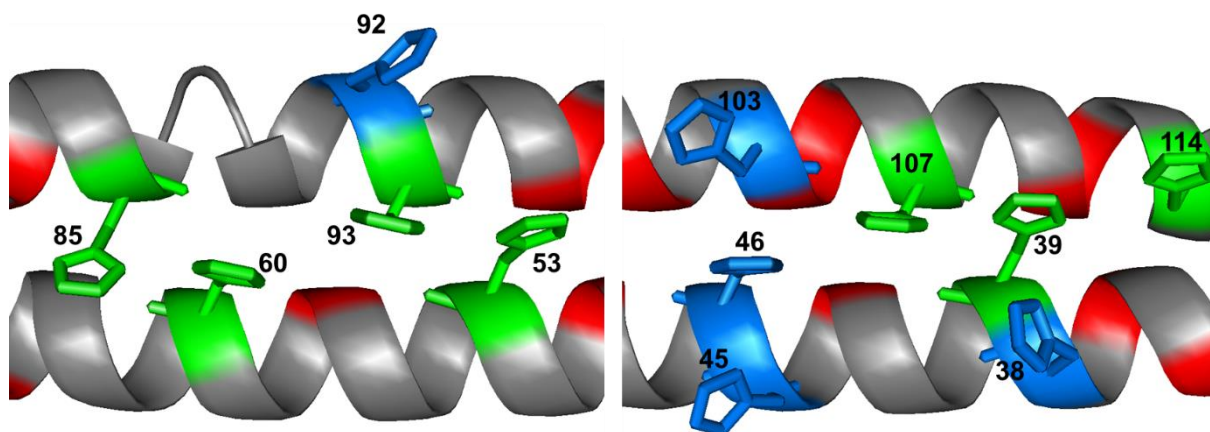
**Figure 21: Relative positioning of histidine residues in the medial part of Dld1.**
Histidines 46 and 107 have been identified as $Zn^{2+}$ binding site by x-ray crystallography and SHELDX analysis. Histidines 60 and 93 as well as 39 and 114 show a similar relative positioning. Alanines are highlighted in red. Histidines are highlighted in blue if they are not part of the zipper. Histidines contributing to the zipper are highlighted in green.

If $Zn^{2+}$ is coordinated by more amino acids than just the two predicted histidines 46 and 107, this argues that either other amino acids of the same Dld1 molecule or from a second Dld1 molecule participate in $Zn^{2+}$ binding.

For the first of the two hypotheses, Dld1 would undergo major structural changes upon metal ion binding, consistent with results from CD spectroscopy with increased $Zn^{2+}$ concentrations. The latter of the two possibilities would indicate that Dld1 forms dimers or oligomers. This hypothesis would be consistent with observations made during normalized gel filtration chromatography, but inconsistent with results from x-ray crystallography and crosslinking experiments. Both experiments, as presented in this thesis, were conducted without the addition of metal ions, although some crosslinking experiments were performed under the addition of metal ions, without any evidence for Dld1 multimerization (data not shown). On the other hand, early IMAC experiments conducted for this thesis, exhibited multiple bands in elution fractions, when Dld1 was eluted together with metal ions, using EDTA instead of imidazole (**Supplemental Figure 3**). However, these results were not reproducible in a controlled manner.

Besides $Zn^{2+}$, Dld1 was able to bind several other metal ions. Together with $Zn^{2+}$, the binding of Dld1 to $Fe^{3+}$ was studied in greater detail. Structural analysis of Dld1 did not give any indication of a dedicated $Fe^{3+}$-binding site. A comparison of available literature on iron-binding proteins shows that typically iron is either bound indirectly via a facilitating molecule, e.g. porphyrin as in hemoglobin or cytochromes (Perutz, 1963; Finzel *et al.*, 1984) or directly coordinated by at least four amino acid ligands and two non amino acid ligands, e.g. in transferrin, lactoferrin or in iron SOD (Baker, 1994; Munoz *et al.*, 2005). Hemoglobin as well as cytochromes form a structural pocket or crevice to accommodate and tightly bind the heme molecule and the iron is further coordinated one distal histidine ligand. As Dld1 does not

assume a globular shape that would allow the coordination of heme or similar facilitating molecules and all binding analysis experiments were conducted directly with $Fe^{3+}$, this modus of iron binding seems to be unlikely for Dld1. Based on the results presented in this thesis, it is far more likely that Dld1 binds to $Fe^{3+}$ directly, although the participating ligands have not been definitely determined. Based on their physiochemical properties, amino acids with side chains containing either carboxylate, thiol or imidazole groups are likely ligands for $Fe^{3+}$ binding. On the basis of this criteria, Dld1 contains 6 aspartic and glutamic acids each and 14 histidines that may serve as $Fe^{3+}$ ligands. As a start, histidine 103 was identified as a likely candidate for $Fe^{3+}$ binding by MST measurements with mutant derivative GFP:Dld1$^{H103A,H107A}$ where the $K_D$ with $Fe^{3+}$ was determined to be twice as high as in comparison to GFP:Dld1. As with $Zn^{2+}$, it is very likely that Dld1 undergoes a significant conformational change upon $Fe^{3+}$ binding as evidenced by the results of CD spectroscopy of Dld1 incubated with $Fe^{3+}$-NTA, where a decrease in alpha helicity was observed. As currently no crystal structure for Dld1 with bound $Fe^{3+}$ is available, further mutational analysis might be the best approach to characterize potentially significant amino acids starting with the candidates outline above.

## 3.6 Challenges of determining metal ion affinities

In this thesis several methodical approaches were made to investigate Dld1's ability to bind metal ions. In a set of qualitative IMAC experiments, *E. coli*-purified Dld1 displayed affinity to $Ni^{2+}$, $Cu^{2+}$, $Zn^{2+}$, $Fe^{2+}$ and $Fe^{3+}$. Subsequently, two further methods were employed to quantify the metal affinity of Dld1, although with only limited success. All ITC measurements at pH 7.5 and pH 6 were inconclusive as either no change in temperature was observed during titration or resulting thermograms could not be aligned with any binding models.

After titrations of $FeCl_3$, a precipitate could be seen in the ITC cell after the measurement was completed, most likely a result of insoluble ferric hydroxide formation, which eliminated $Fe^{3+}$ from the solution and inhibited any detectable binding with Dld1. The reason why the residual ITC measurements at pH 7.5, 6 and 5 for $CuCl_2$ and $ZnCl_2$ were inconclusive remain speculative. A reasonable explanation for measurements were no temperature change was measured is that the amount of Dld1 used in the measurement cell was insufficient to induce a detectable temperature change, i.e. the signal was outside of the instruments dynamic range. Furthermore, metal ions could have rendered themselves inert to binding (similarly to $FeCl_3$), e.g. by reacting with the buffer during the setup period for the measurement. ITC measurements for which the resulting thermograms could not be aligned with binding models could be explained by a suboptimal experimental setup, e.g. dilution warmth of the metal ion or reaction of the metal ion with the buffer could have resulted in an overlay of multiple temperature signals and let to an inconclusive result. Finally, it has to be said that ITC is a very sensitive method and has a multitude of variables, including reaction cell temperature,

selection of buffer system, buffer/salt concentration, titrand and titrant concentration, number, duration, volume and spacing of injections as well as stirring speed and reference power, all of which have a significant impact on the result of the measurement. Due to the lack of experience and binding reference data for Dld1, experimental setup for all ITC measurement founded on the "standard protocol", i.e. 20 injections and a final 2-fold molar excess of metal ion over protein, which might be suboptimal for some 1:1 binding reactions (Tellinghuisen, 2012). Although the attempt was made to optimize the settings for all three tested metal ions, e.g. change of pH/buffer system, in the end time limitations prevented optimal ITC measurements for Dld1 binding $Zn^{2+}$ as well as $Cu^{2+}$ and conclusive data was only obtained for Dld1 binding to $Fe^{3+}$. The $K_D$ for Dld1 binding to $Fe^{3+}$ was determined as approx. 7 µM. Since Dld1 is largely unstructured at this pH, and a correlation between alpha helical folding and metal ion binding was established, it can be speculated that the affinity is stronger at a neutral pH.

In parallel to ITC experiments, and attempt was made to determine the affinity of Dld1 to $Zn^{2+}$, $Cu^{2+}$ and $Fe^{3+}$ via MST. Since the method relies on monitoring fluorescence and Dld1 is devoid of tyrosine or tryptophan, GFP:Dld1 was used instead of Dld1. While a $K_D$ for GFP:Dld1 binding of $Cu^{2+}$ could not be obtained due to fluorescence quenching, the $K_D$ for GFP:Dld1 binding of ferric citrate was determined as approx. 3.8 µM and GFP:Dld1 binding of $Zn^{2+}$ as approx. 1.3 µM. While the $K_D$ for the binding of $Zn^{2+}$ is likely a good estimate, the $K_D$ for GFP:Dld1 binding of $Fe^{3+}$ is most likely lower as ferric citrate had to be used to keep $Fe^{3+}$ in solution at neutral pH. Citrate forms complexes with $Fe^{3+}$ and competes with GFP:Dld1, which limits $Fe^{3+}$ availability and artificially increases the determined $K_D$. Although it is feasible to determine the $K_D$ and therefore affinity of GFP:Dld1 to $Fe^{3+}$ by mathematical elimination of citrate from the binding reaction, certain assumptions have to be made about the aqueous speciation of ferric citrate. Applying such a mathematical elimination, the actual affinity constants of different phenolic acids for $Fe^{3+}$ have been calculated (Yang *et al.*, 2014). While ITC measurements of different phenolic acids titrated with ferric citrate determined affinity constants between 4 and $10 \times 10^3 \, M^{-1}$, the mathematical elimination of citrate led to a drastic increase of affinity constants to $3 \times 10^{34} \, M^{-1}$ to $4 \times 10^{35} \, M^{-1}$. However, the mathematical elimination was based on the presumption that ferric citrate only formed mono-iron di-citrate complexes. Electron spray ionization mass spectrometry measurements have shown that ferric citrate speciation depends on pH and stoichiometry of both binding partners (Silva *et al.*, 2009). Although the aforementioned species is dominant at neutral pH and with a 10-fold molar excess of citrate over ferric iron, trinuclear and tetranuclear species were also identified. Furthermore, if ferric iron and citrate are present at a molar ratio of 1:2, oligomeric complexes are favored over the mono-iron di-citrate complex. In conclusion, the actual affinity of GFP:Dld1 to $Fe^{3+}$ is most likely

higher than the one determined by MST, but a mathematical elimination of citrate likely leads to false results due to wrong assumptions and is therefore self-defeating.

A direct comparison of results obtained for Dld1 binding of $Fe^{3+}$/ferric citrate from all three methods concerning reveals a surprising inconsistency. A lower pH during IMAC experiments lead to an observable increase of immobilized Dld1 on the $Fe^{3+}$ and $Fe^{2+}$ loaded columns, indicating an increase in binding affinity. In contrast, lowering the pH from 7.5 to 5 between MST and ITC experiments conducted with ferric citrate or $Fe^{3+}$, doubled the determined dissociation constant and therefore lowered the affinity of Dld1 to $Fe^{3+}$. As all IMAC experiments were conducted under aerobic conditions, $Fe^{2+}$ likely oxidized to $Fe^{3+}$ during the column preparation. Subsequently, as with $Fe^{3+}$ loaded columns, the majority of $Fe^{3+}$ might have reacted to iron hydroxide as soon as the column was first equilibrated with neutral pH buffer, rendering a large proportion of the column inert to binding of Dld1, resulting in presence of Dld1 in flow-through and was fractions. If this is accurate, than the conclusion drawn from $Fe^{2+/3+}$-IMACs at pH 7.5 are likely false.

In conclusion, Dld1 exhibits affinity to all metal ions tested during IMACs. Only for Dld1 binding if $Zn^{2+}$ and $Fe^{3+}$, $K_D$s were determined which reside in low micro molar range. A decrease of pH resulting in decrease alpha helical structure most likely decreases Dld1's ability to bind $Fe^{3+}$ and most likely other metal ions. Especially experiments with $Fe^{2+}$ and $Fe^{3+}$ were challenging due to the reactive nature of both ions at aerobic an pH neutral conditions demanding the use of either lowering the pH or the use of chelators. Therefore the determined $K_D$ for Dld1 binding of ferric citrate in MST measurements is most likely several magnitudes lower, although an exact calculation did not seem feasible. With an optimized methodical setup, mutant Dld1 derivatives were used in MST experiments to determine if specific conserved histidine residues had any impact on Dld1's affinity to $Zn^{2+}$ and $Fe^{3+}$.

## 3.7 Dld1 interferes with radical reactions

Co-localization of Dld1, reactive $Fe^{3+}$ and ROS in CWAs, in combination with Dld1's ability to bind $Fe^{3+}$, led to the speculation that Dld1 might sequester $Fe^{3+}$ to interfere with $Fe^{3+}$-catalyzed redox reactions during *P. indica* / barley interaction. To test this hypothesis, the effect of Dld1 on $Fe^{3+}$-catalyzed oxidation of DAB by $H_2O_2$ was investigated. The results clearly demonstrated that Dld1 is unable to prevent the initial oxidation of DAB to a Quinone iminium cation radical (**Figure 22**). Moreover, the determined affinity of Dld1 to $Fe^{3+}$ both at pH 5 and pH 7.5 is relatively low compared to known iron scavenging molecules such as siderophores. Together, these results make it unlikely that $Fe^3$ scavenging is the primary role of Dld1 during *P. indica* / barley interaction. However, Dld1 might utilize its affinity to $Fe^{3+}$ to localize at CWAs in order fulfill it biological function.
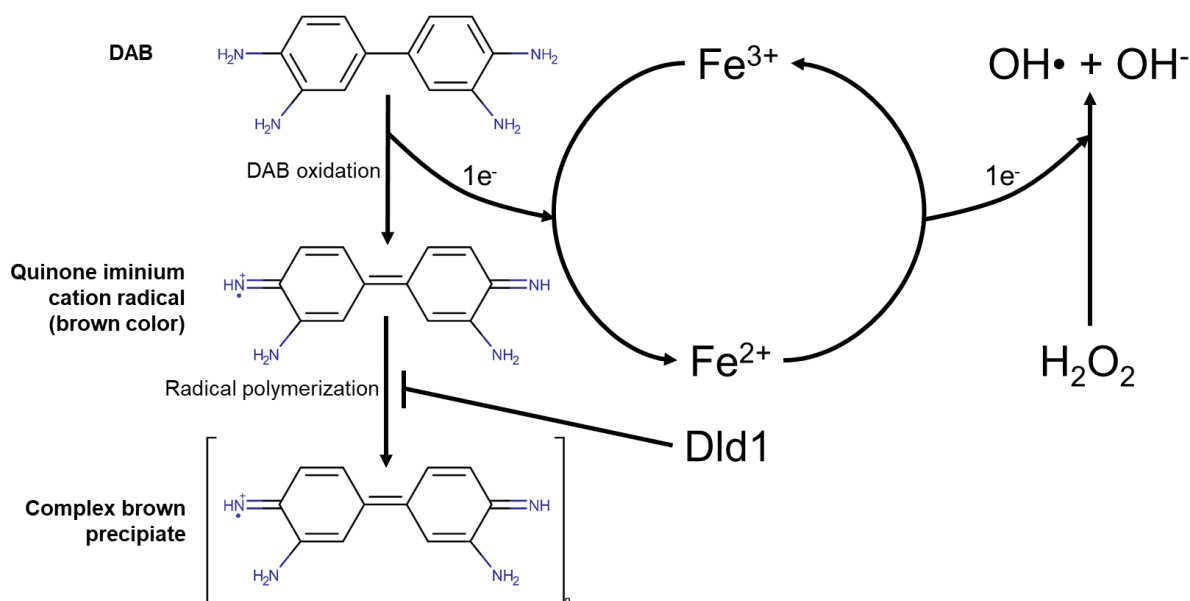
**Figure 22: Model for $Fe^{3+/2+}$ catalyzed DAB oxidation assay.**
DAB transfers one electron ($e^-$) to $Fe^{3+}$, resulting in a redistribution of electron pair bonds throughout the benzene rings. An intermediate Quinone iminium cation radical (brown color) is formed, which self-reacts and polymerizes to a complex brown precipitate. $Fe^{2+}$ further transfers one electron to $H_2O_2$ which results in one molecule of hydroxide ($OH^-$) and hydroxyl radical ($OH•$), each. Results obtained from the $Fe^{3+}$ catalyzed DAB oxidation assay in this thesis argue that Dld1 interfered with the radical polymerization of the Quinone iminium cation radical.

While Dld1 is unable to prevent the oxidation of DAB, respective experiments showed that Dld1 interferes with the subsequent radical polymerization of DAB. ROS, such as $H_2O_2$ are produced in response to microbial penetration attempts and have been functionally implicated in the maturation and fortification of CWAs (Brown *et al.*, 1998; McLusky *et al.*, 1999; Soylu *et al.*, 2005). Here, ROS do not only serve as signalling molecules, but have been directly implicated in chemical reactions, such as crosslinking of antimicrobial proteins and phenolics within the plant cell wall and polymerization of ferulic acid, an interconnected building block of the plant wall, which is crucial for cell wall fortification (Zimmerlin *et al.*, 1994; Wojtaszek *et al.*, 1997). Based on the nature of ROS, radical intermediates are likely to be present during these reactions. Since an interference with radical polymerization reactions has been demonstrated for Dld1, it is tempting to speculate that Dld1 might function as a radical scavenger *in planta* within CWAs during *P. indica* / barley interaction.

## 3.8 A functional hypothesis for Dld1 during *P. indica* barley colonization

Based on the localization and biochemical data obtained during the practical work for this thesis, the following hypothesis is postulated for Dld1's biological function during *P. indica* / barley interaction.

During the early stages of barley colonization, *P. indica* seeks to establish a biotrophic interaction with barley root epidermal and cortex cells. In order to exchange nutrients with barley, *P. indica* has to penetrate the cell wall of barley root cells. Barley evidently senses *P. indica* as a microbial invader, most likely by the recognition of MAMPs and signals

associated with damaging of its cell wall(s). The recognition triggers an array of cellular defense responses, including the targeted reallocation of intracellular $Fe^{3+}$ to the cell wall location, where a *P. indica* penetration has been recognized. There, $Fe^{3+}$ mediates ROS cycling and the production of $H_2O_2$, which serves as chemical inducer for the maturation and fortification of localized CWAs by radical crosslinking of phenolics, antimicrobial proteins, polymerization of ferulic acid and callose deposition in order to repel the microbial invader.

Meanwhile, *DLD1* is upregulated in the penetrating *P. indica* cells. Dld1 is guided into the secretory pathway and ultimately secreted onto the barley cell wall. Here Dld1 co-localizes with $Fe^{3+}$ via its affinity for metal ions. As radical scavenger, Dld1 interferes with the radical crosslinking and polymerization reactions induced by $H_2O_2$ and iron, thereby preventing the maturation and fortification of CWAs. Ultimately, *P. indica* breaks though the weakened CWA and establishes a biotrophic interaction with the host plant cell.

## 3.9 Outlook

Dld1's localization, as well as structural, biophysical and biochemical properties were analyzed and discussed in detail and a hypothesis for its biological function was postulated. However, there are a number of aspects to this novel protein that are still elusive and prompt further research effort.

The proposed biological function for Dld1 remains very speculative, as it only draws from a artificial *in vitro* assay. Naturally, DAB is no substrate in the plant cell wall. Zimmerlin *et al.* have demonstrated the polymerization of ferulic acid *in vitro* by addition of $H_2O_2$ and a plant cell wall peroxidase. If the functional hypothesis postulated above is correct, the peroxidase could be substituted by $Fe^{3+}$ and the assay could be conducted with and without the presence of Dld1. If Dld1 is a radical scavenger, it should interfere with the formation of ferulic acid polymers. The formation or absence of a ferulic acid polymer could be observed using a suitable mass spectromic method.

Although Dld1's capability to bind several metal ions has been analyzed and discussed extensively in this thesis, no definite metal ion binding sites were identified. From the presented results, it seems more likely that at least $Zn^{2+}$ and $Fe^{3+}$ binding is mediated by an at least partially different set of amino acids. One approach to achieve a better understanding of potential metal binding sites would be single and cumulative exchange of amino acids in Dld1 purified from *E. coli*, which are potentially relevant for metal ion binding followed by a qualitative or quantitative metal ion binding assay. The most promising candidates for this approach would certainly be the 14 histidines throughout Dld1, as these amino acids readily participate in metal ion binding and seem to be critical for Dld1's pH sensitive structure. A second, cruder approach would be the generation of truncated versions of Dld1 to home in on parts of the protein, which are critical for metal binding followed by a qualitative or quantitative metal ion binding assay.

The disadvantage of this particular approach originates from Dld1's coiled coil structure as distant parts of the protein might work in conjunction to facilitate metal ion binding. Deletion of one part of the protein might impair metal ion binding, but this does not necessarily mean that the deleted part contains all relevant ligands for the binding of the respective metal ion. A third approach, would be the crystallization of purified Dld1 followed by crystal soaking with metal ion solutions to achieve crystallization with the respective metal ion in close proximity to potential amino acid ligands. This approach is promising as conditions under which Dld1 is likely to form crystals have already been identified.

The hypothesis discussed in this work focuses on Dld1's potential to interfere with $Fe^{2+/3+}$ catalyzed radical reactions. This means that Dld1 does not interact with any of the plant host proteins, but only interacts with the plant host's iron pool deposited at the CWAs. However there are numerous potential interaction partners during the initial stage of *P. indica* colonization that might give a significant insight into Dld1's potential biological function. This includes in particular a variety of metal-ion-containing, ROS-generating enzymes, e.g. peroxidases, SODs and oxidases. The most promising approach to identify potential interaction partners would be a yeast-2-hybrid screening using Dld1 as bait and a combined *P. indica* / barley cDNA library as prey. In fact, this experiment was previously conducted in the workgroup of Prof. Dr. Zuccaro, but impurities, most likely originating at the cDNA library vendor, led to inconclusive results and a repetition in the framework of this thesis was not considered feasible due to time constraints.

Although a hypothesis for Dld1's biological function has been discussed in this thesis, the supporting results only focus on *in vitro* structural, biophysical or biochemical properties as well as *in planta* localization of the protein. Hence, further *In vivo* experiments are crucial to validate this hypothesis. One approach to analyze the biological function of Dld1 would be the creation of a deletion mutant followed by the evaluation *P. indica* colonization by confocal microscopy and by determining the *P. indica* / barley gDNA ratio as described previously (Hilbert *et al.*, 2012). Unfortunately, *P. indica* is a dikaryotic organism and to date does not allow gene deletion by any of the methods that have been established for other fungal model organisms. Instead a sophisticated RNA interference (RNAi) method has been established for *P. indica* and successfully utilized for analyzing the impact of target gene silencing on successful plant colonization (Hilbert *et al.*, 2012; Lahrmann *et al.*, 2013). A first attempt for RNAi mediated silencing for *DLD1* has been during the practical work for this thesis, however the relative decrease of RNA transcripts was neither verified via Northern blot nor qPCR. Due to the significance of a *DLD1*-silenced *P. indica* strain, additional efforts should be undertaken to generate a respective RNAi mutant. One potential caveat for the interpretation of the results of colonization experiments with a *DLD1* RNAi strain is the fact that the *P. indica* genome harbors approximately 30 genes encoding proteins very similar to Dld1. The proteins are in

fact so similar that several of the DELD family proteins might be functionally redundant. If this is the case, RNAi silencing of a single encoding gene might not have a significant impact on colonization. There are essentially two ways to try to circumvent this challenge. Firstly, a significant number of DELD family protein encoding genes could be silenced by sequentially introducing a number or RNAi constructs. However, this approach would be laborious and difficult to achieve as only a limited number of resistance markers are available for *P. indica* transformation. Secondly, a sort of 'common denominator RNAi construct' could be designed by alignment of all DELD family protein encoding genes. This construct could be introduced in a single transformation and might lead to silencing of a significant number of target genes and result in a macroscopic impact on colonization.

Another possibility to shed light on Dld1's biological relevance would be the introduction of the *DLD1* gene into another fungus with subsequent evaluation of ROS and metal ion tolerance. A Dld1-producing *U. maydis* mutant has already been generated outside the framework of this thesis, which showed a higher tolerance against ROS and iron. Additionally, colonies of this mutant exhibit a dark brown coloring, which increases even more when the mutant is grown on iron-rich media. Further investigations are needed to identify the respective pigment and uncover the underlying biological mechanism of the increased tolerability. However, these preliminary results indicate that Dld1 might confer ROS and iron tolerance, two abiotic stresses *P. indica* evidently experiences during colonization of a host plants such as barley.

In this thesis, potential functions of the highly conserved C-terminal RSIDELD motif of *P. indica*'s DELD family proteins were examined in respect to metal ion binding and protein localization. No significant impact was observed, when the motif was deleted from the full-length protein. Based on published literature, two hypotheses about potential functions of a short, conserved, terminally located motif are discussed below in conjunction with experimental approaches.

Effector proteins are secreted during host colonization to modulate host immunity. In addition to secretion, a subset of effector proteins are presumed to be transported into the host cell cytoplasm. In some pathogenic species, conserved translocation motifs have been identified and characterized. In the plant pathogenic oomycetes a conserved RxLR motif has been determined to be essential for protein translocation into the host plant cell cytoplasm (Whisson *et al.*, 2007; Dou *et al.*, 2008; Wawra *et al.*, 2017). The RxLR motif is located in proximity to the signal peptide cleavage site and often accompanied by a secondary conserved motif. Although the RxLR motif has been determined as essential for number of translocated oomycete effectors, a general mechanism for translocation utilizing the motif remains to be discovered (Wawra *et al.*, 2012). The human malaria pathogen *P. falciparum* targets essential remodeling and virulence proteins across the vacuolar membrane and into the cytoplasm of

erythrocytes. This transport is guided by the so called '*Plasmodium* export element' or short PEXEL motif consisting of the amino acids Arg-x-Leu-x-Glu/Asp/Gln (where x representing any amino acid) (Hiller *et al.*, 2004; Marti *et al.*, 2004). Similar to the RxLR motif, the PEXEL motif is located in close proximity to the N-terminal signal peptide cleavage site of the translocated proteins. Whereas the RxLR motif can often be found within the next 40 amino acids of the cleavage site, the PEXEL motif is often directly next to the cleavage site and is further processed by proteases in the ER, which in the end results in N-acetylation of the protein (Chang *et al.*, 2008; Boddey *et al.*, 2009). In fungi, there are several examples for the translocation of effectors proteins into host plant cells (Kale *et al.*, 2010; Djamei *et al.*, 2011; Plett *et al.*, 2011; Tanaka *et al.*, 2014). However, the existence of a shared or a conserved translocation mechanism is still unclear. It is tempting to speculate that the RSIDELD motif of Dld1 and the DELD family proteins might mediate protein translocation. Similarly to the positioning of the RxLR and PEXEL motif at the N-terminus, the structurally exposed positioning of the RSIDELD motif at the C-terminus might facilitate protein-protein interaction necessary for protein translocation. *In planta* confocal microscopy of *U. maydis* strains producing mCherry tagged Dld1 with and without the RSIDELD motif did not show any difference in protein localization and certainly did not show any protein translocation into maize cells. However, a *P. indica*-dependent translocation mechanism mediated by the RSIDELD motif could not have been observed in this particular experimental setup. Moreover, for an unknown reason, the detection of translocated effectors of *U. maydis* via confocal microscopy has been proven ineffective in previous studies (Lo Presti *et al.*, 2017). To reliably analyze a potential role of the RSIDELD motif in protein translocation, a transgenic *P. indica* strain constitutively producing Dld1 with an N-terminal fluorescence tag after the signal peptide cleavage site should be examined via confocal microscopy during barley colonization. Immunodetection of Dld1 with transmission electron microscopy under the same culturing conditions should be undertaken in addition to verify the localization of the protein during colonization. As a control, a *P. indica* strain expressing the same construct but without the RSIDELD motif should be examined. In addition, *P. indica* strains producing a secreted fluorescent protein with and without the C-terminal addition of the RSIDELD motif should also be examined to investigate whether the RSIDELD motif alone would be sufficient to mediate a potential translocation. In conclusion, the hypothesis that the RSIDELD motif could potentially mediate protein translocation in host plant cells is very tempting, especially when a conserved fungal translocation motif is lacking to date, but so far any supporting evidence for this hypothesis is lacking.

The most well studies C-terminally located protein motifs, are ER or Golgi retention motifs present in a variety of proteins throughout a number of species. Based on the results obtained from *in vitro* and *in planta* localization of Dld1, where the protein has been shown to be secreted

in independent experimental setups, it is unlikely that the RSIDELD motif mediates ER or Golgi retention. However, in these experiments Dld1 was always produced outside of *P. indica*. This might open the possibility that the RSIDELD motif only interacts with *P. indica* proteins that facilitate ER or Golgi retention. Moreover, one of the most prominent and best studied conserved ER retentions signals is the C-terminal KDEL or HDEL sequence, which shares three terminal amino acids with RSIDELD motif (Munro & Pelham, 1987). The K/HDEL sequence is recognized and bound by one or multiple corresponding receptors in the cis-Golgi or pre-Golgi compartment and returned to the ER via retrograde transport (Lewis & Pelham, 1990; Semenza *et al.*, 1990). One could speculate that a *P. indica*-specific RSIDELD receptor might fulfil this role. A potential experimental approach to analyze whether the RSIDELD motif mediates ER or Golgi retention, would be determining the localization of Dld1 fused N-terminally with a fluorescent protein produced by *P. indica* under a constitutive promotor. The respective strain should be examined via confocal microscopy. However, a potential ER or Golgi localization should be validated by Immunoblot experiments, as a constitutive production of the Dld1 fusion protein might lead to false positive ER and Golgi localization as a result of an overload of the cells secretion system. In these immunoblots, the relative amount of secreted Dld1 fusion protein should be comparably low to the amount of protein extracted from *P. indica* cells, if the RSIDELD motif facilitates ER or Golgi retention. In a secondary, broader approach, the RSIDELD motif could be used as bait in a yeast-2-hybrid screening to identify potential K/HDEL receptor like interaction partners, which return the protein to the ER or Golgi via retrograde transport.

# 4. Material & Methods

## 4.1 Material and chemicals

### 4.1.1 Chemicals

All chemicals that were used during experiments described in this thesis were, if not mentioned differently, from *p. a.* quality and were purchased primarily from the companies BD (Franklin Lakes, USA), GE Healthcare (Uppsala, Sweden), Merck (Darmstadt), Invitrogen (Darmstadt), Roth (Karlsruhe) and Sigma-Aldrich (Taufkirchen).

### 4.1.2 Buffers and solutions

Standard buffers and solutions were made according to Ausubel *et al.* (2002) and Sambrook *et al.* (1989). Special buffers and solutions are listed below the respective methods. If required, buffers and solutions were autoclaved for 20 min at 121°C. Heat sensitive buffers and solutions were instead sterile filtered (pore sized 0.2 µm; Merck, Darmstadt).

### 4.1.3 Enzymes and antibodies

Restriction enzymes were purchased from New England Biolabs (NEB, Frankfurt/Main). For cloning purposes the DNA polymerases Easy-A Hi-Fi Cloning Enzyme (Agilent Technologies, Santa Clara, USA) and *Pfu* DNA Polymerase (Promega Corporation, Madison, USA) were used. *Taq* Polymerase (Thermo Fisher Scientific, Waltham, USA) was used for amplifications in colony PCR reactions. DNA molecules were ligated with T4-DNA ligase (Thermo Fisher Scientific, Waltham, USA). For enzymatic degradation of RNA RNase A (Thermo Fisher Scientific, Waltham, USA) was used. Primary and secondary antibodies for immunoblot assays were purchased from Sigma-Aldrich (Taufkirchen, Germany), Cell Signalling Technology (Danvers, USA), Clontech Laboratories (Mountain View, USA). For a detailed listing of used antibody please refer to section 4.6.2.

### 4.1.4 Kits used in this thesis

For purification of PCR products and DNA fragments from agarose gels the Wizard® SV Gel and PCR Clean-Up System (Promega Corporation, Madison, USA) was used. Extraction and purification of plasmids from *E. coli* was implemented with the QIAprep® Mini Plasmid Kit (Qiagen, Hilden). Mutation and insertion of bases into plasmids were ensued using the QuickChange Multi Site-Directed Mutagenesis Kit (Stratagene, LaJolla, USA). Further specialized Kits are listed under the respective methods they were used for.

## 4.2 Cultivation of microorganisms

### 4.2.1 Cultivation and growth media

Media for the cultivation and growth of microorganisms are listed in **Table 2**. If not mentioned otherwise, all media were autoclaved at 121°C for 5 min.

**Table 2: Media used for cultivation and growth of microorganisms.**

| Name | Organism | Contents |
|------|----------|----------|
| dYT [-Agar] | *E. coli* | 1.6% (w/v) Tryptone |
| | | 1% (w/v) Yeast extract |
| | | 0.5% (w/v) NaCl |
| | | [1.5% (w/v) Agar] |
| Lysogeny broth (LB) [-Agar] | *E. coli* | 0.5% (w/v) Yeast extract |
| | | 1% (w/v) Tryptone |
| | | 1% (w/v) NaCl |
| | | [1.5% (w/v) Agar] |
| YEPS$_{light}$ | *U. maydis* | 1% (w/v) Yeast extract |
| | | 1% (w/v) Peptone |
| | | 1% (w/v) Sucrose |
| Potato-Dextrose (PD) Agar | *U. maydis* | 2.4% (w/v) Potato-dextrose broth |
| | | 2% (w/v) Agar |
| NSY-Glycerol | *U. maydis* | 0.8% (w/v) Nutrient Broth |
| | | 0.1% (w/v) Yeast extract |
| | | 0.5% (w/v) Sucrose |
| | | 69.6% (v/v) Glycerole |
| Complete medium (CM) [Agar] | *P. indica* | 5% (v/v) 20X CM salt solution |
| | | 2% (w/v) Glucose |
| | | 0.2% (w/v) Peptone |
| | | 0.1% (w/v) Yeast extract |
| | | 0.1% (w/v) Casamino acids |
| | | 0.1% (v/v) CM microelements |
| | | [1.5% (w/v) Agar] |
| 20X CM salt solution | *P. indica* | 12% (w/v) $NaNO_3$ |
| | | 1.04% (w/v) KCl |
| | | 1.04% (w/v) $MgSO_4$ heptahydrate |
| | | 3.04% (w/v) $KH_2PO_4$ |
| 1,000X CM microelements | *P. indica* | 0.6% (w/v) $MnCl_2$ tetrahydrate |
| | | 0.15% (w/v) $H_3BO_3$ |
| | | 0.265% (w/v) $ZnSO_4$ heptahydrate |
| | | 0.075% (w/v) KI |
| | | 0.00024% (w/v) $Na_2MO_4$ dihydrate |
| | | 0.013 (w/v) $CuSO_4$ pentahydrate |

## 4.2.2 Cultivation of *E. coli*

*E. coli* bacteria were grown at 37°C with 200 rpm shaking. If necessary liquid and solid media were supplemented with the antibiotics listed below. For storage of permanent cultures at -80°C, 25% glycerol were added.

**Table 3: Antibiotics used for the cultivation of *E. coli*.**

| Antibiotic | Final concentration [µg/mL] |
|---|---|
| Ampicillin (Amp) | 100 |
| Kanamycin (Kan) | 40 |
| Chloramphenicol (Cam) | 34 |

## 4.2.3 Cultivation of *U. maydis*

*U. maydis* sporidia cultures were grown at 28°C with 200 rpm shaking. Overnight cultures were grown in YEPS$_{light}$. As solid medium, PD plates were used. If necessary 2 µg/mL Carboxin (Cbx) was added. For storage of permanent cultures at -80°C, overnight cultures were mixed with 50% NSY-Glycerol.

## 4.2.4 Cultivation of *P. indica*

*P. indica* mycelium cultures were grown at 28°C with 130 rpm shaking. CM was used as liquid and solid medium. If necessary 80 µg/mL Hygromycine B (Hyg) was added for selection. For storage of permanent cultures at -80°C, spores were harvested and diluted in 50% glycerol.

## 4.2.5 Determination of cell density in bacterial and fungal cultures

Cell density of *E. coli* and *U. maydis* cultures were determined using a Novaspec II Photometer (Pharmacia Biotech/GE Lifesciences, Uppsala, Sweden) by measuring optical density at 600 nm (OD$_{600}$). If the measured OD$_{600}$ exceeded 0.8 the culture was diluted.

## 4.3 Strains, oligonucleotides and plasmids

### 4.3.1 *E. coli* strains

The *E. coli* strains used in this work are listed in **Table 4** with all relevant information.

**Table 4: *E. coli* strains used in this study.**

| Strain Name Genotype | Purpose | Reference/Purchased from |
|---|---|---|
| **Top 10** [F- mcrA Δ(mrr-hsdRMS-mcrBC) φ80lacZΔM15 ΔlacX74 nupG recA1 araD139 Δ(ara-leu)7697 galE15 galK16 rpsL(Str$^R$) endA1 λ$^-$] | Cloning/ Plasmid amplification | Thermo Fisher Scientific, Waltham, USA |
| **BL21(DE3)pLysS** [F$^-$ *ompT gal dcm lon hsdS$_B$($r_B^-$ $m_B^-$)* λ(DE3 [*lacI lacUV5-T7 gene 1 ind1 sam7 nin5*]) [*malB$^+$*]$_{K-12}$(λ$^S$) pLysS[*T7p20 ori$_{p15A}$*](Cm$^R$)] | Progenitor strain for heterologous production of proteins | Thermo Fisher Scientific, Waltham, USA |
| **Tuner(DE3)pLysS** [F– ompT hsdSB (rB– mB–) gal dcm lacY1(DE3) pLysS (Cm$^R$)] | Progenitor strain for heterologous production of proteins | Merck Millipore, Billerica, USA |
| *E. coli* **<pRSET-GST:DLD1woSP>** BL21(DE3)pLys p[*P$_{T7}$:GST:DLD1$^{20-135}$* (Amp$^R$)] | Heterologous production of Dld1 | This thesis |
| *E. coli* **<pRSET-GST:DLD1woSP$^{H107A}$>** BL21(DE3)pLys p[*P$_{T7}$:GST:DLD1$^{20-135(H107A)}$* (Amp$^R$)] | Heterologous production of Dld1$^{H107A}$ | This thesis |
| *E. coli* **<pRSET-GST:DLD1woSP$^{ΔRSIDELD}$>** BL21(DE3)pLys p[*P$_{T7}$:GST:DLD1$^{20-128}$* (Amp$^R$)] | Heterologous production of Dld1$^{ΔRSIDELD}$ | This thesis |

| Strain Name Genotype | Purpose | Reference/Purc hased from |
|---|---|---|
| **E. coli <pRSET-GST:EGFP>** Tuner(DE3)pLysS p[$P_{T7}$:GST:EGFP (Amp$^R$)] | Heterologous production of eGFP | This thesis |
| **E. coli <pRSET-GST:EGFP:DLD1woSP>** BL21(DE3)pLys p[$P_{T7}$:GST:EGFP:DLD1$^{20-135}$ (Amp$^R$)] | Heterologous production of eGFP:Dld1 | This thesis |
| **E. coli <pRSET-GST:EGFP:DLD1woSP$^{H107A}$>** BL21(DE3)pLys p[$P_{T7}$:GST:EGFP:DLD1$^{20-135(H107A)}$ (Amp$^R$)] | Heterologous production of eGFP:Dld1$^{H107A}$ | This thesis |
| **E. coli <pRSET-GST:EGFP:DLD1woSP$^{H103A,H107A}$>** BL21(DE3)pLys p[$P_{T7}$:GST:EGFP:DLD1$^{20-135(H103A,H107A)}$ (Amp$^R$)] | Heterologous production of eGFP:Dld1$^{H103A,H107A}$ | This thesis |
| **E. coli <pRSET-GST:EGFP:DLD1woSP$^{\Delta RSIDELD}$>** BL21(DE3)pLys p[$P_{T7}$:GST:EGFP:DLD1$^{20-128}$ (Amp$^R$)] | Heterologous production of eGFP:Dld1$^{\Delta RSIDELD}$ | This thesis |

## 4.3.2 *U. maydis* strains

All *U. maydis* strains that were generated during this work originate from the solopathogenic strains *U. maydis* SG200 (Kämper *et al.*, 2006) and are listed in **Table 5** with all relevant information. For the integration of genes in the *ip* locus *(sdh2)* plasmids were used that harbor a Cbx-resistant *ip* allel (*ipR*; Broomfield and Hargreaves, 1992). Respective plasmids were linearized with *Ssp*I prior to transformation. Resulting strains were verified by PCR on genomic DNA and southern blot analysis.

**Table 5: *U. maydis* strains used in this study.**

| Strain Name Genotype | Purpose | Reference/Purchased from |
|---|---|---|
| **SG200** *[a1 : mfa2 bW2 bE1]* | Progenitor strain | Kämper *et al.*, 2006 |
| **U. maydis <p123-mCherry>** *[a1 : mfa2 bW2 bE1] ip$^R$[P$_{otef}$:mCherry]ip$^S$* | Lysis control strain in secretion assay | Doehlemann *et al.*, 2009 |
| **U. maydis <p123-PIT2SP:mCherry:DLD1woSP >** *[a1 : mfa2 bW2 bE1] ip$^R$[P$_{otef}$:Pit2$^{1-22}$:mCherry:DLD1$^{20-135}$]ip$^S$* | Positive control strain in secretion assay | This thesis |
| **U. maydis <p123-DLD1SP:mCherry:DLD1woSP >** *[a1 : mfa2 bW2 bE1] ip$^R$[P$_{otef}$:DLD1$^{1-29}$:mCherry:DLD1$^{20-135}$]ip$^S$* | Analysis of Dld1 secretion | This thesis |
| **U. maydis <p123-DLD1SP:mCherry:DLD1woSP$^{\Delta RSIDELD}$>** *[a1 : mfa2 bW2 bE1] ip$^R$[P$_{otef}$:DLD1$^{1-29}$:mCherry:DLD1$^{20-128}$]ip$^S$* | Analysis of Dld1 secretion | This thesis |

## 4.3.3 *P. indica* strains

All *P. indica* strains that were generated during this work originate from the *P. indica* DSM11827 isolate (obtained from: Deutsche Sammlung von Mikroorganismen und Zellkulturen, Braunschweig; Varma *et al.*, 1999) and are listed in **Table 6**. Prior to *P. indica* transformation, respective plasmids were linearized by *Nae*I restriction.

**Table 6:** *P. indica* **strains used in this thesis.**

| Strain Name<br>Genotype | Purpose | Reference/Purchased from |
|---|---|---|
| *P. indica* | Progenitor strain | Varma *et al.*, 1999 |
| *P. indica* <pGOGFP><br>*[P$_{gpd}$:oGFP:T$_{Nos}$]* | Lysis control strain in secretion assay | Hilbert *et al.*, 2012 |
| *P. indica* <pGOGFP:DLD1><br>*[P$_{gpd}$:oGFP:DLD1:T$_{Nos}$]* | Analysis of Dld1 secretion | This thesis |

## 4.3.4 Oligonucleotides

All oligonucleotides used in this study were synthesized by and purchased from either Sigma-Aldrich (Taufkirchen) or MWG (Martinsried) and are listed in **Supplemental Table 2**.

## 4.3.6 Plasmids

### 4.3.6.1 Plasmids used for heterologous production of recombinant proteins in *E. coli*

**pRSET-GST-PP (Schreiner *et al.*, 2008)** - This plasmid is modified from the Thermo Fisher Scientific (Waltham, USA) pRSET plasmid by exchanging the sequence encoding a hexahistidine (His$_6$) tag for GST. Additionally the sequence encoding the GST tag is preceded at its 3' end by a sequence encoding a 3C protease cleavage site, which enables the cleavage of the GST tag from the fusion protein with the respective protease, which is sold as PreScission Cleavage Protease (GE, Uppsala, Sweden). The plasmid furthermore confers ampicillin resistance to transformed *E. coli* cells.

**pRSET-GST:DLD1woSP (this study)** - This plasmid was generated by the amplification of the *P. indica* gene PIIN_05872 (*DLD1)* from cDNA synthesized from RNA extracted from *P. indica* colonized barley roots 3 dpi. The DNA sequence encoding the *in silico* predicted signal peptide was not amplified. The PCR product was restricted by *Bam*HI and *Hind*III and ligated into pRSET-GST-PP downstream of the 3C protease cleavage site. It serves the purpose of heterologous production of GST:Dld1 in *E. coli* BL21(DE3)pLys.

**pRSET-GST:DLD1woSP$^{H107A}$ (this study)** - This plasmid originates from pRSET-GST:DLD1woSP. It was generated by site-directed mutagenesis of the base triplet, which encodes Dld1 histidine at position 107 to alanine (CAC to GCC). It serves the purpose of heterologous production of GST:Dld1$^{H107A}$ in *E. coli* BL21(DE3)pLys.

**pRSET-GST:DLD1woSP$^{H103A,H107A}$ (this study)** - This plasmid originates from pRSET-GST:DLD1woSP$^{H107A}$. It was generated by site-directed mutagenesis of the base triplet, which encodes Dld1 histidine at position 103 to alanine (CAC to GCC). It serves the purpose of heterologous production of GST:Dld1$^{H103A,H107A}$ in *E. coli* BL21(DE3)pLys.

**pRSET-GST:DLD1woSP$^{\Delta RSIDELD}$ (this study)** - This plasmid was generated by the amplification of the *P. indica* gene *DLD1* from cDNA synthesized from RNA extracted from

*P. indica* colonized barley roots 3 dpi. The DNA sequence encoding the *in silico* predicted signal peptide and the C-terminal RSIDELD motif was not amplified. Instead of the RSIDELD motif, a premature stop codon was introduced. The PCR product was restricted by *BamH*I and *Hind*III and ligated into pRSET-GST-PP downstream of the 3C protease cleavage site. It serves the purpose of heterologous production of GST:Dld1$^{\Delta\text{RSIDELD}}$ in *E. coli* BL21(DE3)pLys.

**pRSET-GST:EGFP (provided by Dr. André Müller from workgroup Prof. Dr. Gunther Döhlemann, University of Cologne; formerly Max-Planck-Institute Marburg)** - This plasmid was generated by amplifying the coding sequence of eGFP, subsequent digestion with *BamH*I and *Hind*III and ligation into pRSET-GST-PP. It serves the purpose of heterologous production of GST:GFP in *E. coli* Tuner(DE3)pLys.

**pRSET-GST:EGFP:DLD1woSP (this study)** - This plasmid originates form pRSET-GST:EGFP. It was generated by inserting the coding sequence of *DLD1* without the sequence encoding the *in silico* predicted signal peptide via Gibson assembly (Gibson *et al.*, 2009) downstream and in frame of the coding sequence of eGFP. It serves the purpose of heterologous production of GST:GFP:Dld1 in *E. coli* BL21(DE3)pLys.

**pRSET-GST:EGFP:DLD1woSP$^{\text{H107A}}$ (this study)** - This plasmid originates from pRSET-GST:EGFP:DLD1woSP. It was generated by site-directed mutagenesis of the base triplet, which encodes Dld1 histidine on position 107 to alanine (CAC to GCC). It serves the purpose of heterologous production of GST:GFP:Dld1$^{\text{H107A}}$ in *E. coli* BL21(DE3)pLys.

**pRSET-GST:EGFP:DLD1woSP$^{\text{H103A,H107A}}$ (this study)** - This plasmid originates from pRSET-GST:EGFP:DLD1woSP$^{\text{H107A}}$. It was generated by site-directed mutagenesis of the base triplet, which encodes Dld1 histidine on position 103 to alanine (CAC to GCC). It serves the purpose of heterologous production of GST:GFP:Dld1$^{\text{H103A,H107A}}$ in *E. coli* BL21(DE3)pLys.

**pRSET-GST:EGFP:DLD1woSP$^{\Delta\text{RSIDELD}}$ (this study)** - This plasmid originates form pRSET-GST:EGFP. It has been generated by inserting the coding sequence of *DLD1* without the sequence encoding the *in silico* predicted signal peptide and the C-terminal RSIDELD motif via Gibson assembly (Gibson *et al.*, 2009) downstream and in frame of the coding sequence of eGFP. Instead of the RSIDELD motif, a premature stop codon was introduced. It serves the purpose of heterologous production of GST:GFP:Dld1$^{\Delta\text{RSIDELD}}$ in *E. coli* BL21(DE3)pLys.

### 4.3.6.2 Plasmids used for protein expression in *U. maydis*

**p123_Potef_Yup1_2XRFP_Cbx (Wang *et al.*, 2011)** - This plasmid was used for all plasmid constructions involving target protein expression in *U. maydis*. It contains a Cbx selection marker gene as well as the synthetic constitutive otef promoter (Potef) for protein expression in *U. maydis*. The plasmid furthermore confers ampicillin to transformed *E. coli* cells.

**p123-PIT2SP:mCherry:DLD1woSP (this study)** - This plasmid originates from p123_Potef_Yup1_2XRFP_Cbx and was generated by restriction digest with *Bam*HI and *Not*I. The DNA sequence encoding the *in silico* predicted signal peptide of Pit2 (Pit2SP; Doehlemann *et al.*, 2011) was constructed by oligonucleotide assembly, restricted by *Bam*HI and *Not*I and ligated downstream of Potef into p123_Potef_Yup1_2xRFP_Cbx. Subsequently a gene fusion of the mCherry coding sequence and *DLD1* were amplified and cloned into p123_Potef_Yup1_2XRFP_Cbx downstream and in frame with the Pit2SP via Gibson assembly (Gibson *et al.*, 2009) downstream of the Potef promoter. The plasmid serves the purpose of producing a fusion protein of Pit2SP, mCherry and Dld1 without signal peptide in *U. maydis*. This serves as a positive control in *U. maydis* secretion assay.

**p123-DLD1SP:mCherry:DLD1woSP (this study)** - This plasmid originates from p123_Potef_Yup1_2XRFP_Cbx and was generated by restriction digest with *Bam*HI and *Not*I. The DNA sequence encoding the *in silico* predicted signal peptide of Dld1 (Dld1SP) was constructed by oligonucleotide assembly, restricted by *Bam*HI and *Not*I and ligated downstream of Potef into p123_Potef_Yup1_2xRFP_Cbx. Subsequently a gene fusion of the mCherry coding sequence and *DLD1* were amplified and cloned into p123_Potef_Yup1_2XRFP_Cbx downstream and in frame with the Pit2SP via Gibson assembly (Gibson *et al.*, 2009) downstream of the Potef promoter. The plasmid serves the purpose of producing a fusion protein of Dld1SP, mCherry and Dld1 without signal peptide in *U. maydis*. It was used in a secretion assay to give evidence if *U. maydis* is able to utilize the *P. indica* originated signal peptide for efficient protein secretion.

**p123-DLD1SP:mCherry:DLD1woSP$^{\Delta RSIDELD}$ (this study)** - This plasmid originates from p123-DLD1SP:mCherry:DLD1woSP and was generated by insertion of a premature stop codon in front of the DNA sequence encoding the C-terminal RSIDELD inside *DLD1* via site-Directed mutagenesis. The plasmid serves the purpose of producing a fusion protein of Dld1SP, mCherry and Dld1 without signal peptide and RSIDELD motif in *U. maydis*. It was used in a fungal secretion assay to give evidence if *U. maydis* is able to utilize the *P. indica* originated signal peptide for efficient protein secretion and whether the RSIDELD motif had an impact on this process.

### 4.3.6.3 Plasmids used for protein expression in *P. indica*

**pGOGFP (Hilbert *et al.*, 2012)** - This plasmids is used for expression of a for *P. indica* codon optimized coding sequence of GFP (synthesized by GenScript Piscataway, NJ, USA) in *P. indica*. It contains the respective gene under the control of the *P. indica* constitutive glyceraldehyde 3-phosphate dehydrogenase promoter (Pgpd) and confers hygromycine resistance to transformed *P. indica* as well as ampicillin resistance to transformed *E. coli* cells. In this study it was used as negative control in *P. indica* fungal secretion assays.

**pGOGFP:DLD1 (this study)** - This plasmid originates from pGOGFP. Full length *DLD1* was amplified and the PCR product was restricted with *Cla*I and *Hind*III and ligated into *Cla*I / *Hind*III restricted pGOGFP, upstream and in frame with the GFP coding sequence. In this study, pGOGFP:DLD1 was used to analyze protein secretion in *P. indica.*

### 4.3.6.3 Plasmids used for protein expression in *H. vulgare*

**Pro35S::eGFP (Schweizer *et al.*, 1999) –** This plasmid was used for transient expression of GFP in barley leaves via ballistic transformation.

**P35S::mCherry (kindly provided by Prof. Kahmann, Max-Planck-Institute Marburg) –** This plasmid was used for transient expression of mCherry in barley leaves via ballistic transformation.

**P35S::DLD1$^{\Delta RSIDELD}$:mCherry:RSIDELD (this study) -** This plasmid was used for transient expression of Dld1$^{\Delta RSIDELD}$:mCherry:RSIDELD in barley leaves via ballistic transformation (particle bombardment). It originates from plasmid P35S::mCherry, where *DLD1$^{\Delta RSIDELD}$* and the RSIDELD motif were inserted up- and downstream of mCherry via Gibson assembly (Gibson *et al.*, 2009).

## 4.4 Basic microbiological methods

## 4.4.1 Transformation of *E. coli*

Preparation of competent cells was done according to Cohen *et al.* (1972) with modifications. 1 mL of an overnight culture of *E. coli* TOP10 / BL21(DE3)pLysS / Tuner(DE3)pLysS were diluted to an $OD_{600}$ of 0.5 with 100 mL of LB medium with 10 mM $MgCl_2$ and 10 mm $MgSO_4$ and grown for 16 hours at 37°C and 200 rpm shaking. Cells were pelleted at 8,000 *g* and the supernatant is discarded. The cell pellet was washed with 33 mL of ice cold RF1 solution and incubated for 60 min at 4°C. The cells were spun down for 15 min at 8,000 *g* and 4°C. Cells were resuspended in 5 mL of ice cold RF2 solution and incubated for 10 min on ice. Cells were subsequently aliquoted in 15 µL transformation reactions in 1.5 mL reaction tubes and stored at -80°C.

For transformation, aliquots were thawed on ice and mixed carefully with 30 µL of RF2 solution. 2 µL of ligation reaction was added and cells were incubated further on ice for 30 min. Subsequently cells were heat shocked at 42°C for 1 min and 500 µL of dYT medium was added. Cell were allowed to regenerate at 37°C for 1 hour at 200 rpm shaking. Afterwards cells were pelleted at 8,000 *g* for 2 min and supernatant was discarded. Cells were resuspended in 200 µL of dYT and plated on dYT plates with antibiotics. Plates were incubated at 37°C overnight.

| RF1 solution | 100 mM RbCl |
|---|---|

| | 50 mM MnCl$_2$ heptahydrate |
| --- | --- |
| | 30 mM CH$_3$CO$_2$K |
| | 10 mM CaCl$_2$ dihydrate |
| | 15% (v/v) Glycerol |
| | pH adjusted to 5.8 |
| | Filter sterilized |
| RF2 solution | 10 mM MOPS |
| | 10 mM RbCl |
| | 75 mM CaCl$_2$ dihydrate |
| | 15% (v/v) Glycerol |
| | pH adjusted to 5.8 |
| | Filter sterilized |

## 4.4.2 *U. maydis* protoplast preparation and transformation

The procedure of protoplast preparation and subsequent transformation used in this study is based on the methods published by Gillissen *et al.* (1992) and Schulz *et al.* (1990).

For protoplastation *U. maydis* SG200 sporidia were grown overnight in 4 mL YEPS$_{light}$ at 28°C with 200 rpm shaking. The culture was diluted 1:300 in 50 mL of YEPS$_{light}$ and incubated further until OD$_{600}$ ≈ 0.8. Cells were spun down at 8,000 *g* for 10 min and washed with 25 mL of SCS, spun down again and resuspended in 2 mL SCS with 2.5 mg/mL Novozyme (Osumi *et al.*, 1989; Novo Nordisc, Kopenhagen, Denmark). Cells were incubated at room temperature for 5 to 15 min and protoplastion was monitored via a light microscope. If approximately half of the cells exhibited a protoplast typical round shape, the reaction was terminated by addition of 10 mL of SCS and centrifugation for 10 min at 8,000 *g* and 4°C for 10 min. The protoplast pellet was washed thrice with 2 mL finally resuspended in 0.5 mL of cold STC. After preparation protoplasts were stored at -80°C in 70 µL aliquots.

For transformation protoplasts were thawed on ice and mixed with 10 to 15 µL of purified plasmid DNA (1 to 5 µg of total DNA), 1 µL of 15 mg/mL heparin and incubated on ice for 10 min. Afterwards 0.5 mL of STC with 40% polyethylene glycol was added followed by an incubation on ice for 15 min. The mixture was then plated on regeneration plates and incubated at 28°C for up to 6 days. Colonies were transferred to PD plates with antibiotics.

| SCS | 20 mM Sodium Citrate |
| --- | --- |
| | 1 M Sorbitol |
| | pH adjusted to 5.8 |
| STC | 100 mM CaCl$_2$ dihydrate |
| | 10 mM Tris hydrochloride |
| | 1 M Sorbitol |
| | pH adjusted to 7.5 |

### 4.4.3 *P. indica* chlamydospore collection

*P. indica* plates were incubated for up to four weeks at 28°C. Approx. 15 mL of sterile 0.002% Tween-20 was poured onto the plates and spores were harvested gently with a Drigalski spatula by stroking and pushing gently onto the surface mycelium. Afterwards surface mycelium was detached from the plate using a sharp scalpel. The spore/mycelium suspension was cleared of mycelium fragments by filtration through a sterile miracloth filter (Merck Millipore, Darmstadt). Spores were pelleted at 8,000 *g* for 7 min and washed thrice with 20 mL of 0.002% Tween-20. Spores were counted in a Neubauer improved cell counting chamber and the solution was adjusted to 500,000 spores/mL. *P. indica* spore solutions spores were directly used for protoplast preparation.

### 4.4.4 *P. indica* protoplast preparation and transformation

5 mL of a *P. indica* spore solution (concentration of 500,000 spores/mL) was diluted in 250 mL CM in a 500 mL culture flask and incubated for seven days at 28°C and 130 rpm shaking. The grown mycelium was filtered through a sterile miracloth filter and washed with 50 mL of 0.9% NaCl. Mycelium was transferred into a sterile blender (Microtron MB 550; Kinematica AG, Lucerne, Switzerland) and crushed with 60 mL of CM for 60 s. 20 mL of crushed mycelium was transferred into 130 mL of CM in a culture flask and regenerated for 3 days at 28°C and 130 rpm shaking. The regenerated mycelium was filtered through sterile miracloth filter, washed with 0.9% NaCl and transferred to a sterile 50 mL reaction tube. 20 mL of SCS with 25 mg/mL Novozmye (sterile filtered) was added and mycelium was incubated for 20 to 30 min at room temperature. Protoplast formation was monitored via a light microscope. After numerous round shaped protoplasts were visible, the reaction was stopped by addition of 20 mL of ice cold STC. Protoplasts were pelleted by centrifugation for 10 min at 4,000 *g* at 4°C and gently washed twice with 5 mL of ice cold STC. Protoplasts were resuspended in 1 mL of ice cold STC and counted with a Neubauer improved cell counting chamber. The protoplast concentration was adjusted to $10^7$ to $10^9$ protoplasts/mL and aliquoted in 70 µL for transformation.

Eight (8) to 10 µg of linearized plasmid DNA and 15 µg heparin was added to one aliquot of *P. indica* protoplasts and the mixture was incubated on ice for 10 min. Subsequently 500 µL of STC with 40% PEG and 10 U of the enzyme, which was used for plasmid linearization, was added and the mixture was incubated for 15 min on ice. The transformation mixture was then mixed with 15 mL of MYP regeneration top medium (without antibiotics, heated to not more than 40°C) and poured onto an already solidified MYP bottom regeneration medium. Plates were then incubated at 28°C for two weeks until small colonies became visible. Colonies were then picked, transferred to fresh CM plates with antibiotics and grown for two weeks at 28°C. Chlamydospores were harvested and (see section 4.4.3), diluted to 10,000 spores/mL and

3 mL were plated on a new CM plate with antibiotics to grow colonies derived from single spores. After two weeks of incubation at 28°C several colonies were selected and genomic integration of the plasmid was verified via PCR and southern blot on genomic DNA.

| | |
|---|---|
| SCS | 20 mM Sodium Citrate |
| | 1 M Sorbitol |
| | pH adjusted to 5.8 |
| STC | 50 mM CaCl$_2$ dihydrate |
| | 10 mM Tris hydrochloride |
| | 1.33 M Sorbitol |
| | pH adjusted to 7.5 |
| MYP top regeneration medium | 0.7% (w/v) Malt extract |
| | 0.1% (w/v) Peptone |
| | 0.05% (w/v) Yeast extract |
| | 0.6% (w/v) Agar |
| MYP bottom regeneration medium | 0.7% (w/v) Malt extract |
| | 0.1% (w/v) Peptone |
| | 0.05% (w/v) Yeast extract |
| | 1.2% (w/v) Agar |

## 4.5 Basic techniques of molecular biology

## 4.5.1 Manipulation of nucleic acids

### 4.5.1.1 Polymerase chain reaction (PCR)

To amplify DNA fragments for subsequent cloning steps or for analytical purposes, polymerase chain reaction was adopted from Mullis *et al.*, 1986. PCR products for subsequent cloning steps were synthesized with Easy-A High-Fidelity PCR Cloning Enzyme (Agilent Technologies, Santa Clara, USA). For analytical purposes *Taq* Polymerase (Thermo Fisher Scientific, Waltham, USA) was used. Standard reaction mixtures for both polymerases are listed below as well as typical thermocycler (TProfessional Basic, Biometra, Jena) programs, following the scheme of initial denaturation, denaturation, annealing, elongation, final elongation. Elongation time was adjusted to the size of the PCR product as well as to the synthesis capability of the polymerase. Oligonucleotide annealing temperatures were calculated *in silico* with SnapGene 3.0 (GSL Biotech, Chicago, USA).

**Easy-A High Fidelity PCR Cloning Enzyme**

|                              | Volume [µL] |
| ---------------------------- | ----------- |
| Distilled water              | to 50.0     |
| 10X Easy-A reaction buffer   | 5.0         |
| dNTPs (25 mM each NTP)       | 0.4         |
| DNA template (100 ng/µL)     | 1.0         |
| Primer #1 (100 ng/µL)        | 1.0         |
| Primer #2 (100 ng/µL)        | 1.0         |
| Easy-A polymerase (5 U/µL)   | 0.5         |
| Total reaction volume        | 50.0        |

|                       | Temperature | Duration              |            |
| --------------------- | ----------- | --------------------- | ---------- |
| **Initial denaturation** | 95°C     | 2 min                 |            |
| **Denaturation**      | 95°C        | 40 s                  |            |
| **Annealing**         | *in silico* | 30 s                  | 30 Cycles  |
| **Elongation**        | 72°C        | 1 min / 1 kb product size |        |
| **Final Elongation**  | 72°C        | 7 min                 |            |

**Taq Polymerase**

|                              | Volume [µL] |
| ---------------------------- | ----------- |
| Distilled water              | to 50.0     |
| 10X *Taq* reaction buffer    | 5.0         |
| 25 mM MgCl$_2$               | 8.0         |
| dNTPs (2 mM each NTP)        | 5.0         |
| DNA template (100 ng/µL)     | 1.0         |
| Primer #1 (100 µM)           | 0.5         |
| Primer #2 (100 µM)           | 0.5         |
| *Taq* polymerase (5 U/µL)    | 0.25        |
| Total reaction volume        | 50.0        |

|                       | Temperature | Duration              |            |
| --------------------- | ----------- | --------------------- | ---------- |
| **Initial denaturation** | 95°C     | 3 min                 |            |
| **Denaturation**      | 95°C        | 30 s                  |            |
| **Annealing**         | *in silico* | 30 s                  | 30 Cycles  |
| **Elongation**        | 72°C        | 1 min / 1 kb product size |        |
| **Final Elongation**  | 72°C        | 10 min                |            |

## 4.5.1.2 Restriction of DNA

Type II restriction endonucleases used for restriction of DNA molecules were exclusively purchased from New England Biolabs (NEB; Frankfurt/Main). The reactions were incubated at temperatures depending on the enzyme(s) used from 1 hour up to 16 hours. A standard restriction mixture is given below.

| | |
|---|---|
| Distilled water | to 20.0 µL |
| DNA | 0.5 to 5.0 µg |
| Specific 10X NEB buffer | 2.0 µL |
| 100X BSA | 0.2 µL |
| Restriction endonuclease | 0.5 U |
| Total reaction volume | 20.0 µL |

## 4.5.1.3 Ligation of DNA fragments

DNA fragments regenerated by endonuclease restrictions were ligated using T4 DNA ligase (Thermo Fisher Scientific, Waltham, USA). A standard ligation mixture is given below:

| | |
|---|---|
| Distilled water | to 20.0 µL |
| Vector backbone DNA | 50.0 ng |
| Insert DNA | 3X molar excess |
| 10X T4 DNA ligase buffer | 2.0 µL |
| T4 DNA ligase (5 U/µL) | 1.0 µL |
| Total reaction volume | 20.0 µL |

## 4.5.1.4 Site directed mutagenesis

Site directed mutagenesis was executed with QuikChange Multi Site-Directed Mutagenesis Kit (Stratagene, Lajolla, USA) as described per manufacturer's instructions.

## 4.5.1.5 Sequencing of nucleic acids

All newly generated DNA molecules were sequenced at MWG (Martinsried) according to chain termination sequencing method (Sanger *et al.*, 1977).

## 4.5.2 Isolation and extraction of nucleic acids

### 4.5.2.1 Plasmid DNA isolation from *E. coli*

Plasmid DNA was isolated from *E. coli* using QIAprep Spin Miniprep or Midiprep Kits (Qiagen, Hilden) as described per manufacturer's instructions, depending on the amount of plasmid DNA to be isolated.

### 4.5.2.2 Genomic DNA extraction from *U. maydis*

Genomic DNA extraction from *U. maydis* was conducted as per modified protocol from Hoffman and Winston (1987). Cells of a 2 mL of *U. maydis* overnight culture were pelleted at

17.000 $g$ for 2 min and the supernatant was discarded. 400 µL of lysis buffer, 500 µL Phenol/Chloroform and 300 µL of glass beads (0.4 to 0.6 mm; Sartorius, Göttingen) were added and cells were lysed for 20 min by rigorous shaking on a Vibrax-VXR shaker (IKA, Staufen) at 2500 rpm. Subsequently the samples were centrifuged at 17,000 $g$ for 15 min, the upper phase was transferred into a new reaction tube and mixed with 1 mL of 100% ethanol for precipitation. DNA was pelleted by centrifugation at 17,000 $g$ for 2 min and supernatant was discarded. The DNA pellet was air dried for 5 min at solved in 60 µL TE buffer with 20 µg/mL RNase A. For RNA digestion the samples were incubated for 10 min at 55°C under light shaking. Extracted DNA was stored at -20°C.

| Lysis buffer | 50 mM Tris hydrochloride |
| --- | --- |
| | 50 mM Na$_2$-EDTA |
| | 1% (w/v) SDS |
| | pH adjusted to 7.5 |
| Phenol/Chloroform | 50% (v/v) Phenol (equilibrated with TE buffer) |
| | 50 (v/v) Chloroform |
| TE buffer | 10 mM Tris hydrochloride |
| | 1 mM Na$_2$-EDTA (pH 8) |

### 4.5.2.3 Genomic DNA extraction from *P. indica*

For isolation of genomic DNA from *P. indica*, mycelium from a liquid culture grown for 10 days was filtered through miracloth filter (Merck Millipore, Darmstadt) and frozen in liquid nitrogen. The mycelium was then ground to fine powder using a liquid-nitrogen-cooled mortar and pistil. Approximately 200 mg of mycelium powder was transferred to a liquid-nitrogen-cooled 2 mL reaction tube, mixed with 1 mL of extraction buffer and incubated for 10 min at room temperature under light shaking. Subsequently 1 mL of CIA was added and the samples were incubated for another 5 min at room temperature. Afterwards the samples were centrifuged for 20 min at 17,000 $g$, the upper aqueous phase was transferred into a fresh 2 mL reaction tube and 200 µL of 100% ethanol were added. After incubation for 5 min at room temperature under light shaking 1 mL of CIA was added and samples were incubated for another 5 min at room temperature. Samples were then centrifuged for 20 min at 17,000 $g$ and the aqueous phase was transferred to a fresh 2 mL reaction tube. Genomic DNA was precipitated by addition of 1 mL of 100% isopropanol and incubation overnight at 4°C. Subsequently DNA was pelleted by centrifugation for 30 min at 17,000 $g$. The pellet was washed twice with 900 µL ice-cold 70% ethanol, air dried for 5 min and then resolved in 50 µL double distilled water. 1 µL of RNase A (10 mg/mL pH 7.4) was added and RNA was digested at 37°C for 60 min. Extracted DNA was stored at -20°C.

| Extraction buffer | 100 mM Tris hydrochloride (pH 7.5) |
| --- | --- |
| | 50 mM Na$_2$-EDTA (pH 8) |

|                                          | 1% (w/v) SDS              |
|                                          | pH adjusted to 7.5        |
| CIA (Chloroform, isoamyl alcohol)        | 24 vol. Chloroform        |
|                                          | 1 vol. isoamyl alcohol    |

## 4.5.3 Separation and detection of nucleic acids

### 4.5.3.1 Agarose gel electrophoresis

Depending on the size of the expected restriction fragments, PCR products or plasmids, agarose concentration in gels was varied between 0.8% and 2%. Agarose (Biozym, Hessisch Oldendorf) was solved in TAE buffer by cooking in a microwave. After the solution had cooled to approximately 60°C, ethidium bromide (Roth, Karlsruhe) to a final concentration of 50 ng/L was added. Nucleic acid separation was performed in an electrophoresis chamber filled with TAE buffer above the gel surface and a power supply at 90 V for 30 to 40 min. Prior to loading nucleic acid samples were mixed with the respective loading dye and carefully filled into the pockets of the solidified gel. Bands were observed under UV light with TS imaging system (Biometra, Göttingen).

| 50X TAE buffer       | 2 M Tris hydrochloride        |
|                      | 2 M Acetic acid               |
|                      | 50 mM EDTA                    |
|                      | pH adjusted to 8              |
| 6X DNA loading dye   | 40% (w/v) Sucrose             |
|                      | 0.25% (w/v) Bromphenolblue    |
| 6X RNA loading dye   | 50 mM MOPS                    |
|                      | 50% (w/v) Sucrose             |
|                      | 0.25% (w/v) Bromphenolblue)   |
|                      | 0.25% (w/v) Xylencyanol FF    |
|                      | pH adjusted to 7.5            |

### 4.5.3.2 Southern blot

Five (5) µg of extracted *U. maydis* or *P. indica* genomic DNA was digested with a suitable restriction endonuclease. Subsequently the DNA was precipitated by addition of 1/10 volume of 3 M potassium acetate and 3 volumes of 100% ethanol. After incubation at room temperature for 5 min, DNA was pelleted by centrifugation for 5 min at 17.000 *g* and the supernatant was discarded. The Pellet was washed with 750 mL of 80% ethanol, air dried for 5 min and resolved in 20 µL of 1X DNA loading dye. DNA fragments were then separated on a 0.8% agarose/TAE gel and transferred onto a nylon membrane (Hybond-N+; GE Healthcare, Uppsala, Sweden) according a protocol modified from Southern (1975). The agarose gel was incubated for 15 min in 0.25 N hydrochloric acid followed by 15 min neutralization in 0.4 N sodium lye. The DNA fragments were transferred overnight in 0.4 N sodium lye, which was sucked from a reservoir through the agarose gel and the Nylon membrane by capillary force

emanating from a stack of papers on top of the assembly. After completion of the transfer, the DNA fragments were immobilized on the membrane via standard UV crosslinking (UVC 500 UV Crosslinker, Amersham Life Science). The membrane was subsequently incubated in a hybridization glass tube with 20 mL southern hybridization buffer for 2 hours at 65°C in a hybridization oven (UVP HB-1000 Hybridizer, Cambridge, UK) for prehybridization. DNA fragments were detected via Digoxygenin labelled DNA probes which were amplified with the PCR DIG labelling mix kits (Roche, Mannheim) as per manufacturer's instructions and denatured by at 100°C for 10 min before use. Probes were diluted in 40 mL hybridization buffer and incubated with the membrane at 65°C overnight. Afterwards the hybridization buffer with the probe was discarded and the membrane was washed twice for 15 min with 40 mL of wash buffer at 65°C. All following steps were conducted at room temperature. The membrane was incubated for 5 min with DIG wash buffer followed by a 30 min incubation with DIG buffer 2. Subsequently the membrane was incubated for 30 min with DIG antibody solution. To strip the membrane of surplus antibody, the membrane was washed twice for 15 min with DIG wash buffer followed by 5 min wash step with DIG buffer 3. Antibody substrate CDP star (Roche, Basel, Switzerland) was diluted 1:100 in DIG buffer 3 and the membrane was incubated for 5 min with substrate solution. Afterwards the membrane was sealed in plastic foil and incubated for 15 min at 37°C. A light-sensitive film (Kodak X-Omaz XAR-5; Rochester, USA) was exposed to the membrane depending on the signal intensity for a duration between 1 and 30 min. The film was developed in a respective machine (QX-60; Konica, Osaka, Japan).

| | |
|---|---|
| 1 M sodium phosphate buffer | Solution 1: 1 M $Na_2HPO_4$ |
| | Solution 2: 1 M $NaH_2PO_4$ hydrate |
| | Start with solution 1 and add solution 2 until pH 7 is reached |
| Hybridization buffer | 500 mM Sodium phosphate buffer, pH 7 |
| | 7% (w/v) SDS |
| Wash buffer | 0,1 M Sodium phosphate buffer, pH 7 |
| | 1% (w/v) SDS |
| DIG buffer 1 | 0.1 M Maleic acid, pH 7.5 |
| | 0.15 M NaCl |
| DIG buffer 2 | 1% (w/v) milk powder solved in DIG buffer 1 |
| DIG buffer 3 | 0.1 M Maleic acid, pH 9.5 |
| | 0.1 M NaCl |
| | 0.05 M $MgCl_2$ |
| DIG wash buffer | 0.1 M Maleic acid, pH 7.5 |
| | 0.15 M NaCl |
| | 0.3% (v/v) Tween-20 |

| CPD star solution | 100 µL CPD Star (Roche, Mannheim) in 10 mL DIG buffer 3 |
|---|---|

## 4.6 Biochemical methods

### 4.6.1 Separation and detection of proteins

Proteins were separated by standard discontinuous SDS-PAGE described by Laemmli (1970). Prior to separation, proteins were denatured in 1X SDS sample loading dye containing 100 mM dithiothreitol (DTT) at 100°C for 5 min. For separation the Mini Protean System (BioRad, Hercules, USA) was used. Gels consisted of an upper, approximately 1.5 cm high stacking gel with 5% polyacrylamide content, which results to stacking of proteins with similar molecular weight resulting in sharper bands after separation and staining. Polyacrylamide content of the lower, approximately 8.5 cm high separation gel, was varied between 10% and 15% depending on the nature of the protein samples to be separated. Standard SDS running buffer was used for electron transfer at 120 to 160 V for 1 hour. Gel staining and protein visualization was done with Instant Blue® Coomassie-based straining (Expedeon, Swavesey, United Kingdom) according to manufacturer's protocol.

| 6X SDS sample loading dye | 4 M Tris hydrochloride, pH 6.8 |
|---|---|
| | 6% (w/v) SDS |
| | 0.15% (w/v) Bromphenolblue |
| | 60% (v/v) Glycerol |
| Stacking gel | 5% (v/v) Acrylamide |
| | 0.1% (w/v) SDS |
| | In 125 mM Tris hydrochloride, pH 6.8 |
| | 0.1% (w/v) Ammonium persulfate |
| | 0.05% (v/v) Tetramethylethlyenediamine |
| Separation gel | 10-15% (v/v) Acrylamide |
| | 0.1% (w/v) SDS |
| | In 375 mM Tris hydrochloride, pH 8,8 |
| | 0.1% (w/v) Ammonium persulfate |
| | 0.05% (v/v) Tetramethylethlyenediamine |
| SDS running buffer | 25 mM Tris-HCl, pH 8.3 |
| | 192 mM Glycin |
| | 4 mM SDS |

### 4.6.2 Protein detection via immunoblot (Western Blot)

Proteins separated during SDS-PAGE were transferred onto a nitrocellulose membrane by semi-dry blotting with Fastblot B33 (Core Life Sciences, Irvine, USA) according to manufacturer's protocol. In order to ensure complete transfer, 3 mm thick Whatman paper was soaked in transfer buffer and placed on the protein anode. The nitrocellulose membrane was briefly washed in distilled water and then soaked in transfer buffer as well and placed on top

of the Whatman paper. Protein gels were prepared for protein transfer by incubation in transfer buffer for 10 min and placed on top of the nitrocellulose membrane. A second in transfer buffer soaked Whatman paper was placed on top of the gel, completing the sandwich assembly. After addition of each layer a plastic pipette was used to remove air bubbles between the different layers of the sandwich assembly. After closing the blotting apparatus with the cathode lid, proteins were transferred from the gel onto the nitrocellulose membrane for 1 hour at 100 mA/gel. To avoid background noise and unspecific signals, the membrane was incubated for 1 hour in blocking solution on a rotary shaker and subsequently washed thrice in TBS-T for 5 min. Subsequently, the membrane was incubated in blocking buffer diluted 1/10 with TBS-T with addition of a specific primary antibody (**Table 7**) for 1 hour. To minimize unspecific signals the membrane was again washed thrice with TBS-T for 5 min. Depending on the primary antibody used the membrane was incubated for 1 hour with a secondary antibody coupled with a HRP conjugate diluted in blocking buffer diluted 1/10 with TBS-T. After three additional washes with TBS-T for 5 min, the membrane was incubated for 5 min with SuperSignal Pico Detection reagent (Thermo Fisher Scientific, Waltham, USA). Light signals were detected by exposition of light sensitive films (Kodak X-Omaz XAR-5) for up to 1 hour, depending on signal strength. Films were developed with QX-60 developing apparatus (Konica, Marunochi, Japan).

| Transfer buffer | 25 mM Tris-HCl |
| --- | --- |
|  | 192 mM Glycine |
|  | 15% (v/v) Methanol |
|  | pH adjusted to 10.4 |
| TBS-T | 50 mM Tris-HCl |
|  | 150 mM NaCl |
|  | pH adjusted to 7.5 |
|  | 0.1% (v/v) Tween-20 |
| Blocking buffer | 5% (w/v) milk powder in TBS-T |

**Table 7: Primary and secondary antibodies used in this study.**

| Antibody | Produced in | Dilution | Manufacturer |
| --- | --- | --- | --- |
| anti-GFP | Mouse | 1:1,000 | Cell Signalling Technology (Danver, USA) |
| anti-mCherry | Rabbit | 1:1,000 | Clontech Laboratories (Mountain View, USA) |
| anti-GST | Rabbit | 1:1,000 | Sigma Aldrich (Taufkirchen, Germany) |
| anti-Dld1 | Rabbit | 1:1,000 | Eurogentec (Seraing, Belgium) |
| anti-Mouse | Rabbit | 1:10,000 | Sigma Aldrich (Taufkirchen, Germany) |

| anti-Rabbit | Goat | 1:2,000 | Sigma Aldrich (Taufkirchen, Germany) |

### 4.6.3 Protein visualization via Coomassie based InstantBlue® staining

For visualization of proteins after SDS-PAGE, gels were submerged and incubated in InstantBlue® (Expedeon; Swavesey, Great Britain) staining solution for 15 min.

### 4.6.4 Determination of protein concentration

### 4.6.4.1 Determination of protein concentration via Bradford assay

Concentration of complex protein mixtures (e. g. total cell lysates) was determined after Bradford (1976). Standard curve was prepared with BSA.

### 4.6.4.2 Determination of protein concentration via absorption coefficient

Since accurate concentration determination after Bradford (1976) heavily relies on the likeliness of amino acid composition between the protein used for the standard curve and the protein or protein mixture for which the concentration is to be determined, the method was not deemed accurate enough for determining concentration of purified proteins. Therefore molar absorption coefficient at 280 nm ($\varepsilon$) was determined with ExPASy ProtParam tool (Gasteiger *et al.*, 2003) using amino acid sequence of the respective purified protein. Subsequenttly, $A_{280}$ of protein solution was determined with a NanoDrop 1000 Spectrophotometer (Thermo Fisher Scientific, Waltham, USA) in technical triplicates and the protein concentration was calculated.

### 4.6.5 Heterologous expression and purification of proteins from *E. coli*

Plasmids pRSET-GST:DLD1woSP, pRSET-GST:DLDwoSP$^{H103A,H107A}$, pRSET-GST:DLD1woSP$^{\Delta RSIDELD}$, pRSET-GST:EGFP, pRSET-GST:EGFP:DLD1woSP, PRSET-GST-EGFP-DLD1woSP$^{H107A,}$ pRSET-GST:EGFP:DLD1woSP$^{H103A,H107A}$ and pRSET-GST:EGFP:DLD1woSP$^{\Delta RSIDELD}$ were transformed into *E. coli* BL21(DE3)pLysS chemo-competent cells (Promega Cooperation, Madison, USA). An overnight culture of respective strains in dYT medium supplemented with 100 µg/mL Ampicillin and 34 µg/mL Chloramphenicol was diluted 1:100 in 1 L of dYT supplemented with 100 µg/mL Ampicillin and 34 µg/mL Chloramphenicol in a 5 L culture flask. Cells were grown at 37°C and 200 rpm shaking to and $OD_{600}$ of 0.7 to 0.9. Subsequently protein expression was induced by addition of 1 mM of IPTG. After induction, cells were shifted to 20°C and further grown for 16 hours at 200 rpm. Cells were harvested by centrifugation for 30 min at 8000 *g* and 4°C (Rotor: SLA-3000, Sorvall LYNX 4000 Superspeed Centrifuge; Thermo Fisher Scientific, Waltham, USA). Cells harvested from 1 L culture volume were solved in 100 mL of lysis buffer, aliquoted in approximately 6X 20 mL and frozen at -20°C for at least 1 hour. After thawing for 1 hour at room temperature, cells were lysed by French Press at 16,000 psi in three subsequent runs (SimAminco French Pressure Cell Press FA078; SLM Instruments, Urbana, USA). Cell lysate

was cleared of cell debris by centrifugation for 30 min at 20,000 *g* and 4°C (Rotor: 22-34, Sorvall LYNX 4000 Superspeed Centrifuge; Thermo Fisher Scientific, Waltham, USA). Supernatant was applied to a gravity flow column (Pierce™ Centrifuge Columns 10 mL; Thermo Fisher Scientific, Waltham, USA) loaded with 1.2 mL matrix of glutathione sepharose 4B (GE Healthcare, Uppsala, Sweden). Column matrix was subsequently washed three times with 10 mL TBS and, depending desired elutionmethod either washed once with 5 mL glutathione elution buffer for protein elution with GST tag, or once with 10 mL of PreScission Cleavage buffer for GST tag cleavage. Cleavage of the GST tag and release of protein from column matrix was performed by incubating the column matrix with 2 mL of cleavage solution for 16 hours at 4°C. The flow through was collected along with two further washes of 2 mL of PreScission Cleavage buffer. Elution fractions were concentrated with Amicon Ultra-4 centrifugal filters (Millipore/Merck, Darmstadt, Germany) with a molecular weight cut-off of 3000 Da to a final volume of approximately 2 mL. The concentrated elution fractions were filtered through a 0.22 µm filter and separated through gel filtration in an ÄKTA pure system with HiLoad 16/600 Superdex 200 pg column (GE Healthcare, Uppsala, Sweden) equilibrated with TBS. Separate peaks of fusion protein were verified and checked for purity via SDS PAGE. Corresponding fractions were pooled and concentrated with Amicon Ultra-4 centrifugal filters to final volume of 500 µL and stored at 4°C for up to 1 week. Protein stability was verified prior to each experiment via SDS PAGE.

| Lysis buffer | 50 mM Tris-HCl |
| --- | --- |
|  | 150 mM NaCl |
|  | 500 mM EDTA |
|  | 1% (v/v) Triton X-100 |
|  | 100 µM PMSF |
|  | pH adjusted to 7.5 |
| TBS | 50 mM Tris-HCl |
|  | 150 mM NaCl |
|  | pH adjusted to 7.5 |
| Glutathione Elution Buffer | 10 mM reduced Glutathione in TBS |
| PreScission Cleavage buffer | 1 mM EDTA |
|  | 1 mM DTT |
|  | in TBS |
| Cleavage solution | 4% (v/v) PreScission® Protease (GE , Uppsala, Sweden) |
|  | in PreScission Cleavage buffer |

## 4.6.6 Determination of oligomeric state by calibrated gel filtration run

Gel filtration column HiLoad 16/600 Superdex 200 pg (GE Healthcare, Uppsala, Sweden) was used with an ÄKTA pure FPLC system (GE Healthcare, Uppsala, Sweden). Calibration of

column was performed with gel filtration Low Molecular Weigth calibration kit (GE Healthcare, Uppsala, Sweden). Partition coefficient ($K_{av}$) was calculated by dividing total column bed volume (120 mL) by peak absorbance retention volume of respective protein ($V_e$). $K_{av}$ was plotted against logarithm of molecular weight (logMw) of respective proteins. A standard curve was compiled with resulting data points.

| Protein | MW [Da] | lgMW | Retention Volume [mL] | Kav |
|---|---|---|---|---|
| Conalbumin | 75000 | 4.88 | 52.76 | 0.43 |
| Carbonic Anhydrase | 29000 | 4.46 | 65.80 | 0.53 |
| Ribonuclease A | 19700 | 4.29 | 78.40 | 0.63 |
| Aprotinin | 6500 | 3.81 | 92.32 | 0.74 |
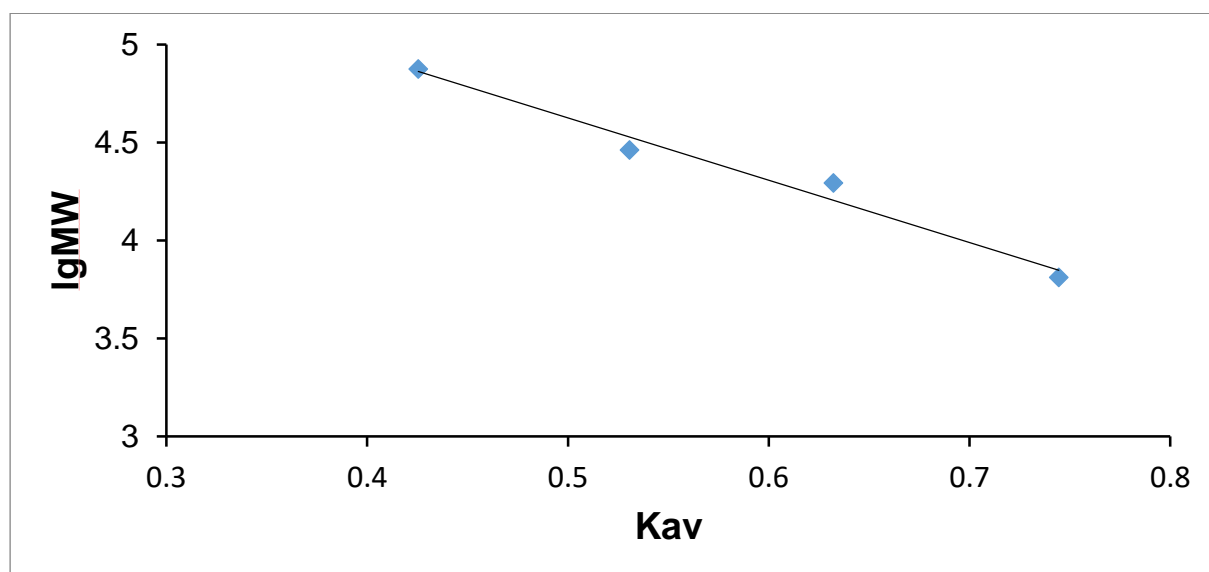


By linear regression a trend line with the formula $y = 1635.8 \cdot e^{-0.059x}$ was determined. This formula was used to calculate the molecular weight from peak absorbance retention volumes.

## 4.6.7 Circular dichroism spectroscopy

For secondary structure measurements, CD spectra were recorded from 208 to 240 nm and the buffer baselines were subtracted with a JASCO J-810 spectropolarimeter or at 20°C with a JASCO J-700 spectropolarimeter. To assay pH dependent stability, 10 µM protein was measured in the respective CD buffer (see below). When indicated, protein samples were preincubated with different metal ions (1 mM). Spectra were recorded in a 1 mm cuvette with a data pitch of 1 nm and a response time of 5 s. Ten (10) individual spectra were averaged.

| | |
|---|---|
| CD buffer pH 7.5 | 50 mM MOPS |
| | 100 mM NaCl |
| | pH adjusted to 7.5 |
| CD buffer pH 6/5/4 | 50 mM MES |
| | 100 mM NaCl |

| | pH adjusted to 6/5/4 |
|---|---|
| CD buffer $Fe^{3+}$ | 50 mM MES |
| | 150 mM NaCl |
| | pH adjusted to 6 |

## 4.6.8 Protein x-ray crystallization

Crystallization trials were performed at 295 K in 96-well sitting-drop vapor-diffusion plates with 50 µl of crystallization reservoir solution and drops consisting of 300 nL Dld1 solution concentrated to 17 mg/mL in crystallization buffer and 300 nL crystallization reservoir solution. For experimental phasing and cryo-protection, single crystals were soaked overnight in a droplet containing reservoir solution supplemented with zinc acetate/PEG solution before loop-mounting and flash-cooling in liquid nitrogen. Data were collected at a wavelength of 1 Å at beamline X10SA (PXII) at the Swiss Light Source (Paul Scherrer Institute, Villigen, Switzerland) at 100 K using a PILATUS 6M detector (DECTRIS). Diffraction images were processed and scaled using the XDS program suite (Kabsch, 1993). Using SHELXD (Sheldrick, George M, 2008), a single strong $Zn^{2+}$ site was identified. After density modification with SHELXE, the resulting electron density map could be traced by Buccaneer (Cowtan, 2006) to a large extent, revealing one protein chain in the asymmetric unit. The model was completed by cyclic manual modeling with Coot (Emsley & Cowtan, 2004) and refinement with Refmac5 (Murshudov *et al.*, 1999). Analysis with Procheck (Laskowski *et al.*, 1996) attested an excellent geometry with all residues in the allowed regions of the Ramachandran plot (Ramachandran *et al.*, 1963).

| Protein crystallization buffer | 30 mM MOPS |
|---|---|
| | 150 mM NaCl |
| | pH adjusted to pH 7.4 |
| Crystallization reservoir solution | 200 mM ammonium sulfate |
| | 100 mM sodium citrate |
| | 15% (w/v) PEG 4000 |
| | pH adjusted to 5.6 |
| Zinc acetate/PEG solution | 10 mM zinc acetate |
| | 15% (v/v) PEG 400 |

## 4.7 Biophysical determination of protein / metal ineraction

### 4.7.1 Immobilized metal affinity chromatography

Concentrated purified protein solutions were dialyzed in ZelluTrans dialysis tubing with 3.5 kDa molecular weight cut off (Roth, Karlsruhe, Germany) for 16 hours at 4°C under constant stirring with 5 L of either TBS, MES or acetate binding buffer. 30 µg of protein diluted in 300 µL of respective binding buffer (depending of the pH analyzed) were applied to Pierce™ Spin Columns – Screw Cap (Thermo Fisher Scientific, Waltham, USA) with 120 µL matrix of

Chelating Sepharose Fast Flow (GE, Uppsala, Sweden) loaded with either $Cu^{2+}$, $Ni^{2+}$, $Zn^{2+}$, $Fe^{3+}$ or $Fe^{2+}$ as per manufacturer's instructions. Protein solutions were incubated with column matrix for 2 hours at 4°C. The flow through was collected by centrifugation at 500 $g$ for 2 min and the column matrix was washed five times with 300 µL of the respective binding buffer. Bound proteins were eluted by washing twice with 300 µL of the respective binding buffer with 500 mM imidazole. Proteins in flow through, wash and elution fractions were precipitated by standard acetone precipitation and analyzed via SDS PAGE.

| TBS binding buffer | 50 mM Tris-HCl |
| --- | --- |
| | 150 mM NaCl |
| | pH adjusted to 7.5 |
| MES binding buffer | 50 mM MES |
| | 150 mM NaCl |
| | pH adjusted to 6 |
| Acetate binding buffer | 50 mM sodium acetate |
| | 150 mM NaCl |
| | pH adjusted to 6 |
| Elution buffers | TBS, MES or acetate binding buffer with addition of 500 mM imidazole |

## 4.7.2 Microscale Thermophoresis

Concentrated purified protein solutions were dialyzed in ZelluTrans dialysis tubing with 3.5 kDa molecular weight cut off (Roth, Karlsruhe, Germany) for 16 hours at 4°C under constant stirring with 5 L of MST buffer. Ligand solutions were prepared freshly before each measurement by solving $ZnCl_2$, $CuCl_2$, ferric citrate or Cellohexaose in buffer dialysate. 100 nM of protein were mixed with a range of ligand concentrations in a volume of 20 µL, incubated for 5 min at room temperature and transferred into MST Premium coated capillaries. Fluorescence during thermophoresis was measured with the Nanotemper Monolith NT.115 (Nanotemper Technologies, Munich, Germany) at a laser power of 30%. Resulting thermophoresis data were analyzed with the NTAnalysis software (Nanotemper Technologies, Munich, Germany).

| MST buffer | 50 mM HEPES |
| --- | --- |
| | 150 mM NaCl |
| | 0.05% (v/v) Tween-20 |
| | pH adjusted to 7.5 |

## 4.7.3 Isothermal titration calorimetry

Concentrated purified protein solutions were dialyzed in ZelluTrans dialysis tubing with 3.5 kDa molecular weight cut off (Roth, Karlsruhe, Germany) for 16 hours at 4°C under constant stirring with 5 L of ITC buffer and diluted to 100 µM final concentration. Ligand solutions were freshly prepared before each ITC measurement by solving $FeCl_3$ in the buffer dialysate. ITC

measurements were performed in a MicroCal iTC 200 system (Malvern Instruments, Malvern, UK) with the following parameters: Total number of injections: 20, cell temperature: 25°C, reference power (µcal/s): 10, initial delay: 60 s, syringe (ligand) concentration: 4 mM, cell (protein) concentration: 0.2 mM, stirring speed: 1000 rpm, injection volume: 2 µL (0.4 µL for first injection), duration of injection: 4 s (0.8 s for first injection), spacing: 150 s, filter period: 5 s. Every ITC run with protein was followed by injection of ligand into buffer, buffer into protein and buffer into buffer, both as control measurements. Resulting thermograms were analyzed with Origin based MicroCal software (MicroCal Inc., Northampton, USA).

| ITC buffer | 50 mM sodium acetate |
|---|---|
| | 150 mM NaCl |
| | pH adjusted to 5 |

## 4.8. Other biochemical assays

## 4.8.1 DAB oxidation assay

Concentrated purified protein solutions were dialyzed in ZelluTrans dialysis tubing with 3.5 kDa molecular weight cut off (Roth, Karlsruhe, Germany) for 16 hours at 4°C under constant stirring with 5 L of DAB assay buffer pH 6 or DAB assay buffer pH 5. DAB, HRP, $FeCl_3$ and $H_2O_2$ stocks were prepared with $ddH_2O$ just prior to each measurement. Measurements were carried out in a total volume of 200 µL in white Greiner high and medium binding 96-well plates with micro-clear bottom (Sigma-Aldrich, Taufkirchen, Germany). Final concentrations of the reagents: $FeCl_3$=20 µM, HRP=5µg, $H_2O_2$=100 µM, Dld1=0.5 to 10 µM, DAB = 50 µM. For HRP catalyzed reaction, protein, HRP and DAB were mixed and incubated at RT in a 96-well-plate for 10 min and $H_2O_2$ was added manually. For metal catalyzed DAB oxidation assays, Dld1, metal and $H_2O_2$ were mixed and incubated at RT in the 96-well-plate for 10 min. DAB solution was injected and the oxidation was monitored by absorbance increase at 460 nm over 5 hours (Infinite® 200 PRO, Tecan, Männedorf, Switzerland).

| DAB assay buffer pH 6 | 50 mM MES |
|---|---|
| | 150 mM NaCl |
| | pH adjusted to 6 |
| DAB assay buffer pH 5 | 50 mM Sodium acetate |
| | 150 mM NaCl |
| | pH adjusted to 5 |

## 4.8.2 Prussian Blue assay

Concentrated purified protein solutions were dialyzed in ZelluTrans dialysis tubing with 3.5 kDa molecular weight cut off (Roth, Karlsruhe, Germany) for 16 hours at 4°C under constant stirring with 5 L of Prussian Blue assay buffer. $FeCl_3$, hemin and DFO stocks were prepared with buffer dialysate just prior to each measurement. Measurements were carried out in a total volume of

100 μL in white Greiner high and medium binding 96 well plates with micro-clear bottom (Sigma-Aldrich, Taufkirchen, Germany). Final concentrations of the reagents: $FeCl_3$=20 μM, DFO=50μM, Dld1=30 to 50 μM. Reagents were mixed and incubated in 96 well plate at room temperature for 10 min prior to measurement. 100 μL of Prussian Blue staining solution (Iron Stain Kit, Sigma-Aldrich, Taufkirchen, Germany) was added and the $A_{680}$ was measured with in a microplate reader (Infinite® 200 PRO, Tecan, Männedorf, Schweiz).

| Prussian Blue assay buffer | 50 mM Sodium acetate |
|---|---|
| | 150 mM NaCl |
| | pH adjusted to 5 |

### 4.8.3 Protein crosslinking with formaldehyde

This method was adapted from Klockenbusch & Kast (2010). Concentrated purified protein solutions were dialyzed in ZelluTrans dialysis tubing with 3.5 kDa molecular weight cut off (Roth, Karlsruhe, Germany) for 16 hours at 4°C under constant stirring with 5 L of protein crosslinking assay buffer. 20 μM protein were diluted in 120 μL reaction volume and incubated at room temperature for 20 min. Afterwards 12.9 μL of a 37.9% (w/v) paraformaldehyde solution was added (final concentration of formaldehyde: 4%), samples were mixed gently and incubated for up to 60 min. Every 5 min, 20 μL samples were transferred to a new 1.5 mL reaction tubes and 5 μL of 5X SDS sample buffer was added. Samples were not cooked prior to SDS PAGE, as this would dissolve potential crosslinks.

| Protein crosslinking assay buffer | 50 mM MES |
|---|---|
| | 150 mM NaCl |
| | pH adjusted to 6 |

### 4.8.6 Polysaccharide binding assay

Concentrated purified protein solutions were dialyzed in ZelluTrans dialysis tubing with 3.5 kDa molecular weight cut off (Roth, Karlsruhe, Germany) for 16 hours at 4°C under constant stirring with 5 L of sterile distilled water. Commercially available polysaccharides cellulose, xylan and chitin (Sigma Aldrich, Taufkirchen, Germany) were ground to fine powder in a mortar for 1 min. 20 mg of polysaccharide powder was transferred to a fresh 1.5 mL reaction tube. 400 μL of sterile distilled water was added and samples were sonicated for 1 min (duty cycle 30%, output control 5; Branson Sonifier 250; Branson Ultrasonics, Danbury, USA). Samples were centrifuged at 17,000 *g* for 1 min and supernatant was discarded. 200 μL of 10 μM protein solution and 400 μL of sterile distilled water was added and reactions were incubated for 1 hour at room temperature on rotary shaker. Polysaccharides were pelleted by centrifugation at 17,000 *g* for 1 min and supernatant was transferred to fresh 1.5 mL reaction tube. 500 μL of 40% (w/v) trichloroacetic acid and 500 μL 100% acetone was added to supernatant and samples were incubated for at room temperature for 1 hour for protein precipitation. After incubated precipitated proteins were pelleted by centrifugation at 17,000 *g* for 30 min and was

with 1 mL of ice cold 100% acetone. Pellet was air dried for 5 min and boiled at 95°C for 10 min after addition of 100 µL 1X SDS sample buffer. Polysaccharide pellets were washed thrice with sterile distilled water and boiled at 95°C for 10 min after addition of 100 µL 1X SDS sample buffer. 15 µL of polysaccharide and supernatant protein preparations were used in SDS PAGE.

## 4.8.7 GST pulldown assay

Concentrated purified GST fusion protein solutions were dialyzed in ZelluTrans dialysis tubing with 3.5 kDa molecular weight cut off (Roth, Karlsruhe, Germany) for 16 hours at 4°C under constant stirring with 5 L of GST pulldown assay buffer pH 6 and pH 7.5. 250 µL of Glutathione Sepharose 4B (GE Healthcare, Uppsala, Sweden) was applied to Pierce™ Spin Columns – Screw Cap (Thermo Fisher Scientific, Waltham, USA) and washed three times with 500 µL of sterile distilled water by centrifugation at 500 $g$ for 2 min. Twenty (20) µg of GST or GST fusion protein solution in a total volume of 500 µL was added to column matrix. The column was sealed and incubated for 30 min at room temperature on a rotary shaker. Flow through was collected by centrifugation at 500 $g$ for 2 min and columns were washed twice with 500 µL of GST pulldown assay buffer. Ten (10) µg of HRP (Sigma-Aldrich, Taufkirchen, Germany), solved in 500 µL of GST pulldown assay buffer, were added to column matrix. The column was sealed and incubated for 30 min at room temperature on a rotary shaker. Flow through was collected by centrifugation at 500 $g$ for 2 min and columns were washed thrice with 500 µL of GST pulldown assay buffer. Bound proteins on matrix were eluted by addition of 500 µL GST pulldown buffer supplemented with 10 mM reduced glutathione. All collected fractions (flow through, wash and elution) were precipitated by addition of 1 mL of 100% acetone and incubation at -20°C for 16 hours. Precipitated proteins were pelleted by centrifugation at 4°C and 17,000 $g$ for 30 min and solved in 20 µL of 1X SDS sample buffer. Samples were analyzed by SDS PAGE.

| GST pulldown assay buffer pH 7.5 | 50 mM Tris-HCl |
| | 150 mM NaCl |
| | pH adjusted to 7.5 |
| GST pulldown assay buffer pH 6 | 50 mM MES |
| | 150 mM NaCl |
| | pH adjusted to 6 |

## 4.9 Fungal methods

## 4.9.1 Separate detection of cytoplasmic and secreted *P. indica* proteins *in vitro*

*P. indica* strains were inoculated in 200 mL CM medium in 500 mL culture flasks by transferring five mycelium plugs in the liquid medium and grown at 28°C with 130 rpm agitation for 7 days. Hyg was added if applicable. Afterwards mycelium was separated from culture supernatant by

pouring the entire culture through a miracloth filter (Merck Millipore, Darmstadt). Mycelium was frozen in liquid nitrogen and ground to a fine powder using a liquid-nitrogen-cooled mortar and pistil. Approximately 100 µL of mycelium powder was transferred to a 2 mL reaction tube and 100 µL 1X SDS sample buffer (Laemmli, 1970) as well as 100 µL of glass beads (diameter=0.5 mm) were added. Lysis was achieved by three runs of vigorous shaking in FastPrep®-24 (MP Biomedicals, Santa Ana, USA) at 6 m/s for 1 min with 1 min sample incubation on ice in between. Cell debris was removed by centrifugation at 15,000 $g$ for 30 s. Fifteen (15) µL lysate was used in SDS PAGE and immunoblots.

For precipitation of secreted proteins, the culture supernatant was passed through a folding filter type 600P (Carl Roth, Karlsruhe, Germany) and a 0.45 µm syringe filter (Millex-GP; Merck Millipore, Darmstadt, Germany) to remove small mycelium fragments and spores. Proteins were precipitated by addition of 10% (v/v, final concentration) trichloroacetic acid and incubation at -20°C overnight and centrifugation at 40,000 $g$. For SDS PAGE, precipitated secreted proteins were resolved in 50 µL of 1X SDS sample buffer and 15 µL were used. GFP-tagged proteins were either detected with anti-GFP antibody (Cell Signalling Technology, Danver, USA) or anti-Dld1 antibody (Eurogentec, Seraing, Belgium). For mass spectromic analysis, precipitated secreted proteins were solved in 50 µL TBS and eventually deglycosylated with Protein Deglycosylation Mix (New England Biolabs, Ipswich, USA) under denaturing conditions as per manufacturer's instructions. Proteins were then analyzed via liquid chromatography electron spray ionization tandem mass spectrometry (LC-ESI-MS/MS; LTQ Orbitrap Discovery; Thermo Fisher Scientific, Waltham, USA) after tryptic digest (FASP™ Protein Digestion Kit; Expedeon, Swavesey, United Kingdom) in the facilities of CEACAD/CMMC Proteomics Facility in Cologne, Germany. Data was analyzed with open-source quantitative proteomics software MaxQuant (Cox & Mann, 2008).

| | |
|---|---|
| TBS | 50 mM Tris-HCl |
| | 150 mM NaCl |
| | pH adjusted to 7.5 |

## 4.9.2 Separate detection of cytoplasmic and secreted *U. maydis* proteins *in vitro*

Detection of SPPit2:mCherry:Dld1woSP, SPDld1:mCherry:Dld1woSP and SPDld1:mCherry:Dld1woSP$^{\Delta RSIDELD}$ proteins along with respective controls in the culture supernatants of *U. maydis* strains was performed as follows: *U. maydis* overnight cultures were diluted to $OD_{600}$ = 0.1 in 50 mL of CM (Holliday, 1974) with 2% glucose and grown at 28°C until $OD_{600}$ reached 0.5. For protein extraction from sporidia, 2 mL culture were pelleted at 5,700 $g$ for 2 min and the supernatant was discarded. Cells were resolved in 100 µL 1X SDS sample buffer (Laemmli, 1970) and 100 µL of glass beads (diameter=0.5 mm) were added. Lysis was

achieved by three runs of vigorous shaking in FastPrep®-24 (MP Biomedicals, Santa Ana, USA) at 6 m/s for 1 min with 1 min sample incubation on ice in between. Cell debris was removed by centrifugation at 15,000 $g$ for 30 s. Fifteen (15) µL lysate was used in SDS PAGE and immunoblots. For precipitation of secreted proteins the residual 48 mL of culture was cleared by centrifugation at 1,000 $g$ for 5 min and subsequent filtration of supernatant through a 0.45 µm syringe filter (Millex-GP; Merck Millipore, Darmstadt, Germany). Proteins were precipitated by addition of 5 mL 100% (v/v) trichloroacetic acid and incubation at -20°C overnight, pelleted at 40,000 $g$ and resolved in 50 µL of 1X SDS sample buffer. Fifteen (15) µL were used in SDS PAGE and immunoblots. mCherry tagged proteins were either detected with anti-mCherry antibody (Clontech Laboratories, Mountain View, USA) or anti-Dld1 antibody (Eurogentec, Seraing, Belgium).

## 4.10. Plant methods

### 4.10.1 Cultivation of maize

The variant Early Golden Bantam (UrbanFarmers, New York City, USA) was used for the *U. maydis* / maize *in planta* microscopy. Plants were cultivated in a temperature-controlled greenhouse with a light / dark cycle of 28°C for 14 hours / 20°C for 10 hours. During the day phase, the illumination intensity was at least 25 kLux to up to 90 kLux with additional sunlight. Four corn grains were sowed per pot in Fruhstorfer soil type "T" and watered once a day.

### 4.10.2 Infection of maize with *U. maydis*

*U. maydis* strains were cultivated overnight in YEPSlight liquid medium to an $OD_{600}$ of approx. 0.6 to 1.0. Cells were harvested by centrifugation at 2,400 $g$ for 3 min and resuspended in sterile water. Cells were centrifuged again and the $OD_{600}$ was adjusted to 3.0 with sterile water with 0.1% (v/v) Tween-29. Verticils of 7-day-old maize seedlings were injected with 500 µL of *U. maydis* cell suspension, whereas the injection site was located approx. 1 cm above the soil surface.

### 4.10.3 Transient transformation of barley leaves via particle bombardment

Barley seeds (*Hordeum vulgare* L. cv Golden Promise) were germinated and pre-grown for one week in soil in growth chamber with a day / night cycle of 16h / 8h (light intensity, 108 µmol $m^{-2}$ $s^{-1}$) and a temperature of 22°C / 18°C. The first leaves were cut and placed with abaxial side on 0.5% water agar plates. Four leaves were used for one technical repetition. Particle bombardment was performed as per manufacturer's instructions with the PDS-1000/HeTM Biolistic Particle Delivery System (Biorad, Munich Germany) using a 900 psi rupture disc, vacuum of up to 27 In Hg and gold microcarriers (1.6 µM). The microcarriers were labelled with 3 µg of plasmid carrying gene of interest and 1 µg of transformation-control plasmid. The

bombarded leaves were kept at room temperature for 3 days in a closed Petri-dish and expression and localization of the fusion proteins was monitored via confocal laser scanning microscopy. In order to analyze the localization of fusion proteins during pathogen attack, bombarded leaves were inoculated with powdery mildew 24 hours after ballistic transformation.

## 4.11 Microscopy

Confocal microscopy images were taken using a TCS-SP5 confocal laser-scanning microscope (Leica, Bensheim, Germany). To visualize the localization of mCherry and mCherry:Dld1 during *U. maydis*-maize interaction, the area 1–3 cm below the site of injection was excised at 3 dpi and directly observed under the microscope. *B. graminis* was stained with Fluorescent Brightener 28 (Sigma, Munich, Germany).

| Fluorescent protein/Fluorophore | Laser (excitation wavelength) | Emission wavelength |
|---|---|---|
| mCherry | DPSS laser (561 nm) | 580 – 630 nm |
| eGFP | Argon laser (488 nm) | 495 – 530 nm |
| Fluorescent brightener 28 | Laser diode (405 nm) | 420 – 450 nm |

# 5. Literature references

**Abramovitch RB, Kim YJ, Chen S, Dickman MB, Martin GB. 2003.** Pseudomonas type III effector AvrPtoB induces plant disease susceptibility by inhibition of host programmed cell death. *The EMBO journal* **22**(1): 60-69.

**Alberts IL, Nadassy K, Wodak SJ. 1998.** Analysis of zinc binding sites in protein crystal structures. *Protein Sci* **7**(8): 1700-1716.

**Allan AC, Fluhr R. 1997.** Two Distinct Sources of Elicited Reactive Oxygen Species in Tobacco Epidermal Cells. *Plant Cell* **9**(9): 1559-1572.

**Askwith C, Eide D, Van Ho A, Bernard PS, Li L, Davis-Kaplan S, Sipe DM, Kaplan J. 1994.** The FET3 gene of S. cerevisiae encodes a multicopper oxidase required for ferrous iron uptake. *Cell* **76**(2): 403-410.

**Askwith C, Kaplan J. 1997.** An oxidase-permease-based iron transport system in Schizosaccharomyces pombe and its expression in Saccharomyces cerevisiae. *Journal of Biological Chemistry* **272**(1): 401-405.

**Ausubel FM. 2002.** *Short protocols in molecular biology: a compendium of methods from current protocols in molecular biology. 2 (2002)*: Wiley.

**Baker EN 1994.** Structure and Reactivity of Transferrins. In: Sykes AG ed. *Advances in Inorganic Chemistry*: Academic Press, 389-463.

**Balesdent MH, Fudal I, Ollivier B, Bally P, Grandaubert J, Eber F, Chèvre AM, Leflon M, Rouxel T. 2013.** The dispensable chromosome of Leptosphaeria maculans shelters an effector gene conferring avirulence towards Brassica rapa. *New Phytologist* **198**(3): 887-898.

**Baltruschat H, Fodor J, Harrach BD, Niemczyk E, Barna B, Gullner G, Janeczko A, Kogel K-H, Schaefer P, Schwarczinger I, et al. 2008.** Salt tolerance of barley induced by the root endophyte Piriformospora indica is associated with a strong increase in antioxidants. *New Phytologist* **180**(2): 501-510.

**Barb WG, Baxendale JH, George P, Hargrave KR. 1951.** Reactions of ferrous and ferric ions with hydrogen peroxide. *Transactions of the Faraday Society* **47**: 462-500

**Barney BM, LoBrutto R, Francisco WA. 2004.** Characterization of a small metal binding protein from Nitrosomonas europaea. *Biochemistry* **43**(35): 11206-11213.

**Baxter A, Mittler R, Suzuki N. 2014.** ROS as key players in plant stress signalling. *Journal of Experimental Botany* **65**(5): 1229-1240.

**Bindschedler LV, Dewdney J, Blee KA, Stone JM, Asai T, Plotnikov J, Denoux C, Hayes T, Gerrish C, Davies DR, et al. 2006.** Peroxidase-dependent apoplastic oxidative burst in Arabidopsis required for pathogen resistance. *The Plant journal : for cell and molecular biology* **47**(6): 851-863.

**Bindschedler LV, Whitelegge JP, Millar DJ, Bolwell GP. 2006.** A two component chitin-binding protein from French bean–association of a proline-rich protein with a cysteine-rich polypeptide. *FEBS letters* **580**(6): 1541-1546.

**Boddey JA, Moritz RL, Simpson RJ, Cowman AF. 2009.** Role of the Plasmodium export element in trafficking parasite proteins to the infected erythrocyte. *Traffic* **10**(3): 285-299.

**Boller T, Felix G. 2009.** A renaissance of elicitors: perception of microbe-associated molecular patterns and danger signals by pattern-recognition receptors. *Annual review of plant biology*.

**Bolwell GP, Daudi A 2009.** Reactive oxygen species in plant–pathogen interactions. *Reactive oxygen species in plant signaling*: Springer, 113-133.

**Bos JI, Kanneganti TD, Young C, Cakir C, Huitema E, Win J, Armstrong MR, Birch PR, Kamoun S. 2006.** The C-terminal half of Phytophthora infestans RXLR effector AVR3a is sufficient to trigger R3a-mediated hypersensitivity and suppress INF1-induced cell death in Nicotiana benthamiana. *The Plant Journal* **48**(2): 165-176.

**Bradford MM. 1976.** A rapid and sensitive method for the quantitation of microgram quantities of protein utilizing the principle of protein-dye binding. *Analytical biochemistry* **72**(1-2): 248-254.

**Broomfield PE, Hargreaves JA. 1992.** A single amino-acid change in the iron-sulphur protein subunit of succinate dehydrogenase confers resistance to carboxin in Ustilago maydis. *Current genetics* **22**(2): 117-121.

**Brown I, Trethowan J, Kerry M, Mansfield J, Bolwell GP. 1998.** Localization of components of the oxidative cross-linking of glycoproteins and of callose synthesis in papillae formed during the interaction between non-pathogenic strains ofXanthomonas campestris andFrench bean mesophyll cells. *The Plant Journal* **15**(3): 333-343.

**Cabras T, Patamia M, Melino S, Inzitari R, Messana I, Castagnola M, Petruzzelli R. 2007.** Pro-oxidant activity of histatin 5 related Cu(II)-model peptide probed by mass spectrometry. *Biochem Biophys Res Commun* **358**(1): 277-284.

**Chang HH, Falick AM, Carlton PM, Sedat JW, DeRisi JL, Marletta MA. 2008.** N-terminal processing of proteins exported by malaria parasites. *Mol Biochem Parasitol* **160**(2): 107-115.

**Cohen SN, Chang AC, Hsu L. 1972.** Nonchromosomal antibiotic resistance in bacteria: genetic transformation of Escherichia coli by R-factor DNA. *Proceedings of the National Academy of Sciences* **69**(8): 2110-2114.

**Collier SM, Moffett P. 2009.** NB-LRRs work a "bait and switch" on pathogens. *Trends in plant science* **14**(10): 521-529.

**Conesa A, Gotz S. 2008.** Blast2GO: A comprehensive suite for functional analysis in plant genomics. *Int J Plant Genomics* **2008**: 619832.

**Cowtan K. 2006.** The Buccaneer software for automated model building. 1. Tracing protein chains. *Acta Crystallographica Section D: Biological Crystallography* **62**(9): 1002-1011.

**Cox J, Mann M. 2008.** MaxQuant enables high peptide identification rates, individualized ppb-range mass accuracies and proteome-wide protein quantification. *Nature biotechnology* **26**(12): 1367.

**Damasceno CM, Bishop JG, Ripoll DR, Win J, Kamoun S, Rose JK. 2008.** Structure of the glucanase inhibitor protein (GIP) family from Phytophthora species suggests coevolution with plant endo-β-1, 3-glucanases. *Molecular Plant-Microbe Interactions* **21**(6): 820-830.

**Daudi A, Cheng Z, O'Brien JA, Mammarella N, Khan S, Ausubel FM, Bolwell GP. 2012.** The apoplastic oxidative burst peroxidase in Arabidopsis is a major component of pattern-triggered immunity. *Plant Cell* **24**(1): 275-287.

**De Jonge R, Van Esse HP, Kombrink A, Shinya T, Desaki Y, Bours R, Van Der Krol S, Shibuya N, Joosten MH, Thomma BP. 2010.** Conserved fungal LysM effector Ecp6 prevents chitin-triggered immunity in plants. *Science* **329**(5994): 953-955.

**Deslandes L, Olivier J, Peeters N, Feng DX, Khounlotham M, Boucher C, Somssich I, Genin S, Marco Y. 2003.** Physical interaction between RRS1-R, a protein conferring

resistance to bacterial wilt, and PopP2, a type III effector targeted to the plant nucleus. *Proceedings of the National Academy of Sciences* **100**(13): 8024-8029.

**Djamei A, Schipper K, Rabe F, Ghosh A, Vincon V, Kahnt J, Osorio S, Tohge T, Fernie AR, Feussner I, et al. 2011.** Metabolic priming by a secreted fungal effector. *Nature* **478**(7369): 395-398.

**Dodds PN, Lawrence GJ, Catanzariti A-M, Ayliffe MA, Ellis JG. 2004.** The Melampsora lini AvrL567 avirulence genes are expressed in haustoria and their products are recognized inside plant cells. *The Plant Cell* **16**(3): 755-768.

**Doehlemann G, Reissmann S, Assmann D, Fleckenstein M, Kahmann R. 2011.** Two linked genes encoding a secreted effector and a membrane protein are essential for Ustilago maydis-induced tumour formation. *Mol Microbiol* **81**(3): 751-766.

**Doehlemann G, van der Linde K, Assmann D, Schwammbach D, Hof A, Mohanty A, Jackson D, Kahmann R. 2009.** Pep1, a secreted effector protein of Ustilago maydis, is required for successful invasion of plant cells. *PLoS Pathog* **5**(2): e1000290.

**Dou D, Kale SD, Wang X, Jiang RH, Bruce NA, Arredondo FD, Zhang X, Tyler BM. 2008.** RXLR-mediated entry of Phytophthora sojae effector Avr1b into soybean cells does not require pathogen-encoded machinery. *Plant Cell* **20**(7): 1930-1947.

**Eaton KA, Gilbert JV, Joyce EA, Wanken AE, Thevenot T, Baker P, Plaut A, Wright A. 2002.** In vivo complementation of ureB restores the ability of Helicobacter pylori to colonize. *Infect Immun* **70**(2): 771-778.

**Eichhorn H, Lessing F, Winterberg B, Schirawski J, Kämper J, Müller P, Kahmann R. 2006.** A ferroxidation/permeation iron uptake system is required for virulence in Ustilago maydis. *The Plant Cell* **18**(11): 3332-3345.

**Emsley P, Cowtan K. 2004.** Coot: model-building tools for molecular graphics. *Acta Crystallographica Section D: Biological Crystallography* **60**(12): 2126-2132.

**Ernst J, Winkelmann G. 1977.** Enzymatic release of iron from sideramines in fungi. NADH: sideramine oxidoreductase in Neurospora crassa. *Biochimica et Biophysica Acta (BBA)-General Subjects* **500**(1): 27-41.

**Felix G, Duran JD, Volko S, Boller T. 1999.** Plants have a sensitive perception system for the most conserved domain of bacterial flagellin. *The Plant Journal* **18**(3): 265-276.

**Finzel BC, Poulos TL, Kraut J. 1984.** Crystal structure of yeast cytochrome c peroxidase refined at 1.7-A resolution. *J Biol Chem* **259**(21): 13027-13036.

**Fraser TH, Bruce BJ. 1978.** Chicken ovalbumin is synthesized and secreted by Escherichia coli. *Proc Natl Acad Sci U S A* **75**(12): 5936-5940.

**Gasteiger E, Gattiker A, Hoogland C, Ivanyi I, Appel RD, Bairoch A. 2003.** ExPASy: The proteomics server for in-depth protein knowledge and analysis. *Nucleic Acids Res* **31**(13): 3784-3788.

**Gernert KM, Surles MC, Labean TH, Richardson JS, Richardson DC. 1995.** The Alacoil: a very tight, antiparallel coiled-coil of helices. *Protein Sci* **4**(11): 2252-2260.

**Gibson DG, Young L, Chuang R-Y, Venter JC, Hutchison III CA, Smith HO. 2009.** Enzymatic assembly of DNA molecules up to several hundred kilobases. *Nature methods* **6**(5): 343.

**Gillissen B, Bergemann J, Sandmann C, Schroeer B, Bölker M, Kahmann R. 1992.** A two-component regulatory system for self/non-self recognition in Ustilago maydis. *Cell* **68**(4): 647-657.

**Greenberg JT, Yao N. 2004.** The role and regulation of programmed cell death in plant–pathogen interactions. *Cellular microbiology* **6**(3): 201-211.

**Greenshields DL, Liu G, Feng J, Selvaraj G, Wei Y. 2007.** The siderophore biosynthetic gene SID1, but not the ferroxidase gene FET3, is required for full Fusarium graminearum virulence. *Molecular plant pathology* **8**(4): 411-421.

**Greenshields DL, Liu G, Wei Y. 2007.** Roles of iron in plant defence and fungal virulence. *Plant Signal Behav* **2**(4): 300-302.

**Hall J, Hazlewood GP, Surani MA, Hirst BH, Gilbert HJ. 1990.** Eukaryotic and prokaryotic signal peptides direct secretion of a bacterial endoglucanase by mammalian cells. *J Biol Chem* **265**(32): 19996-19999.

**Harford C, Sarkar B. 1997.** Amino Terminal Cu(II)- and Ni(II)-Binding (ATCUN) Motif of Proteins and Peptides: Metal Binding, DNA Cleavage, and Other Properties. *Accounts of Chemical Research* **30**(3): 123-130.

**Hart MM, Trevors JT. 2005.** Microbe management: application of mycorrhyzal fungi in sustainable agriculture. *Frontiers in Ecology and the Environment* **3**(10): 533-539.

**Helmerhorst EJ, Troxler RF, Oppenheim FG. 2001.** The human salivary peptide histatin 5 exerts its antifungal activity through the formation of reactive oxygen species. *Proc Natl Acad Sci U S A* **98**(25): 14637-14642.

**Hemetsberger C, Herrberger C, Zechmann B, Hillmer M, Doehlemann G. 2012.** The Ustilago maydis effector Pep1 suppresses plant immunity by inhibition of host peroxidase activity. *PLoS pathogens* **8**(5): e1002684.

**Hilbert M, Voll LM, Ding Y, Hofmann J, Sharma M, Zuccaro A. 2012.** Indole derivative production by the root endophyte Piriformospora indica is not required for growth promotion but for biotrophic colonization of barley roots. *New Phytol* **196**(2): 520-534.

**Hiller NL, Bhattacharjee S, van Ooij C, Liolios K, Harrison T, Lopez-Estrano C, Haldar K. 2004.** A host-targeting signal in virulence proteins reveals a secretome in malarial infection. *Science* **306**(5703): 1934-1937.

**Holliday R 1974.** Ustilago maydis. *Bacteria, Bacteriophages, and Fungi*: Springer, 575-595.

**Howard DH. 1999.** Acquisition, transport, and storage of iron by pathogenic fungi. *Clinical Microbiology Reviews* **12**(3): 394-404.

**Hückelhoven R. 2007.** Cell wall–associated mechanisms of disease resistance and susceptibility. *Annu. Rev. Phytopathol.* **45**: 101-127.

**Hückelhoven R, Fodor J, Preis C, Kogel KH. 1999.** Hypersensitive cell death and papilla formation in barley attacked by the powdery mildew fungus are associated with hydrogen peroxide but not with salicylic acid …. *Plant Physiology*.

**Hückelhoven R, Kogel K-H. 2003.** Reactive oxygen intermediates in plant-microbe interactions: Who is who in powdery mildew resistance? *Planta* **216**(6): 891-902.

**Izard JW, Kendall DA. 1994.** Signal peptides: exquisitely designed transport promoters. *Mol Microbiol* **13**(5): 765-773.

**Johnson L. 2008.** Iron and siderophores in fungal–host interactions. *Mycological research* **112**(2): 170-183.

**Jones JD, Dangl JL. 2006.** The plant immune system. *Nature* **444**(7117): 323-329.

**Kabsch W. 1993.** Automatic processing of rotation diffraction data from crystals of initially unknown symmetry and cell constants. *Journal of applied crystallography* **26**(6): 795-800.

**Kale SD, Gu B, Capelluto DG, Dou D, Feldman E, Rumore A, Arredondo FD, Hanlon R, Fudal I, Rouxel T, et al. 2010.** External lipid PI3P mediates entry of eukaryotic pathogen effectors into plant and animal host cells. *Cell* **142**(2): 284-295.

**Kämper J, Kahmann R, Bölker M, Ma L-J, Brefort T, Saville BJ, Banuett F, Kronstad JW, Gold SE, Müller O. 2006.** Insights from the genome of the biotrophic fungal plant pathogen Ustilago maydis. *Nature* **444**(7115): 97.

**Kim H-S, Desveaux D, Singer AU, Patel P, Sondek J, Dangl JL. 2005.** The Pseudomonas syringae effector AvrRpt2 cleaves its C-terminally acylated target, RIN4, from Arabidopsis membranes to block RPM1 activation. *Proceedings of the National Academy of Sciences of the United States of America* **102**(18): 6496-6501.

**Klockenbusch C, Kast J. 2010.** Optimization of Formaldehyde Cross-Linking for Protein Interaction Analysis of Non-Tagged Integrin *BioMed Research International* **2010**.

**Koppenol WH. 2001.** The Haber-Weiss cycle – 70 years later. *Redox Report* **6** (4).

**Kuang H, Woo S-S, Meyers BC, Nevo E, Michelmore RW. 2004.** Multiple genetic processes result in heterogeneous rates of evolution within the major cluster disease resistance genes in lettuce. *The Plant Cell* **16**(11): 2870-2894.

**Laemmli UK. 1970.** Cleavage of structural proteins during the assembly of the head of bacteriophage T4. *Nature* **227**(5259): 680.

**Lahrmann U, Ding Y, Banhara A, Rath M, Hajirezaei MR, Döhlemann S, von Wirén N, Parniske M, Zuccaro A. 2013.** Host-related metabolic cues affect colonization strategies of a root endophyte. *Proceedings of the National Academy of Sciences* **110**(34): 13965-13970.

**Lahrmann U, Strehmel N, Langen G, Frerigmann H, Leson L, Ding Y, Scheel D, Herklotz S, Hilbert M, Zuccaro A. 2015.** Mutualistic root endophytism is not associated with the reduction of saprotrophic traits and requires a noncompromised plant innate immunity. *New Phytologist* **207**(3): 841-857.

**Landschulz WH, Johnson PF, McKnight SL. 1988.** The leucine zipper: a hypothetical structure common to a new class of DNA binding proteins. *Science* **240**(4860): 1759-1764.

**Laskowski RA, Rullmann JAC, MacArthur MW, Kaptein R, Thornton JM. 1996.** AQUA and PROCHECK-NMR: programs for checking the quality of protein structures solved by NMR. *Journal of biomolecular NMR* **8**(4): 477-486.

**Lesuisse E, Simon-Casteras M, Labbe P. 1998.** Siderophore-mediated iron uptake in Saccharomyces cerevisiae: the SIT1 gene encodes a ferrioxamine B permease that belongs to the major facilitator superfamily. *Microbiology* **144**(12): 3455-3462.

**Lewis MJ, Pelham HR. 1990.** A human homologue of the yeast HDEL receptor. *Nature* **348**(6297): 162-163.

**Liu G, Greenshields DL, Sammynaiken R, Hirji RN, Selvaraj G, Wei Y. 2007.** Targeted alterations in iron homeostasis underlie plant defense responses. *J Cell Sci* **120**(Pt 4): 596-605.

**Lo Presti L, Zechmann B, Kumlehn J, Liang L, Lanver D, Tanaka S, Bock R, Kahmann R. 2017.** An assay for entry of secreted fungal effectors into plant cells. *New Phytol* **213**(2): 956-964.

**Longnecker N, Welch RM. 1990.** Accumulation of apoplastic iron in plant roots : a factor in the resistance of soybeans to iron-deficiency induced chlorosis? *Plant Physiol* **92**(1): 17-22.

**Maier RH, Cattani RA. 1965.** Accumulation of Iron in Higher Plant Cell Walls. *Life Sci* **4**: 391-395.

**Marti M, Good RT, Rug M, Knuepfer E, Cowman AF. 2004.** Targeting malaria virulence and remodeling proteins to the host erythrocyte. *Science* **306**(5703): 1930-1933.

**McLeod A, Smart CD, Fry WE. 2003.** Characterization of 1, 3-β-glucanase and 1, 3; 1, 4-β-glucanase genes from Phytophthora infestans. *Fungal Genetics and Biology* **38**(2): 250-263.

**McLusky SR, Bennett MH, Beale MH, Lewis MJ, Gaskin P, Mansfield JW. 1999.** Cell wall alterations and localized accumulation of feruloyl-3′-methoxytyramine in onion epidermis at sites of attempted penetration by Botrytis allii are associated with actin polarisation, peroxidase activity and suppression of flavonoid biosynthesis. *The Plant Journal* **17**(5): 523-534.

**Mei B, Budde AD, Leong SA. 1993.** sid1, a gene initiating siderophore biosynthesis in Ustilago maydis: molecular characterization, regulation by iron, and role in phytopathogenicity. *Proceedings of the National Academy of Sciences* **90**(3): 903-907.

**Melino S, Rufini S, Sette M, Morero R, Grottesi A, Paci M, Petruzzelli R. 1999.** Zn(2+) ions selectively induce antimicrobial salivary peptide histatin-5 to fuse negatively charged vesicles. Identification and characterization of a zinc-binding motif present in the functional domain. *Biochemistry* **38**(30): 9626-9633.

**Melino S, Santone C, Di Nardo P, Sarkar B. 2014.** Histatins: salivary peptides with copper(II)- and zinc(II)-binding motifs: perspectives for biomedical applications. *FEBS J* **281**(3): 657-672.

**Miller G, Schlauch K, Tam R, Cortes D, Torres MA, Shulaev V, Dangl JL, Mittler R. 2009.** The plant NADPH oxidase RBOHD mediates rapid systemic signaling in response to diverse stimuli. *Sci. Signal.* **2**(84): ra45-ra45.

**Molina L, Kahmann R. 2007.** An Ustilago maydis gene involved in H2O2 detoxification is required for virulence. *Plant Cell* **19**(7): 2293-2309.

**Mueller AN, Ziemann S, Treitschke S, Aßmann D, Doehlemann G. 2013.** Compatibility in the Ustilago maydis–maize interaction requires inhibition of host cysteine proteases by the fungal effector Pit2. *PLoS pathogens* **9**(2): e1003177.

**Mullis K, Faloona F, Scharf S, Saiki R, Horn G, Erlich H 1986**. Specific enzymatic amplification of DNA in vitro: the polymerase chain reaction. *Cold Spring Harbor symposia on quantitative biology*: Cold Spring Harbor Laboratory Press. 263-273.

**Munoz IG, Moran JF, Becana M, Montoya G. 2005.** The crystal structure of an eukaryotic iron superoxide dismutase suggests intersubunit cooperation during catalysis. *Protein Sci* **14**(2): 387-394.

**Munro S, Pelham HR. 1987.** A C-terminal signal prevents secretion of luminal ER proteins. *Cell* **48**(5): 899-907.

**Murshudov GN, Vagin AA, Lebedev A, Wilson KS, Dodson EJ. 1999.** Efficient anisotropic refinement of macromolecular structures using FFT. *Acta Crystallographica Section D: Biological Crystallography* **55**(1): 247-255.

**Nürnberger T, Brunner F, Kemmerling B, Piater L. 2004.** Innate immunity in plants and animals: striking similarities and obvious differences. *Immunological reviews* **198**(1): 249-266.

**Oide S, Moeder W, Krasnoff S, Gibson D, Haas H. 2006.** NPS6, encoding a nonribosomal peptide synthetase involved in siderophore-mediated iron metabolism, is a conserved

virulence determinant of plant pathogenic ascomycetes. *The Plant Cell* **18**(10): 2836-2853.

**Ong ST, Ho JZS, Ho B, Ding JL. 2006.** Iron-withholding strategy in innate immunity. *Immunobiology* **211**(4): 295-314.

**Osumi M, YAMADA N, KOBORI H, TAKI A, NAITO N, BABA M, NAGATANI T. 1989.** Cell wall formation in regenerating protoplasts of Schizosaccharomyces pombe: study by high resolution, low voltage scanning electron microscopy. *Microscopy* **38**(6): 457-468.

**Panton LJ, McPhie P, Maloy WL, Wellems TE, Taylor DW, Howard RJ. 1989.** Purification and partial characterization of an unusual protein of Plasmodium falciparum: histidine-rich protein II. *Mol Biochem Parasitol* **35**(2): 149-160.

**Papalexis V, Siomos MA, Campanale N, Guo X, Kocak G, Foley M, Tilley L. 2001.** Histidine-rich protein 2 of the malaria parasite, Plasmodium falciparum, is involved in detoxification of the by-products of haemoglobin degradation. *Mol Biochem Parasitol* **115**(1): 77-86.

**Peng M, Kuc J. 1992.** Peroxidase-generated hydrogen peroxide as a source of antifungal activity in vitro and on tobacco leaf disks. *Phytopathology* **82**(6): 696-699.

**Perutz MF. 1963.** X-ray analysis of hemoglobin. *Science* **140**(3569): 863-869.

**Plett JM, Kemppainen M, Kale SD, Kohler A, Legue V, Brun A, Tyler BM, Pardo AG, Martin F. 2011.** A secreted effector protein of Laccaria bicolor is required for symbiosis development. *Curr Biol* **21**(14): 1197-1203.

**Porciatti E, Milenkovic M, Gaggelli E, Valensin G, Kozlowski H, Kamysz W, Valensin D. 2010.** Structural characterization and antimicrobial activity of the Zn(II) complex with P113 (demegen), a derivative of histatin 5. *Inorg Chem* **49**(19): 8690-8698.

**Priller JPR, Reid S, Konein P, Dietrich P, Sonnewald S. 2016.** The Xanthomonas campestris pv. vesicatoria type-3 effector XopB inhibits plant defence responses by interfering with ROS production. *PLoS One* **11**(7): e0159107.

**Puhar A, Sansonetti PJ. 2014.** Type III secretion system. *Current Biology* **24**(17): R784-R791.

**Raffaele S, Win J, Cano LM, Kamoun S. 2010.** Analyses of genome architecture and gene expression reveal novel candidate virulence factors in the secretome of Phytophthora infestans. *BMC genomics* **11**(1): 637.

**Ramachandran GN, Ramakrishnan C, Sasisekharan V. 1963.** Stereochemistry of polypeptide chain configurations. *J Mol Biol* **7**: 95-99.

**Rooney HC, van't Klooster JW, van der Hoorn RA, Joosten MH, Jones JD, de Wit PJ. 2005.** Cladosporium Avr2 inhibits tomato Rcr3 protease required for Cf-2-dependent disease resistance. *Science* **308**(5729): 1783-1786.

**Rossman AY. 2009.** The impact of invasive fungi on agricultural ecosystems in the United States. *Biological Invasions* **11**(1): 97-107.

**Rouxel T, Grandaubert J, Hane JK, Hoede C, Van de Wouw AP, Couloux A, Dominguez V, Anthouard V, Bally P, Bourras S. 2011.** Effector diversification within compartments of the Leptosphaeria maculans genome affected by Repeat-Induced Point mutations. *Nature Communications* **2**: 202.

**Sabatini LM, Azen EA. 1989.** Histatins, a family of salivary histidine-rich proteins, are encoded by at least two loci (HIS1 and HIS2). *Biochem Biophys Res Commun* **160**(2): 495-502.

**Sambrook J, Fritsch EF, Maniatis T. 1989.** *Molecular cloning: a laboratory manual*: Cold spring harbor laboratory press.

**Sanger F, Nicklen S, Coulson AR. 1977.** DNA sequencing with chain-terminating inhibitors. *Proceedings of the National Academy of Sciences* **74**(12): 5463-5467.

**Schneider EL, Marletta MA. 2005.** Heme binding to the histidine-rich protein II from Plasmodium falciparum. *Biochemistry* **44**(3): 979-986.

**Schreiner P, Chen X, Husnjak K, Randles L, Zhang N, Elsasser S, Finley D, Dikic I, Walters KJ, Groll M. 2008.** Ubiquitin docking at the proteasome through a novel pleckstrin-homology domain interaction. *Nature* **453**(7194): 548.

**Schrettl M, Bignell E, Kragl C, Joechl C, Rogers T, Arst HN, Haynes K, Haas H. 2004.** Siderophore biosynthesis but not reductive iron assimilation is essential for Aspergillus fumigatus virulence. *Journal of Experimental Medicine* **200**(9): 1213-1219.

**Schulz B, Banuett F, Dahl M, Schlesinger R, Schäfer W, Martin T, Herskowitz I, Kahmann R. 1990.** The b alleles of U. maydis, whose combinations program pathogenic development, code for polypeptides containing a homeodomain-related motif. *Cell* **60**(2): 295-306.

**Schulze-Lefert P. 2004.** Plant immunity: the origami of receptor activation. *Current biology : CB* **14**(1): 4.

**Schwecke T, Göttling K, Durek P, Dueñas I, Käufer NF, Zock-Emmenthal S, Staub E, Neuhof T, Dieckmann R, von Döhren H. 2006.** Nonribosomal Peptide Synthesis in Schizosaccharomyces pombe and the Architectures of Ferrichrome-Type Siderophore Synthetases in Fungi. *ChemBioChem* **7**(4): 612-622.

**Schweizer P, Pokorny J, Abderhalden O, Dudler R. 1999.** A transient assay system for the functional assessment of defense-related genes in wheat. *Molecular Plant-Microbe Interactions* **12**(8): 647-654.

**Scott DR, Weeks D, Hong C, Postius S, Melchers K, Sachs G. 1998.** The role of internal urease in acid resistance of Helicobacter pylori. *Gastroenterology* **114**(1): 58-70.

**Semenza JC, Hardwick KG, Dean N, Pelham HR. 1990.** ERD2, a yeast gene required for the receptor-mediated retrieval of luminal ER proteins from the secretory pathway. *Cell* **61**(7): 1349-1357.

**Sheldrick GM. 2008.** A short history of SHELX. *Acta Crystallographica Section A: Foundations of Crystallography* **64**(1): 112-122.

**Sherameti I, Tripathi S, Varma A, Oelmüller R. 2008.** The root-colonizing endophyte Pirifomospora indica confers drought tolerance in Arabidopsis by stimulating the expression of drought stress–related genes in leaves. *Molecular Plant-Microbe Interactions* **21**(6): 799-807.

**Silva AM, Kong X, Parkin MC, Cammack R, Hider RC. 2009.** Iron(III) citrate speciation in aqueous solution. *Dalton Trans*(40): 8616-8625.

**Southern EM. 1975.** Detection of specific sequences among DNA fragments separated by gel electrophoresis. *J Mol Biol* **98**(3): 503-517.

**Soylu S, Brown I, Mansfield JW. 2005.** Cellular reactions in Arabidopsis following challenge by strains of Pseudomonas syringae: from basal resistance to compatibility. *Physiological and molecular plant pathology* **66**(6): 232-243.

**Suzuki N, Miller G, Morales J, Shulaev V, Torres MA, Mittler R. 2011.** Respiratory burst oxidases: the engines of ROS signaling. *Current opinion in plant biology* **14**(6): 691-699.

**Tanaka S, Brefort T, Neidig N, Djamei A, Kahnt J, Vermerris W, Koenig S, Feussner K, Feussner I, Kahmann R. 2014.** A secreted Ustilago maydis effector promotes virulence by targeting anthocyanin biosynthesis in maize. *Elife* **3**: e01355.

**Tellinghuisen J. 2012.** Designing isothermal titration calorimetry experiments for the study of 1:1 binding: problems with the "standard protocol". *Anal Biochem* **424**(2): 211-220.

**Tian M, Win J, Song J, van der Hoorn R, van der Knaap E, Kamoun S. 2007.** A Phytophthora infestans cystatin-like protein targets a novel tomato papain-like apoplastic protease. *Plant Physiology* **143**(1): 364-377.

**Tomb JF, White O, Kerlavage AR, Clayton RA, Sutton GG, Fleischmann RD, Ketchum KA, Klenk HP, Gill S, Dougherty BA, et al. 1997.** The complete genome sequence of the gastric pathogen Helicobacter pylori. *Nature* **388**(6642): 539-547.

**Torres MA, Dangl JL, Jones JD. 2002.** Arabidopsis gp91phox homologues AtrbohD and AtrbohF are required for accumulation of reactive oxygen intermediates in the plant defense response. *Proceedings of the National Academy of Sciences of the United States of America* **99**(1): 517-522.

**Torres MA, Jones JD, Dangl JL. 2006.** Reactive oxygen species signaling in response to pathogens. *Plant Physiology* **141**(2): 373-378.

**Torres MA, Jones JDG, Dangl JL. 2005.** Pathogen-induced, NADPH oxidase–derived reactive oxygen intermediates suppress spread of cell death in Arabidopsis thaliana. *Nature genetics.*

**Tsuda K, Katagiri F. 2010.** Comparing signaling mechanisms engaged in pattern-triggered and effector-triggered immunity. *Current opinion in plant biology* **13**(4): 459-465.

**Tsuda K, Sato M, Stoddard T, Glazebrook J, Katagiri F. 2009.** Network properties of robust immunity in plants. *PLoS genetics* **5**(12): e1000772.

**Unger C, Kleta S, Jandl G, Tiedemann Av. 2005.** Suppression of the Defence-Related Oxidative Burst in Bean Leaf Tissue and Bean Suspension Cells by the Necrotrophic Pathogen Botrytis cinerea. *Journal of Phytopathology* **153**(1): 15-26.

**Vadassery J, Ranf S, Drzewiecki C, Mithöfer A, Mazars C, Scheel D, Lee J, Oelmüller R. 2009.** A cell wall extract from the endophytic fungus Piriformospora indica promotes growth of Arabidopsis seedlings and induces intracellular calcium elevation in roots. *The Plant Journal* **59**(2): 193-206.

**van den Burg HA, Harrison SJ, Joosten MH, Vervoort J, de Wit PJ. 2006.** Cladosporium fulvum Avr4 protects fungal cell walls against hydrolysis by plant chitinases accumulating during infection. *Molecular Plant-Microbe Interactions* **19**(12): 1420-1430.

**Van der Hoorn RA, De Wit PJ, Joosten MH. 2002.** Balancing selection favors guarding resistance proteins. *Trends in plant science* **7**(2): 67-71.

**Varma A, Verma S, Sahay N, Bütehorn B, Franken P. 1999.** Piriformospora indica, a cultivable plant-growth-promoting root endophyte. *Applied and Environmental Microbiology* **65**(6): 2741-2744.

**Vinella D, Fischer F, Vorontsov E, Gallaud J, Malosse C, Michel V, Cavazza C, Robbe-Saule M, Richaud P, Chamot-Rooke J, et al. 2015.** Evolution of Helicobacter: Acquisition by Gastric Species of Two Histidine-Rich Proteins Essential for Colonization. *PLoS Pathog* **11**(12): e1005312.

**Waller F, Achatz B, Baltruschat H, Fodor J, Becker K, Fischer M, Heier T, Hückelhoven R, Neumann C, von Wettstein D. 2005.** The endophytic fungus *Piriformospora indica*

reprograms barley to salt-stress tolerance, disease resistance, and higher yield. *Proceedings of the National Academy of Sciences of the United States of America* **102**(38): 13386-13391.

**Wang L, Berndt P, Xia X, Kahnt J, Kahmann R. 2011.** A seven-WD40 protein related to human RACK1 regulates mating and virulence in Ustilago maydis. *Molecular microbiology* **81**(6): 1484-1498.

**Wawra S, Agacan M, Boddey JA, Davidson I, Gachon CM, Zanda M, Grouffaud S, Whisson SC, Birch PR, Porter AJ, et al. 2012.** Avirulence protein 3a (AVR3a) from the potato pathogen Phytophthora infestans forms homodimers through its predicted translocation region and does not specifically bind phospholipids. *J Biol Chem* **287**(45): 38101-38109.

**Wawra S, Belmonte R, Löbach L, Saraiva M, Willems A, van West P. 2012.** Secretion, delivery and function of oomycete effector proteins. *Current opinion in microbiology* **15**(6): 685-691.

**Wawra S, Trusch F, Matena A, Apostolakis K, Linne U, Zhukov I, Stanek J, Kozminski W, Davidson I, Secombes CJ, et al. 2017.** The RxLR Motif of the Host Targeting Effector AVR3a of Phytophthora infestans Is Cleaved before Secretion. *Plant Cell* **29**(6): 1184-1195.

**Wellems TE, Howard RJ. 1986.** Homologous genes encode two distinct histidine-rich proteins in a cloned isolate of Plasmodium falciparum. *Proc Natl Acad Sci U S A* **83**(16): 6065-6069.

**Whisson SC, Boevink PC, Moleleki L, Avrova AO, Morales JG, Gilroy EM, Armstrong MR, Grouffaud S, van West P, Chapman S, et al. 2007.** A translocation signal for delivery of oomycete effector proteins into host plant cells. *Nature* **450**(7166): 115-118.

**Wojtaszek P, Trethowan J, Bolwell GP. 1997.** Reconstitution in vitro of the components and conditions required for the oxidative cross-linking of extracellular proteins in French bean (Phaseolus vulgaris L.). *FEBS letters* **405**(1): 95-98.

**Yamaoka Y. 2010.** Mechanisms of disease: Helicobacter pylori virulence factors. *Nat Rev Gastroenterol Hepatol* **7**(11): 629-641.

**Yang S, Bai G, Chen L, Shen Q, Diao X, Zhao G. 2014.** The interaction of phenolic acids with Fe(III) in the presence of citrate as studied by isothermal titration calorimetry. *Food Chem* **157**: 302-309.

**Yi M, Valent B. 2013.** Communication between filamentous pathogens and plants at the biotrophic interface. *Annual review of phytopathology* **51**: 587-611.

**Yoda H, Hiroi Y, Sano H. 2006.** Polyamine oxidase is one of the key elements for oxidative burst to induce programmed cell death in tobacco cultured cells. *Plant Physiology*.

**Zeidler D, Zähringer U, Gerber I, Dubery I, Hartung T, Bors W, Hutzler P, Durner J. 2004.** Innate immunity in Arabidopsis thaliana: lipopolysaccharides activate nitric oxide synthase (NOS) and induce defense genes. *Proceedings of the National Academy of Sciences of the United States of America* **101**(44): 15811-15816.

**Zeng YB, Yang N, Sun H. 2011.** Metal-binding properties of an Hpn-like histidine-rich protein. *Chemistry* **17**(21): 5852-5860.

**Zhang M, Li Q, Liu T, Liu L, Shen D, Zhu Y, Liu P, Zhou J-M, Dou D. 2014.** Two cytoplasmic effectors of Phytophthora sojae regulate plant cell death via interactions with plant catalases. *Plant Physiology*: pp. 114.252437.

**Zhang Z, Henderson C, Gurr SJ. 2004.** Blumeria graminis secretes an extracellular catalase during infection of barley: potential role in suppression of host defence. *Molecular plant pathology* **5**(6): 537-547.

**Zimmerlin A, Wojtaszek P, Bolwell GP. 1994.** Synthesis of dehydrogenation polymers of ferulic acid with high specificity by a purified cell-wall peroxidase from French bean (Phaseolus vulgaris L.). *Biochemical Journal* **299**(3): 747-753.

**Zuccaro A, Lahrmann U, Güldener U, Langen G, Pfiffi S, Biedenkopf D, Wong P, Samans B, Grimm C, Basiewicz M. 2011.** Endophytic life strategies decoded by genome and transcriptome analyses of the mutualistic root symbiont Piriformospora indica. *PLoS pathogens* **7**(10): e1002290.

# 6. Supplemental Material
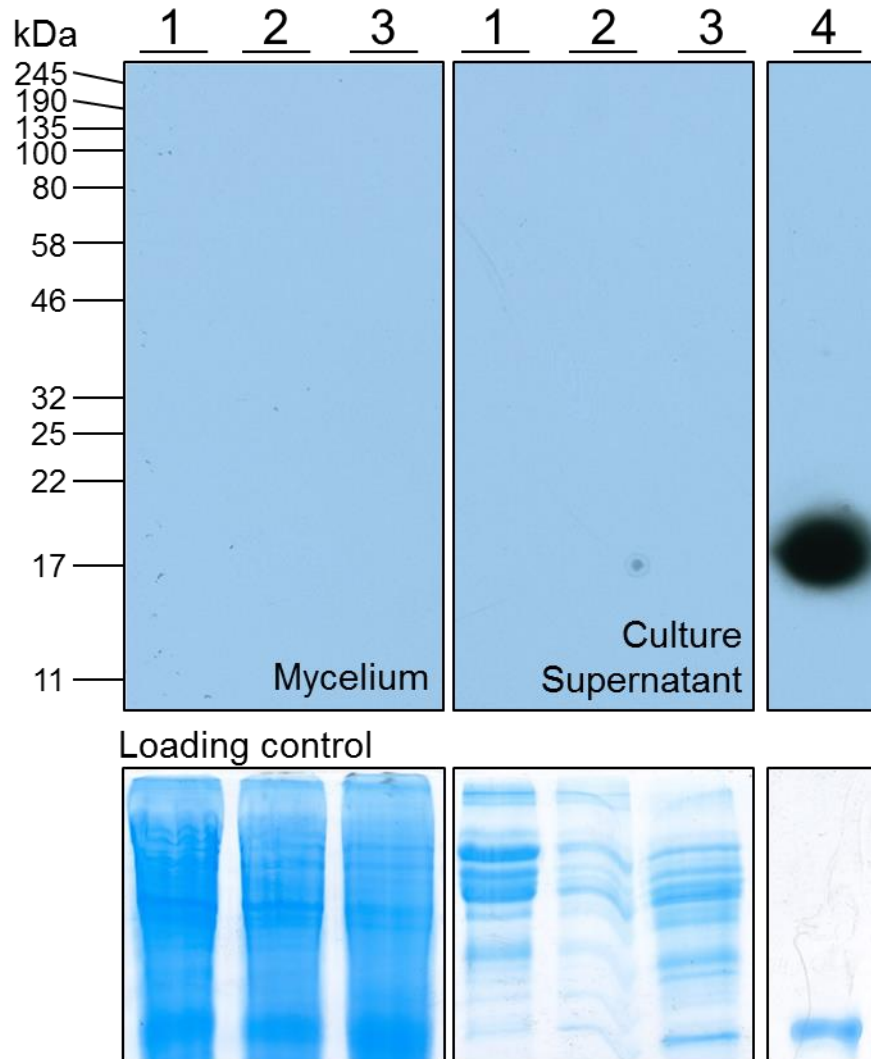


**Supplemental Figure 1: Anti-Dld1 immunoblot-based *P. indica* secretion assay.**
*P. indica* strains were inoculated in CM and cultivated at 28°C for seven days. Mycelium was separated from culture supernatant by filtration, frozen in liquid nitrogen, ground to fine powder, lysed by mechanical disruption and proteins were extracted with SDS sample buffer. Culture supernatant proteins were precipitated with TCA, washed and resolved in equal amounts of SDS sample buffer. *E. coli* purified Dld1 was used as a positive control. Proteins were analyzed by anti-Dld1 immunoblot: Mycelium as well as culture supernatant protein preparation were devoid of signals. In contrast, *E. coli* purified Dld1 exhibited a distinct signal at approx. 15 kDa, consistent with the molecular weight of Dld1 without signal peptide (12.7 kDa). Coomassie staining of gels was used to ensure that equal amounts of proteins were used in the assay.
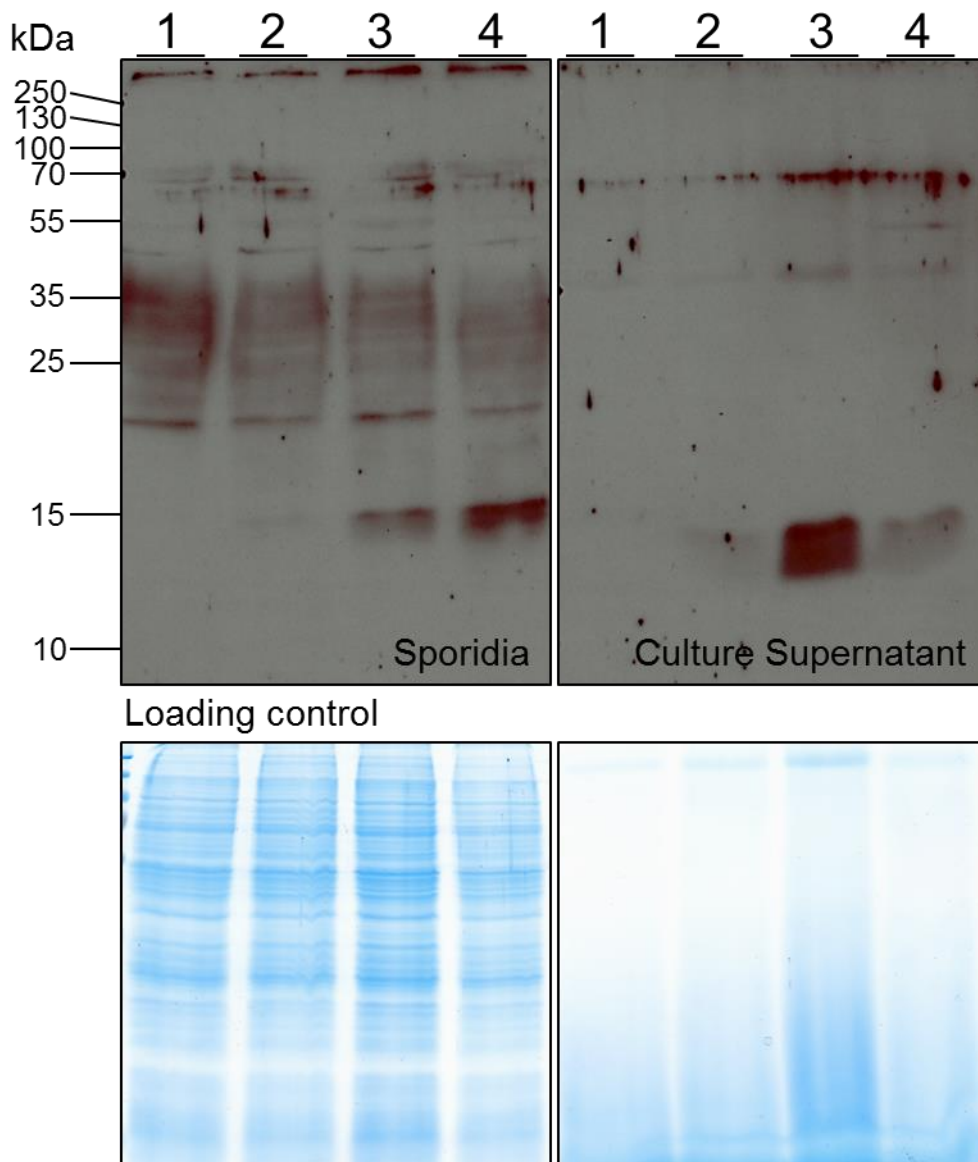
**Supplemental Figure 2: Figure 23: Anti-mCherry immunoblot-based *U. maydis* secretion assay.**
*U. maydis* strains were grown in complete medium (CM) until $OD_{600} = 0.5$. Sporidia and culture supernatant were separated by centrifugation and filtration. Sporidia were lysed and proteins extracted with SDS sample buffer. Proteins from culture supernatant were precipitated with TCA, washed and resolved in equal amounts of SDS sample buffer. Sporidia and culture supernatant protein preparations were analyzed by anti-Dld1 immunoblot. Sporidia proteins from all *U. maydis* strains exhibited several signals from approx. 20 kDa to 70 kDa. All three *U. maydis* <p123:DLD1> clones exhibited a distinct signal with varying intensity at approx. 15 kDa, consistent with the molecular weight of full length Dld1 ($M_W = 14.7$ kDa). A signal at this height was not visible in negative control strain *U. maydis* SG200. Culture supernatant proteins of all *U. maydis* strains exhibited indistinct signals at approx. 70 kDa and 40 kDa. Cultures supernatant proteins of all three *U. maydis* <p123:DLD1> clones exhibited a distinct signal with varying intensity just below 15 kDa, consistent with the molecular weight of Dld1 without the signal peptide ($M_W = 12.7$ kDa). A signal at this height was not visible in negative control strain *U. maydis* SG200. Coomassie staining of gels was used to ensure that equal amounts of proteins were used in the assay.
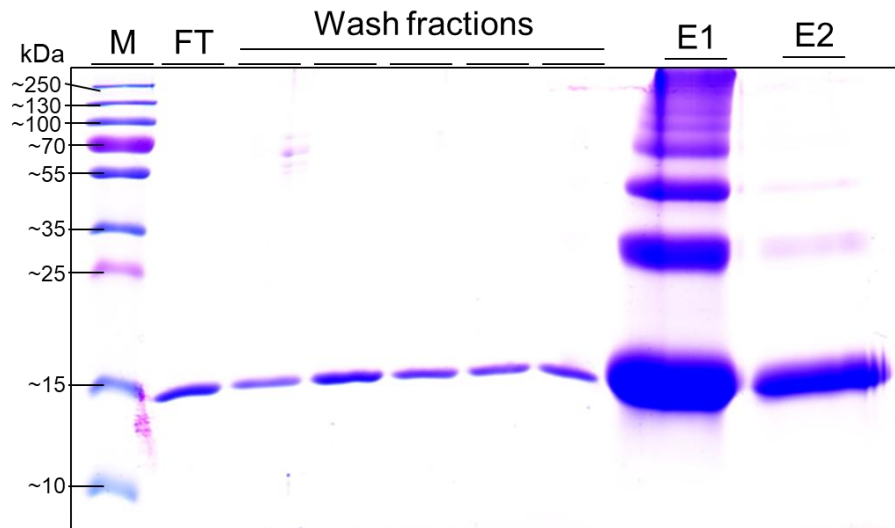
**Supplemental Figure 3: Fe$^{3+}$-IMAC occasionally exhibited multiple band patterns.** SDS-PAGE with fractions from Fe$^{3+}$-IMAC experiment. Metal chelating sepharose was loaded with Fe$^{3+}$, Fe$^{2+}$. Purified Dld1 was incubated with prepared matrix at pH 6. Flow-through (FT) was collected and matrix was washed five times with respective assay buffer. Bound proteins were eluted by competition with EDTA in the elution buffer (E1 and E2). Proteins in all fractions (flow-through, wash and elution) were precipitated, solved in SDS sample buffer and analyzed by SDS-PAGE followed by Coomassie-based staining. Dld1 was present in FT and all wash fractions in low amounts. In E fractions, an intense multiple band pattern was observed starting from approx. 15 kDa.

**Supplemental Table 1: Combined proteins identified from *P. indica* <pGOGFP:DLD1> peptide mass fingerprinting analysis.**

Deglycosylation increased the number of identified proteins from 10 to 53. 47 out of the 53 identified proteins contain a signal peptide predictable with SignalP 4.1.

| *P. indica* gene number | Sequence description | Predicted signal peptide | Molecular weight |
|---|---|---|---|
| PIIN_00112 | probable carboxypeptidase | 19 | 49.14 |
| PIIN_00424 | probable extracellular elastinolytic metalloproteinase precursor | 19 | 68.30 |
| PIIN_00425 | probable extracellular elastinolytic metalloproteinase precursor | - | 66.15 |
| PIIN_01065 | related to bacterial leucyl aminopeptidase precursor | 17 | 44.27 |
| PIIN_01237 | macrofage activating glycoprotein | 17 | 41.17 |
| PIIN_01377 | related to serine protease | 21 | 65.19 |
| PIIN_02021 | expansin family protein | 21 | 26.22 |
| PIIN_02169 | carbohydrate esterase family 4 protein | 18 | 55.11 |
| PIIN_02172 | carbohydrate esterase family 4 protein | 17 | 49.31 |
| PIIN_02492 | related to subtilisin-like serine protease | 18 | 95.81 |
| PIIN_02585 | ribonuclease t2 | - | 45.45 |
| PIIN_03013 | glycoside hydrolase family 16 protein | 21 | 39.43 |
| PIIN_03186 | protein | 17 | 40.75 |
| PIIN_03191 | glyoxal oxidase | 26 | 71.59 |
| PIIN_03211 | hypothetical protein PIIN_03211 [Piriformospora indica DSM 11827] | - | 13.53 |
| PIIN_03333 | ubiquitin isoform cra_a | - | 21.97 |
| PIIN_04111 | glycoside hydrolase family 3 protein | 18 | 80.86 |
| PIIN_04141 | isoamyl alcohol | 19 | 68.80 |
| PIIN_04365 | glucooligosaccharide oxidase | 30 | 56.10 |
| PIIN_04487 | laccase | 47 | 60.57 |
| PIIN_04543 | hypothetical protein PIIN_04543 [Piriformospora indica DSM 11827] | 20 | 16.96 |
| PIIN_04685 | related to aminopeptidase | 22 | 46.11 |
| PIIN_04931 | aminopeptidase | 25 | 49.30 |
| PIIN_04932 | aminopeptidase | 20 | 42.55 |
| PIIN_04941 | aminopeptidase | 20 | 42.74 |
| PIIN_05022 | expansin family protein | 17 | 25.73 |
| PIIN_05108 | malate dehydrogenase | 18 | 25.49 |
| PIIN_05222 | glycoside hydrolase family 16 protein | 19 | 30.83 |
| PIIN_05242 | deuterolysin m35 metalloprotease | 18 | 36.33 |
| PIIN_05281 | thaumatin-like protein | 17 | 27.61 |
| PIIN_05456 | hypothetical protein PIIN_05456 [Piriformospora indica DSM 11827] | 21 | 22.87 |
| PIIN_05901 | hypothetical protein PIIN_05901 [Piriformospora indica DSM 11827] | - | 28.92 |
| PIIN_06108 | acid phosphatase | 16 | 31.13 |
| PIIN_06568 | aspartic protease | 18 | 43.18 |
| PIIN_06613 | macrofage activating glycoprotein | 20 | 36.42 |
| PIIN_07425 | c5-1 protein | 18 | 25.97 |

| *P. indica* gene number | Sequence description | Predicted signal peptide | Molecular weight |
|---|---|---|---|
| PIIN_07640 | alpha-glucosidase | 22 | 98.84 |
| PIIN_07689 | carboxypeptidase cpds | 41 | 56.11 |
| PIIN_08245 | family 32 glycoside hydrolase | 18 | 75.68 |
| PIIN_08262 | secreted protein | 19 | 42.83 |
| PIIN_08288 | gmc oxidoreductase | 23 | 70.34 |
| PIIN_08292 | macrofage activating glycoprotein | 19 | 19.32 |
| PIIN_08474 | copper radical oxidase | 19 | 161.20 |
| PIIN_08513 | hypothetical protein PIIN_08513 [Piriformospora indica DSM 11827] | 30 | 27.70 |
| PIIN_08982 | hypothetical protein PIIN_08982 [Piriformospora indica DSM 11827] | 20 | 23.31 |
| PIIN_09023 | copper radical oxidase | 19 | 75.16 |
| PIIN_09051 | probable extracellular elastinolytic metalloproteinase precursor | 19 | 64.55 |
| PIIN_09116 | glycoside hydrolase family 15 protein | 20 | 64.34 |
| PIIN_09220 | glycoside hydrolase family 16 protein | 20 | 35.57 |
| PIIN_09383 | extracellular protease | 25 | 39.84 |
| PIIN_09677 | glycoside hydrolase family 28 protein | 18 | 47.78 |
| PIIN_09759 | glycoside hydrolase family 16 protein | 20 | 46.28 |
| PIIN_09847 | protein | - | 40.23 |
| PIIN_10060 | glycoside hydrolase family 37 protein | 18 | 87.13 |
| PIIN_10082 | protein | 22 | 80.29 |
| PIIN_10350 | hypothetical protein PIIN_10350 [Piriformospora indica DSM 11827] | 18 | 21.00 |

**Supplemental Table 2: Oligonucleotides used in this study.**

| Name | Sequence (5' to 3') | Restriction site | Purpose |
|---|---|---|---|
| F_Dld1_SP | *CGATCGATATGCGCGTCGGTTTCTATGCC CTACTTTTTGCCTCGGCTGCACTCTTGGCG TCCACTGCTCCGCTTCCGAACCCCCCGAT GACCCCAGCGGAATTCAAGCTTCCCGGGG CG* | none | Oligo assembly Dld1 signal peptide |
| R_Dld1_SP | *CGCCCCGGGAAGCTTGAATTCCGCTGGGG TCATCGGGGGGTTCGGAAGCGGAGCAGT GGACGCCAAGAGTGCAGCCGAGGCAAAAA GTAGGGCATAGAAACCGACGCGCATATCG ATCG* | none | Oligo assembly Dld1 signal peptide |
| 05872woDELD_HindIII | <u>*AAGCTT*</u>*CTACTTGGTGCCAGGGGCGGGTG TT* | *Hind*III | Amplification and cloning of *DLD1* without sequence encoding RISDELD motif and with premature Stop Codon |
| 05872mutAla | *GCTGAACGCGCCGCTGCTACGGCCAACAG AG* | none | Site-directed mutagenesis of *DLD1* |
| 05872wSP_pA_F | *AATGCGCGTCGGTTTCTATGCCC* | none | Amplification of full-length *DLD1* and subsequent cloning in TOPO vector |
| 05872wSPwoSP_R | *CTAATCCAGCTCGTCTATGCTCC* | none | Amplification of full-length *DLD1* and subsequent cloning in TOPO vector |
| 05872_GSTbamh1_F | *GCC*<u>*GGATCC*</u>*GCTCCGCTTCCGAACCCCCC* | *BamH*I | For cloning of *DLD1woSP* into pRSET-A-GST and pRSET-A-GST-GFP-PP |
| 05872_GSThind3_R | *GCCAAGCTTCTAATCCAGCTCGTCTATGC* | *Hind*III | For cloning of DLD1woSP into pRSET-A-GST-PP/pRSET-A-GST-GFP-PP |
| SPDLD1-TEF_F | *ACAACATCATCCACGGGATCCATGCGCGT CGGTTTCTATGC* | none | For the cloning of SPDLD1_mCherry_DLD1woSP and DLD1 full length |
| DLD1-TEF_R | *GATCTGCAGCCGGGCGGCCGCCTAATCCA GCTCGTCTATGCTC* | none | For the cloning of SPDLD1_mCherry_DLD1woSP and DLD1 full length |
| SPPit2-TEF_F | *ACAACATCATCCACGGGATCCATGCTGTTT CGCTCAGCCTT* | none | For the cloning of SPPit2_mCherry_DLD1woSP |
| DLD1-DELDSTOP_F | *CTGCACAGTCAAACATAGGCCCCTGGCAC CAAG* | none | Introduction of stop codon just before RSIDELD motif in DLD1 |
| DLD1-DELDSTOP_R | *CTTGGTGCCAGGGGCCTATGTTTGACTGT GCAG* | none | Introduction of stop codon just before RSIDELD motif in DLD1 |

| | | | |
|---|---|---|---|
| GA_DLD1woSP_F | *GTACAAGGCTCCGCTTCCGAACCC* | none | Gibson assembly of construct pRSET-GST-GFP-DLD1 |
| GA_DLD1woSP_R | *CTTCGAATTCCTAATCCAGCTCGTCTATGCTCC* | none | Gibson assembly of construct pRSET-GST-GFP-DLD1 |
| GA_pRSET-GST-GFP_F | *GCTGGATTAGGAATTCGAAGCTTGATCCGGCT* | none | Gibson assembly of construct pRSET-GST-GFP-DLD1 |
| GA_pRSET-GST-GFP_R | *AGCGGAGCCTTGTACAGCTCGTCCATGCC* | none | Gibson assembly of construct pRSET-GST-GFP-DLD1 |
| GA_GFP-DLD1woRSIDELD_F_R | *CTTCGAATTCCTACTTGGTGCCAGGGGC* | none | Gibson assembly of pRSET-GST-GFP-DLD1woSPwoRISIDELD |
| GA_GFP-DLD1woRSIDELD_V_F | *ACCAAGTAGGAATTCGAAGCTTGATCCGGCT* | none | Gibson assembly of pRSET-GST-GFP-DLD1woSPwoRISIDELD |
| DLD1-OE_F | *AGCTGAAAAAATATCGATAAGCTTATGCGCGTCGGTTTCTATGC* | none | Cloning of DLD1 in pGOGFP |
| DLD1-OE_R | *GCTGCAGGAATTCGATATCCTAATCCAGCTCGTCTATGCTCC* | none | Cloning of DLD1 in pGOGFP |